RL-TR-94-70
Final Technical Report
June 1994

(1)

TROPOSCATTER AT THE KU BAND

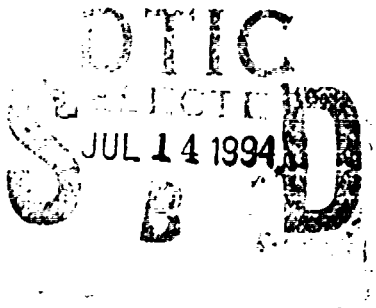

Dartmouth College

Robert K. Crane and Magnus Wennemyr

APPROVED FOR PUBLIC RELEASE; DISTRIBUTION UNLIMITED.

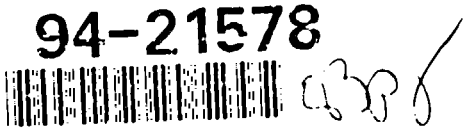

Rome Laboratory
Air Force Materiel Command
Griffiss Air Force Base, New York

This report has been reviewed by the Rome Laboratory Public Affairs Office (PA) and is releasable to the National Technical Information Service (NTIS). At NTIS it will be releasable to the general public, including foreign nations.

RL-TR-94-70 has been reviewed and is approved for publication.

APPROVED: Uve H.W. Lammers

UVE H. W. LAMMERS
Project Engineer

FOR THE COMMANDER: John K. Schindler

JOHN K. SCHINDLER
Director of Electromagnetics & Reliability

If your address has changed or if you wish to be removed from the Rome Laboratory mailing list, or if the addressee is no longer employed by your organization, please notify RL (ERCP) Hanscom AFB MA 01731. This will assist us in maintaining a current mailing list.

Do not return copies of this report unless contractual obligations or notices on a specific document require that it be returned.

REPORT DOCUMENTATION PAGE

Form Approved
OMB No. 0704-0188

1. AGENCY USE ONLY (Leave Blank)	2. REPORT DATE	3. REPORT TYPE AND DATES COVERED
	June 1994	Final Sep 90 - Sep 91

4. TITLE AND SUBTITLE
TROPOSCATTER AT THE KU BAND

5. FUNDING NUMBERS
C - F30602-88-D-0025,
Task E-O-7139
PE - 28010F
PR - 478T
TA - OO
WU - P3

6. AUTHOR(S)
Robert K. Crane and Magnus Wennemyr

7. PERFORMING ORGANIZATION NAME(S) AND ADDRESS(ES)
Dartmouth College
Thayer School of Engineering
Hanover NH 03755

8. PERFORMING ORGANIZATION REPORT NUMBER
N/A

9. SPONSORING/MONITORING AGENCY NAME(S) AND ADDRESS(ES)
Rome Laboratory (ERCP)
31 Grenier Street
Hanscom AFB MA 01731-3010

10. SPONSORING/MONITORING AGENCY REPORT NUMBER
RL-TR-94-70

11. SUPPLEMENTARY NOTES
Rome Laboratory Project Engineer: Uve H.W. Lammers/ERCP/(617) 377-5383

12a. DISTRIBUTION/AVAILABILITY STATEMENT
Approved for public release; distribution unlimited.

12b. DISTRIBUTION CODE

13. ABSTRACT (Maximum 200 words)

Troposcatter data were collected with a wideband measurement system for a period of five months spanning parts of the winter, spring, and summer seasons of 1991. The system provided multipath delay measurements with a 2.5 nsec resolution. Measurements of received signal level, Doppler frequency shift and multipath delay spread were obtained on the 161 km troposcatter path from Prospect Hill in Waltham, MA. to Mt. Tug in Lebanon, NH. These observations are the latest in a longer measurement program to characterize the propagation channel for tropospheric scatter communications systems operating at frequencies near 16 GHz (Ku band). Simultaneous observations at 5 GHz (C band) were made during the last month of the observing program to provide calibration and a statistical comparison with earlier observations made using a different Ku band transmission system.

14. SUBJECT TERMS	15. NUMBER OF PAGES
Troposcatter, Ku-band, rain attenuation, Multipath delay Spread, Tactical communications	88
	16. PRICE CODE

17. SECURITY CLASSIFICATION OF REPORT	18. SECURITY CLASSIFICATION OF THIS PAGE	19. SECURITY CLASSIFICATION OF ABSTRACT	20. LIMITATION OF ABSTRACT
UNCLASSIFIED	UNCLASSIFIED	UNCLASSIFIED	UL

Troposcatter at the Ku Band

Abstract

Troposcatter data were collected with a wideband measurement system for a period of 5 months spanning parts of the winter, spring and summer seasons of 1991. The system provided multipath delay measurements with a 2.5 nsec resolution. Measurements of received signal level, Doppler frequency shift and multipath delay spread were obtained on the 161 km troposcatter path from Prospect Hill in Waltham, Massachusetts to Mt. Tug in Lebanon, New Hampshire. These observations are the latest in a longer measurement program to characterize the propagation channel for tropospheric scatter communications systems operating at frequencies near 16 GHz (Ku band). Simultaneous observations at 5 GHz (C band) were made during the last month of the observing program to provide calibration and a statistical comparison with earlier observations made using a different Ku band transmission system.

The results obtained with the wideband system were similar to those collected earlier. The intent of the measurement program with the wideband system was to make multipath delay spread measurements with better delay resolution than had been obtained before. Model calculations had suggested that the delay spread should be significantly narrower than previously reported and narrower than assumed in the design of troposcatter modulation systems. The prior observations made during this program employed a channel measurement system with an 80 nsec resolution. The observations with that system were consistent with the hypothesis that the atmospheric channel had a multipath delay structure that was significantly narrower than had been assumed and too narrow to observe with the existing equipment. The newer system had sufficient delay resolution to allow a comparison between the observations and predictions. The results show that the atmospheric channel has a wider bandwidth than previously assumed (a narrower multipath delay).

Statistically, the median delay spread values for the 1991 spring time period, which had with the longest run of data, ranged from 98 nsec for the afternoon hours to 110 nsec during the evening for times with scattering by clear air turbulence. These values are narrower than the 173 to 184 nsec median values obtained with the older system during the spring of 1990 for the same time periods respectively. They are also narrower than the 150 to 160 nsec values that have been used in system design.

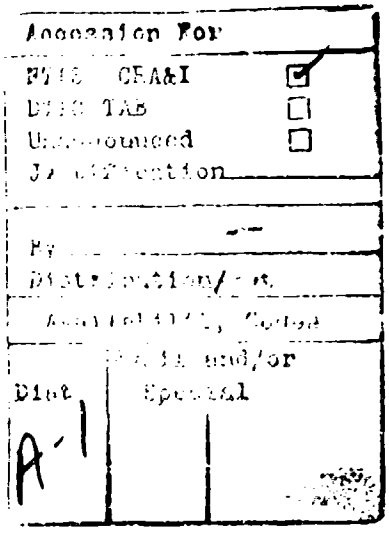

Table of Contents

List of Tables

List of Illustrations

Acknowledgements

The experiment described in this report was sponsored by the Joint Tactical Communications (TRI-TAC) Program Office, Electronics System Division (ESD) and the Rome Laboratory (RL). The work at the Thayer School of Engineering, Dartmouth College was supported by ESD and RL through the RL Post-Doctoral Program. Uve. H. W. Lammers and Richard A. Marr of the Electronics Directorate (RL/ERCP) at Hanscom AFB were responsible for the operation of the transmitter site. They also refurbished the radio frequency hardware for the wideband transmission system.

The receiver site on Mt. Tug is the cable head for Twin State Cable of West Lebanon, NH. The generosity of Twin State Cable in allowing us to use the facility and their tolerance to the occasional bouts of interference that we produced is greatly appreciated.

A number of graduate students at the Thayer School of Engineering have been involved in this project over its five year lifetime. For this final year of the project, only Magnus was left to carry on and prepare this report.

TROPOSCATTER AT THE KU BAND

1. Introduction

1.1 Program objectives

The objectives of this study were to use the wideband troposcatter system to characterize the channel for use in a digital communications system at operating at a carrier frequency near 16 GHz.

1.2 Summary of Results

The analysis of the observations made with the wideband troposcatter measurement system is presented in the Appendix to this final report.

Data collection for this phase of the experiment started in January 1991 and continued through the June 1991 with occasional outages due interference in several of the TV channels caused (apparently) by the first IF of the Ku band receiver. In total, 800 hours of observations were collected during the winter period, 1308 in the spring and 359 in the summer. C-band measurements were started in the latter part of the spring and continued during the summer period. A total of 642 hours of simultaneous C and Ku band measurements were obtained.

Analysis of a Wideband Troposcatter Propagation Channel at the Ku Band

Magnus Wennemyr
Master of Science Thesis
October 1991

Thayer School of Engineering
Dartmouth College, Hanover, New Hampshire

ABSTRACT

Tropospheric scatter is a conglomerate term describing the course-of-propagation alteration of electromagnetic wave energy due to weather mechanisms, allowing for transhorizonal communication in the microwave ranges. This study tests the viability of using the higher frequency ranges (the test frequency was 15.731 GHz) for this type of communication. At the present time, troposcatter communication systems are limited to the lower frequencies (up to 5GHz), due to concerns of attenuation at the higher frequencies during rainy conditions.

Data were collected on a wideband system (400 MBit/sec) over a period of five months. This system provides an unprecedented resolution of turbulence in the lower troposphere. During the last month, data were also collected simultaneously with a reference C band system (4.95 GHz). Characteristics of the signal level, Doppler shift and multipath delay were recorded, and hourly median values of these quantities were analyzed. Diurnal and seasonal changes were observed, and the data categorized according to the dominant scattering mode for each hour. Three modes were considered: turbulent volume scatter, rain scatter, and ducting.

The observations made on the 161km long path between Prospect Hill, MA, and Mt.Tug, NH,show that rain is beneficial for wave propagation at this high frequency. The increased forward scatter associated with the rain offsets the attenuation caused by scattering away from the path between the transmitter and receiver. Turbulent, thin-layer, volume scattering dominated the propagation process 90 percent of the time. As a theory of propagation, this clear air phenomenon was consistent with the results. Diurnal variations were strongest in the summer, significantly increasing both the Ku and C band signal levels during afternoon hours. Seasonal variations were evident as well. In particular, an important observation of seasonal change was a delay spread increase of 50 percent from winter to summer.

Chapter 1
Introduction

1.1 Introduction

The purpose of this study was to test the viability of using a higher frequency range for Tropospheric Scatter (troposcatter) Communication. Although the frequency range in question - near and around the test frequency of 15.731 GHz - is already in use for other types of communication and remote sensing devices, it has been assumed that troposcatter would be too severely attenuated at such small wavelengths, especially in rain conditions, for reliable use in a radio communications service. (The 15.4 to 17.3 GHz range is allocated for RADAR services; the closest fixed service allocation is 14.8 to 15.25 GHz.) If contrasting theories were to prove accurate, however, the funders of the project would be able to use the new frequencies. These theories which rely on a theoretical framework, rather than empirical one, predict that propagation of frequencies in the 15 GHz range will be enhanced during rain; this would be the result of an increase in scattering during rain, counteracting the accompanying attenuation. Antenna gain can be maintained at higher frequencies while reducing the antenna size - such a reduction would make troposcatter systems portable. Furthermore, used as a tool for observation of meteorological processes, this bistatic RADAR system has resolved the vertical Doppler and scatterer strength components of the lower troposphere to an unprecedented degree.

1.2 Transhorizonal Microwave Propagation in the Troposphere

The troposphere is the innermost layer of the atmosphere, ranging from ground level up to 10-16 kilometers height depending on the geographic location. The mean temperature decreases with height within this layer. Beyond the tropopause - a constant temperature layer between the troposphere and the stratosphere - the temperature again increases. All weather conditions manifest themselves in the troposphere, significantly affecting the propagation of those radio waves with wavelengths on the order of the various inhomogeneities in the refractive index. The unpredictable and complex nature of weather obscures interpretation of these effects. Most significant of the regions where these discontinuities exist are strong layers of clear-air turbulence and volumes containing the different forms of precipitation.

Tropospheric scattering is a conglomerate term describing the course of propagation alteration of electromagnetic wave energy due to these weather mechanisms, allowing for transhorizonal communications in the microwave ranges. By several mechanisms, weather - defined as the temperature, pressure, humidity, wind velocity, and precipitation configuration of the troposphere - enables the establishment of communication links of over 1000 km. pathlengths. Conversely, by the same phenomena unpredictable changes in the weather can also inadvertantly cause interference between distant co-channel services.

Although the introduction of satellite communication reduced the need for transhorizonal troposcatter systems for general communications, and aside from their use in special circumstances (due to the low investment costs and the particular capabilities desirable to the military), they are useful in studying the interference problem for systems operating at the same range of frequencies (e.g. the European Community COST 210 project uses troposcatter data to set satellite communication design guidelines for avoiding interference.) Moreover, these systems are used for the study of meteorology; by identifying the processes that alter the transmitted signals by inference from differences in the transmitted and received signals, knowledge is gained about weather processes and structure. This last application is most useful in clear air, during such conditions the different components of the multi-path delay signature (i.e. the power received as a function of the transmit-to-receive timelag) can realistically be considered to represent a vertical profile of the scatterer strength.

1.3 The Troposcatter Link

The troposcatter link shown in Fig 1.1 consisted of 1) a transmitter at Prospect Hill, Waltham MA, maintained by Rome Laboratory personnel and 2) a receiving station on Mt.Tug, Lebanon NH, constructed and maintained by Thayer School graduate students over a period of five years.

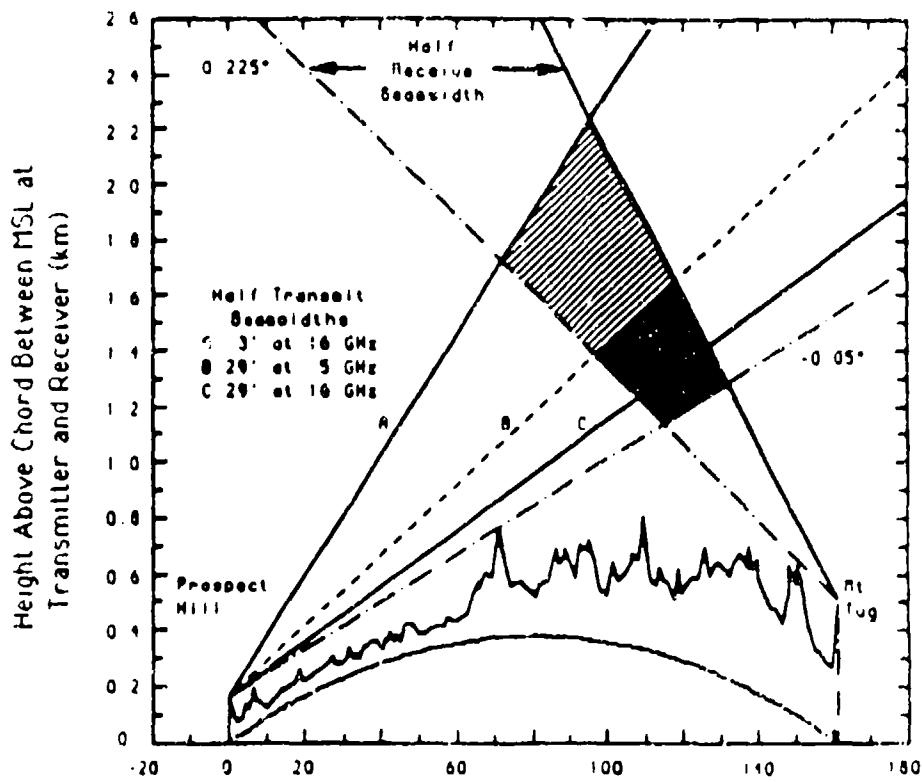

Figure 1.1: Prospect Hill - Mt.Tug path profile for a 4/3 effective earth radius. The lowest beam paths shown indicate the center of the conical 1/2 power sections of the transmitted beams.

The angle of the pointing of the antennas with the horizon is small, producing a very small common scattering volume. As a result, this system is ideal both for studying the interference phenomenon which occurs over similar paths between ground-based, microwave communication systems, and for achieving the aforementioned high vertical resolution. The armed forces use this type of system because of the difficulty of linking with the small scattering volume without access to the transmitter-receiver sites, providing added security from interference and unwanted listeners. The possibility of using smaller antennas means that these systems could become portable by vehicles.

1.4 Project Summary

Building of the link was begun by setting up the microwave (Ku band - at 15.731 GHz) receiver [Levins 1986]. A lower frequency receiver (C band - at 4.95 GHz) was set up as a standard for comparison [Sullivan 1987]. This frequency was chosen to be high enough to lie within the same subrange of turbulent scales (the 'inertial' range of turbulence, discussed in Section 2.3.2, where scattering strength is predicted to follow a log-linear frequency dependence) in order to accurately evaluate clear air frequency relationships. The frequency was also low enough so that a substantial amount of data and experience were available for comparison. Since the C-band had only this purpose, it employed simple, continuous wave (CW) transmission. To provide information as to the delay characteristics of the channel, a phase-modulated 1023 bit long pseudo-random noise (PRN) code at 12.5 MBit/s (narrowband) was applied to the experimental Ku band. [Stamboulis 1987 and Anderson 1989 further add to the system description.] Later a 400 MBit/s (wideband) PRN code was added to the system to increase the spatial resolution [Chandra 1990]. Preliminary assessment of the link and summary of the narrowband results until spring 1990 have already been made [Hoppe 1989, Prabhu 1991, Crane 1991, Crane&Prabhu 1991]. This thesis presents an analysis of the wideband system results.

1.5 Personal Contribution to Project

Aside from the daily routine of collecting and analyzing the data, only minor work was required for maintenance of the receiver hardware. The wideband receiver installation was completed during the fall of 1990, during which time the transmitter was inoperational. New software for data collection was developed, based on the collection program for the narrow-band system, and limitations on the computer at the receiver end was tested. A recurring problem, caused by a faulty clocking of the PRN code generator, was eventually fixed. When the C band was put into use in May, interference problems interrupted the collection campaign. Interference from the C band onto the Ku band was successfully dealt with, by switching the systems on and off during their near-simultaneous measurements toward the end of the collection campaign. The local cable TV company complained of interference, for which reason operation

was shut down several times while a solution was found. The data processing software was rewritten in its entirety, and a method greatly diminishing the effects of the unwanted, irregular, relative drift of the frequency Cesium beam standards was developed. This method was required in order to make possible a precise defining of the spatial location of the scatterers.

1.6 Objective of the Study

The purpose of this report is to present the effects of the different weather phenomena - with an emphasis on rain - on 16 GHz microwave propagation in the troposphere. The data discussed represents measurements collected during a six month period. The use of the C band at the end of the spring was primarily as a reference signal. Since the transmission characteristics depend on a variety of factors, one expects deviation from theoretical predictions, wherefore the data are presented in a statistical format, and their validity investigated. The data are presented in a format to be used for a communication link. High level fields are in that case of little interest; rather, low-level fields are of primary concern. The most important parameters investigated are the transmission loss, the multipath delay spread (placing limitations on channel bandwidth), and the Doppler frequency spread (a necessary parameter for many modulation schemes).

1.7 Summary of Signal Processing and Results

In order to characterize the communication channel and provide the means for interpretation of the meteorological pheonomena, information was collected of the power received, the mean Doppler frequency shifts and the Doppler frequency spread, the multipath delay spread, as well as power and Doppler measurements at different delays. Because of the limitations of the IBM PC used for data collection at the reciver site, only sixteen scans of the PRN code - plus data for a spectrum at the delay with the maximum power - were possible during an hour. The in-phase and quadrature components of the power were sampled 60 times at each tap of the code, in order to average out Rayleigh fading on the channel. Hourly medians of the different quantities were then arranged in various ways to allow investigation of the diurnal and seasonal changes in the data, as well as the effect due to different weather conditions - the 'modes of propagation'. In order to statistically predict the occurrence of low-level fields, large Doppler spreads, and of large delay spreads, distribution models for these quantities were fitted to the data.

1.7.1 Diurnal and Seasonal Variations

As expected, the transmission losses were smallest during the afternoon when warm, moist, turbulent, air contributed more to the forward scattering process. The variation during the winter was minimal, but

increased to an average of about 8 dB during the summer (June 1st-20th). There was a progressive increase in this variation during the spring months. There is a less clearly defined diurnal variation of the multipath delay spread; it tends to increase during the later hours of the day, following the increase in the signal level. The general signal level increases during the warmer months (a difference of 4-5 dB), but is offset by a very large increase, 30-50%, in the delay spread values. The algorithm used for the delay spread estimate is more sensitive than that used in previous reports, and signal-to-noise ratio effects are estimated to have been negligible. The log-normal distribution model fits the signal level data extremely well, at both frequencies: the multipath delay spread and Doppler spread values were normally distributed. Only the Doppler spread measurement is seriously in question. It is, apparently, tainted by the 60 Hz noise evident on the frequency spectra.

1.7.2 Modes of Propagation

Three modes of propagation were investigated: turbulent volume scatter, rain, and ducting. Turbulent scatter accounted for 90% of the hourly median values, with the remainder primarily dominated by rain scatter. Rain on the path was found to amplify the Ku band signal, contrary to expectations based on projections made from lower-frequency experimental data, but in agreement with the theoretical framework of the turbulent, thin-layer, volume scatter model. This agrees with the results from the previous two years. For neither of the months investigated, during rainy conditions, was either the median signal level lower than that of turbulent scatter, or the percentage of extremely low reception levels higher. In general, the Ku band was more sensitive to rain, reflected in the greater change in Doppler frequency shift during rain. Conversely, the C band was more sensitive to ducting, a condition where extended negative gradients are coupled into, with effects similar to that of waveguides. During the few hours when this occured - which was primarily during the night hours - there is a significant deviation from the norm, wherefore it is considered an entirely separate phenomena from turbulent scatter. The C band, and the Ku band to a lesser extent, is strongly amplified during ducting.

1.8 Conclusions

This study, along with the previous results of this same data collection campaign, show conclusively that the Ku band is reliable for troposcatter communications usage. The thin-layer, turbulent volume scatter model accurately predicts the results in clear air, both in terms of total power received and the signal delay profile. Rain is shown only to enhance the signal levels, but was also accompanied by a slight Doppler spread increase. It is, however, less severe than the seasonal Doppler spread variation. The wideband system has proven very useful for a detailed study of the delay profile; this aids significantly in evaluating

theoretical models and investigating weather phenomena. An immediate advantage of the wideband system is that it allows a more accurate evaluation of the categorization of data into the various propagation modes.

Chapter 2
Tropospheric Propagation Models

2.1 Absorption

The fundamental reason for the difficulties encountered in the use of microwave frequencies is the increased attenuation experienced in precipitation because of comparable relative sizes of the electromagnetic wavelengths and the water droplets. Figure 2.1 indicates the increased attenuation due to absorption and scattering at the higher frequencies. For this reason it was thought impractical to use the Ku band for beyond-the-horizon communication.

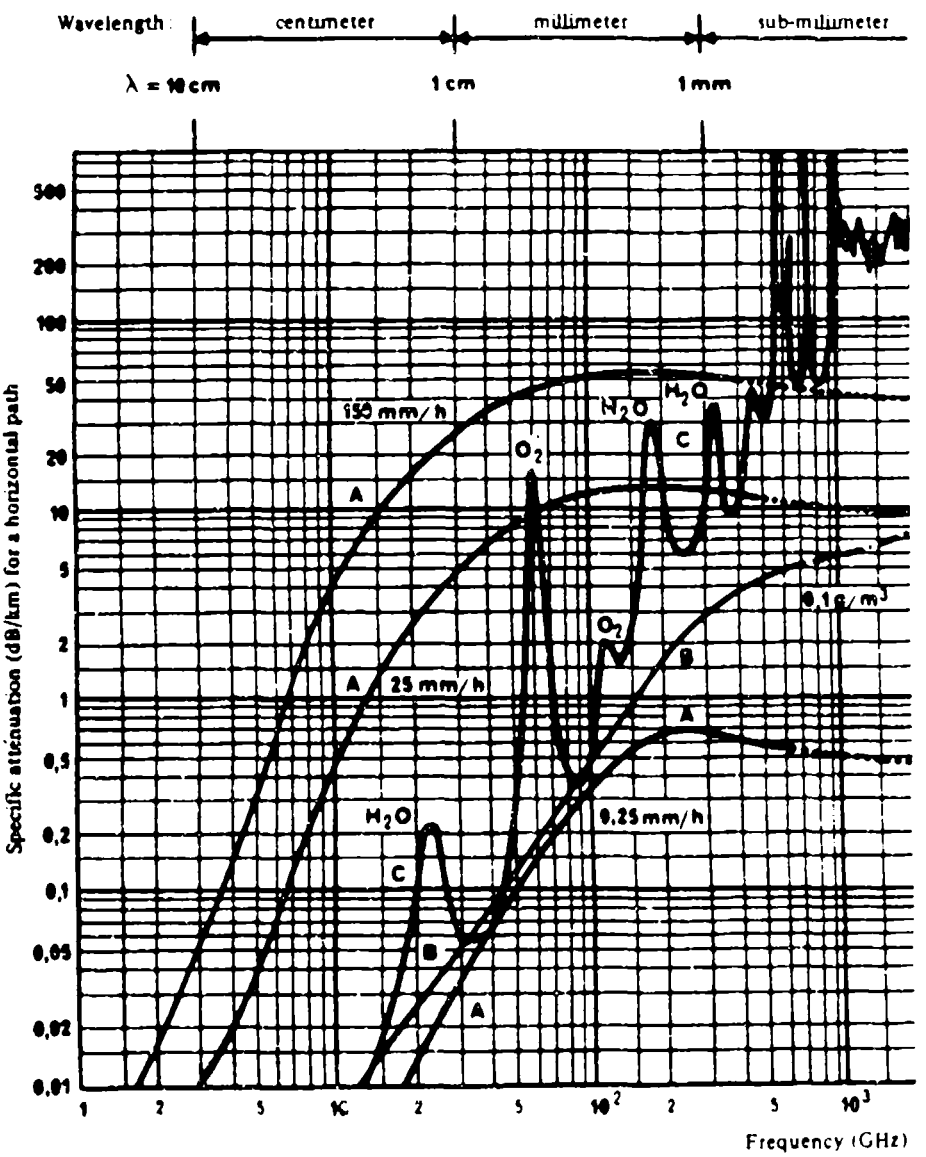

FIGURE 2.1: Attenuation due to gaseous constituents and precipitation [CCIR 1991]

Scattering of the radiowaves causes attenuation, as does the absorbtion caused by water drops with a lossy dielectric. This attenuation due to precipitation is added to the attenuation due to the gaseous constituents in the air, also a frequency dependent effect, to form the total attenuation loss. The most accurate estimates of attenuation by gases (primarily water vapour and oxygen) and by moderate to heavy rainfall are derived empirically, taking into account such factors as rainrate and angle to the horizon. Good theoretical approximations of the attenuation have been reached for smaller - and thus more spherically shaped - raindrop sizes [Doviak 1984, Sect.3.3]. The attenuation is included in the RADAR equation as integrals over the distance of the paths to and from the scatterers.

2.2 Refractive Index

It is the refractive index (n) fluctuations (or, those of the relative permittivity, which is directly related to n) in the air which cause the refraction or reflection of radiowaves back toward the earth. For the clear air these fluctuations are caused by turbulent mixing of the mean gradient of the potential refractive index (reflecting changes due to the accompanying adiabatic changes in temperature), and in cases of precipitation by the gradient of the refractive index across the different media.

The complex refractive index of rain is expressed as $m = n - jk$, where k is the absorption coefficient, a function of wavelength and temperature. A determination of the refractive index is the first step toward finding the backscatter cross Section of a particular phenomenon.

The refractive index of the atmosphere depends primarily on the water vapour pressure which, unlike the composition of dry air, is highly variable:

$$N = 77.6\frac{P}{T} + 3.73\times10^{5}\frac{e}{T} \qquad : P(mb);\ T(K);\ e(mb) \tag{1}$$

where e is the water vapour pressure and the radio refractivity $N = (n-1)\times10^{6}$, so defined because numerically the fluctuations of n tend to be extremely small. The dependence on vapour is due to the permanent dipole of the H2O molecule, heavily influencing the propagation of short waves. These quantities are not independent of each other: pressure changes lead to temperature variations, and the vapour pressure is proportional to the pressure p by $e = 1.62pq$, where q is the concentration of water vapour. Signals received will then be negligible unless temperature perturbations are very strong when water vapour contributions are small. This dependence on the water vapour content explains much of the observed seasonal variability and climate effects on the power received.

Only if there is a sufficiently rapid spatial fluctuation of the refractive index will the electromagnetic energy bend down toward the earth, where dN/dh<-157 per km. In addition to the small-scale variations due to turbulence there is a systematic smooth, mean variation of about -40N/km (varying from day to day, as well as seasonally) in the lowest part of the troposphere, which in effect raises the horizon so that the effective earth radius becomes 4/3 times the earth's radius, by straight application of Snell's law.

The magnitude of the ratio of the discontinuity of the refractive index to the wavelength can also determine the mode of propagation. For instance, because higher gradients would be needed for short wavelengths to be reflected, there is a dependence on the ratio such that reflections are less likely to occur in clear air conditions at the shorter wavelengths. It is therefore possible to relate the mode of propagation to a function of the characteristics of the turbulence and the transmission wavelength, given assumptions about its formation and structure. In this particular case, at the higher frequency the mode of propagation would be turbulent volume scatter. As is common practice and most consistent with present theory, results were divided according to the modes of turbulent scatter, ducting and rain scatter.

2.3 Turbulence in the Troposphere

2.3.1 General

By the late 1960's it was generally accepted that clear air turbulence accounted for the low-intensity signal received with tropospheric scatter systems, while short-term high-intensity reception occured as the result of other mechanisms [Tatarskii, 1971, p152] such as ducting, reflection and precipitation scatter. Interpretations of radar backscatter observations had been attempted as early as the late 1930's [Friend 1939, by Ottersten, 1969]. In the early 60's explanations of such "Angel scatter" focused on smooth refractive index discontinuity reflections [Atlas, 1964, by Ottersten]. Because of the diffuse nature of the echoes, however, it was realized that irregular, turbulent fluctuations in the refractive index as a volume scatter phenomena could at times be a more appropriate model [Atlas and Hardy, 1966]. [Tatarskii, 1961, 1971 developed mathematical theory of turbulence effects on radiowave propagation.] It was determined that a theory proposing that the troposphere was composed of turbulent "blobs" whose spatial extent would be described by an exponential correlation function [Booker and Gordon, 1950 p 403] did not fully explain experimental RADAR results; the same experiments seemed to confirm the correctness of the turbulent volume scatter theory for the high frequency range. Instead turbulence appeared to be associated with stratified layer structures [Richter 1969, p1266]. On the basis of comparisons of model-to-experiment results, it was concluded that specular reflections from these layers are less important at the higher frequencies where the turbulent layer scattering mode dominates, with transition frequencies roughly in the low GHz range [Crane, 1981]. RADAR studies conclusively confirmed the Kolmogorov theories of the turbulence spectrum upon which Tatarskii's studies and the idea of turbulent volume scatter were based

[Kropfli, 1968]. Multifrequency troposcatter findings varied greatly, however, and they in no way showed such conclusive results, calling into question not the Kolmogorov turbulence energy spectrum or Tatarskii's theories, but rather the place of those theories in analysis of trans-horizonal phenomena. For this reason the idea of specular reflections remained a viable alternative to thin layer volume scattering, although no better at predicting results at the higher frequencies; thus, the data collected at lower frequencies - by the National Bureau of Standards - is still the basis for models of the higher frequency paths used by the International Radio Consultative Committee (CCIR) [CCIR,1990, Rice et.al, Tech.Note101]. As recently as the 80's, Gossard [1984] has proposed that layer-reflections may be caused by stacked, thin, volume-filling layers with more complicated and unpredictable frequency dependence, again lending credence to the simpler reflection model even at the higher frequencies. Other directions have been investigated as well, such as fractal modelling of the random volume scattering media [Rastrogi, 1989], without much impact in the field. Skolnik [1974] has a review of the different models. As many felt that Tatarskii's ideas were accurate (because of agreement with RADAR/Aircraft simultaneous measurements), and since a multifrequency experiment had not yet been performed at the frequency range deemed appropriate (previous higher-frequency studies have focused on the high level fields for the interference problem), the present study is important to provide an indication of the importance of the range of frequencies tested. Previous study in this present data collection campaign were partly a further investigation into these theories on the questions of layer reflection vs. turbulent scatter. It was the finding that indeed the frequency dependence described by the turbulent volume scattering model is consistent with the results [Crane 1988].

It is only with the complete understanding of these processes that a full description of the path loss predictions of the RADAR equation (predicting the relation of the received to the transmitted power) can be achieved. This theoretical prediction is important, since empirical predictions for the higher frequency ranges, relying on lower frequency measurements, prove inadequate. Remaining important questions related to turbulence structure include both the amount of beamfilling and the frequency of occurrence of scattering layers.

2.3.2 Turbulence Scales

Turbulence is commonly thought of as the result of windshearing and buoyancy forces causing mixing of air masses of different types (i.e.with different temperature, humidity etc.). Large-sized inhomogeneities break up into smaller and smaller discontinuities, or eddies, such that the velocity, temperature, humidity, pressure and dielectric constant characteristics of such regions become random functions of position and

ume. Kolmogorov [by Tatarskii, 1971, pp.48-] proposed that for large Reynold's numbers[1] the motion can be considered as random, incompressible, flow at low speeds (compared to the speed of sound) and that the small-scale velocity field can be considered homogenous and isotropic. With continued relative motion of the different air masses creating eddies of large spatial scales, there will be a spectrum of eddy sizes at any one time, with kinetic energy continually redistributed from the large to the smaller scales. The region of the spectra containing the large eddies (on the order of 100 m) - with "outer scale of turbulence" Lo - contains the greatest density of the average kinetic energy (per unit mass). The definition of this parameter varies widely. Tatarskii's thin layer outer scale is a function of the turbulent eddy dissipation rate, the thickness of the layer, the velocity changes across the layer, the mean wind shear, and the covariances of the velocity and turbulent heat. The smallest region (on the order of 1 mm) with an "inner scale of turbulence" represents the bulk of energy dissipation beyond which the destructive action of viscosity and diffusion have nullified most turbulent activity:

$$L_i = \sqrt[4]{\frac{\nu^3}{\varepsilon}} \qquad ; \nu = \text{kinematic viscosity of fluid} \tag{2}$$

Kolmogorov proposed in 1947 that the turbulence structure in the 'inertial subrange' well in between these two scales is dependent only on the rate of energy dissipation per unit mass, ε, equalling the rate of the flux of energy toward the smaller scales. Scales in this range are too large for viscocity effects to be noticeable. The energy spectrum function then becomes, by dimensional analysis:

$$E(K) = A\varepsilon^{2/3}k^{-5/3} \qquad ; k = \frac{2\pi}{\lambda} \tag{3}$$

where A is a constant [Doviak 1981, p346]. Wavelengths for RADAR and satellite communication often lie in this inertial subrange, as do the vertical wavenumbers used for the Mt.Tug-Prospect Hill experiment (See Figure 2.2). Note that for tropospheric scattering, which occurs at an angle to the horizontal, the apparent wavelength in the z-direction, the factor under consideration here, is of a much greater value than the transmission wavelength, but is still within the inertial subrange.

1

$$Re = \frac{vL}{\nu}$$

where v and L are the characteristic velocity and scale of flow,
and ν is the kinematic viscocity

2.3.3 Effect of Turbulence on Wave Propagation and the Structure Constant

For this model of turbulence formation, the propagation mode and transition frequency discussed earlier are believed to be found approximately by [Crane 1981, p.656]:

$$\frac{\lambda}{2\sin\theta/2} > L_O \quad ; \theta \text{ is the scattering angle} \tag{4}$$

where, if the inequality is true, specular reflections are expected to dominate, and, if the converse is true, thin volume scattering dominates. Due to the shorter wavelength at the higher frequencies, the refractive index variations span several Fresnel lengths. In that case statistical correlation modeling is more appropriate than the plane wave reflection models used for the longer wavelengths - where the variations in n are smaller than the Fresnel length [Crane 1988]. According to this model, volume scattering should dominate the clear air turbulence propagation on the Prospect Hill to Mt.Tug path since the frequencies are high and only a narrow range of the wavespace (centered around $L = 0.5\lambda$) is expected to contribute to the scattering.

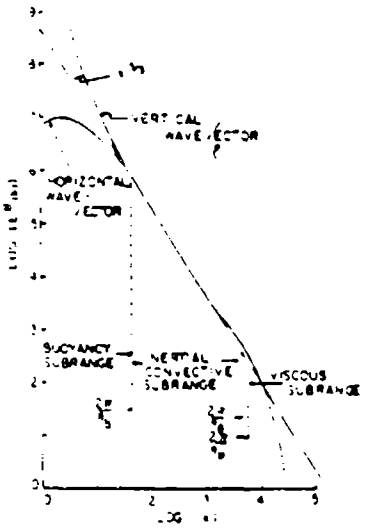

Figure 2.2 One-dimensional spectrum of refractive index fluctuations. Note that the lower wavenumber for the inertial subrange will move in an unpredictable fashion according to variations in the turbulent structure. [Crane 1981]

The spatial variations of the fluctuations in the refractive index are usually represented not by the spectral energy function given earlier or the related autocorrelation function, but rather in terms of the structure function defined as:

$$D_n(\vec{r}) = \langle [n(\vec{r}_1 + \vec{r}) - n(\vec{r}_1)]^2 \rangle \tag{5}$$

where r is the distance between two measurement points, n' the deviation from the mean value of the index of refraction, and the symbols <> denote an ensemble average. With the earlier assumptions of isotropy and homogeneity, the structure function ceases to be the function of a vector distance. This function is used since, by virtue of its being a first difference, it filters out slow variations in the fluctuation measurements, as long as the distance r is not too great. This fact is important to non-stationary processes such as the spatial fluctuation of the refractive index in the atmosphere. In other words, it is usable even though large-scale irregularities are neither homogeneous nor isotropic in the turbulent troposphere. Further, it allows the following simple formulation describing turbulence in the inertial range [Kolmogorov 1947, by Dewan, 1980, pp.9-21]:

(6)

$$D_n(r) = C_n^2 r^{2/3}$$

This is Kolmogorov's original result, based on the assumptions that the potential temperature and specific humidity are conserved and passive. Cn is called the structure constant, defined as:

(7)

$$C_n^2 = \frac{\langle n'^2 \rangle}{L^{2/3}}$$

In other words, the structure constant provides a measure of the refractive index fluctuations relative to the eddy sizes. It is directly related to the energy dissipation rate by:

(8)

$$C_n^2 = \alpha \varepsilon^{2/3} \qquad ; \alpha \approx 1$$

where the energy dissipation consists of both heating and diffusion factors. The structure constant as a function of height thus provides a basis for comparison of the intensity of turbulence as given by the Kolmogorov spectrum, measured by different means with spatially different data collection capabilities, e.g. by RADAR, Sondes, airplanes.

The three-dimensional index of refraction variance spectrum derived from the Fourier integral of the gradient of the structure function of Eqn.6 over the entire wave number space yields:

(9)

$$\Phi_n(K) = 0.033 C_n^2 K^{-11/3} \quad ; \left(\frac{2\pi}{L_o} < k[\bar{m}(\bar{r}) - \bar{n}(\bar{r})] < \frac{2\pi}{L_i}\right)$$ [2]

---

2 Here:

$K = k[\bar{m}(\bar{r}) - \bar{n}(\bar{r})]$ is the scattering vector.

asdf

Note the strong dependence on the scattering angle. This important result is what enables the interpretation of the resolution of the power signature at the different delays to correspond to the vertical structure of the turbulent layers. In the one-dimensional case, this dependence on the wavenumber becomes of the power -5/3.[3] Note that this structure applies to the refractive index spectrum as a derivative of the fact that the temperature as well as the velocity fluctuations exhibit this spectral wavenumber dependence.

This result can then be applied toward the formulation of the scattering cross Section for a final definition of the RADAR equation. From general Bragg scatter, the resulting wavelength dependence of the cross Section is [Doviak 1984, p385]:

$$\eta = 8\pi^2 k^4 \Phi_n(K) m \qquad (10)$$

$m = \sin^2\chi$ is a polarization mismatch factor
χ is the angle of the polarization of the incident wave to the scattering direction

Because its value is near unity at the angles under consideration, the polarization factor is ignored in the computer models for the path. These formulas, along with correct modelling of the propagation path geometries and accurate assumptions about the general structure of turbulence, establishes the groundwork for the relation of the reception characteristics to the intensity of clear air turbulence.

In the final version of the RADAR equation this wavelength dependence is of the power -1/3. Previous experiments have yielded ambivalent results as to this frequency dependency, ranging from -1 to 3 [Eklund and Wickerts, 1968]. As Figure 2.2 shows, however, it is important to ensure that the frequencies lie well within the inertial subrange of the Kolmogorov spectrum for the turbulent volume scatter to apply. The boundary between the buoyancy and inertial subranges is not a fixed one; rather, it is dependent on the particular weather conditions. This project has represented the first such study since the many previous

---

$\bar{m}(\bar{r})$ = unit vector from the transmitter to the scatterer,

$\bar{n}(\bar{r})$ = unit vector from the scatterer to the receiver,

such that they define a scattering angle making:

$K = 2k\sin\frac{\theta}{2}$, where again $k = \frac{2\pi}{\lambda}$

3 The structure function has been related to the energy of the turbulence, and the spectrum of the structure function, (V in the one-dimensional case) is related to the spectral energy density E by:

$$\Phi(k) = \frac{E(k)}{2\pi k^2} = \frac{1}{2\pi k}\frac{dV(k)}{dk}$$

studies have been in too low a range, the frequencies lying now in the inertial subrange, now in the buoyancy subrange.

2.3.4 Turbulence Structure

Several studies, by use of radio-sondes and aircraft as well as RADAR, have clarified the structure of turbulence in the troposphere. They show that the entire troposphere can be thought of as containing a weak 'background' turbulence. High-intensity layers, measuring from tens of meters to a few hundred meters thick, and of up to several tens of kilometers in horizontal extent, lie within this 'background' turbulence. These high-intensity layers are much more likely than the background turbulence to be detected by RADAR. They are less often detected by aircraft, however, and sondes never reveal their horisontal extent. These layers contribute a large portion of the scattered signal in troposcatter systems during clear air conditions, depending on the vertical extent of the layers, their spatial placement, and the strength of the turbulence-generating shearing forces. Appearing randomly over time, in uniform spatial distribution, the layers cause every part of the common volume to be turbulent at some time [Crane 1980]. For this reason - and since any one wavelength is responsive only to a particular, narrow, range of scale of turbulence - the strong layering effect is expected to occur only within a limited volume a small percentage of the time.

The occurrence of particular structures should be taken into account for proper prediction of signal reception in clear air. For instance, RADAR echoes often show wave patterns in clear air. In the common case of vertical wind shear, such waves would presumably exhibit stronger refractivity variance in its upper and lower extremes when breaking waves are formed [Ottersten 1969]. This may only be detected as two distinct layers to a troposcatter system. Along with ducting, these cases are more pertinent to the understanding of interference phenomena. Thermals, or convective bubbles, are expected to reach the lower edge of the common volume at about ten a.m.

2.4 Ducting

Although ducting is a special case of clear turbulence, it is usually not considered as such. During ducting, layers with particularly high dn/dh boundaries form parallel planes; sometimes microwaves can enter the guides and become trapped, in a waveguide-like fashion. A much larger portion of the transmitted signal will in this case be directed toward the receiver. Because of the unsteady nature of the ducts and the fact that they will probably not be quite planar makes modelling of this phenomenon very difficult. Further complexity is introduced since the coupling into the duct of the different modes - and the resulting spectral dependence - is difficult to predict. In general the lower frequency is, as one would expect, considerably more sensitive to this high-level power phenomenon. (Further reduction of the frequency, however causes

the vertical extent of the duct to become more important.) From observations of long time-lags between the constructive and destructive interference patterns that sometimes exist in the waveguide [Crane 1981], the ducting mean Doppler is expected to be very low.

2.5 Precipitation

There is more detailed knowledge of rain formation and characteristics; its drop size, shape and distribution effects on radio wave propagation are comparatively well understood, primarily because of the relative ease in comparing data collected by different means and the simpler descriptive nature of this phenomenon. Rain formation during the different periods of the year has also been studied extensively, and snow and ice particle distribution can be predicted with some accuracy at different heights from rain measurements and height profiles of temperature and humidity. Rain is eminently detectable; it is easily differentiated from other forms of scatter by a large positive Doppler signature. (We have defined positive Doppler as that which shortens the wave pathlength. Rain, with a downward motion toward the straight line passing throught the earth that connects the two antennas, has precisely this effect.) The backscatter cross Section of a water drop per unit volume - the Rayleigh approximation - is [Crane 1974]:

$$\eta = \left(\frac{\pi^5}{\lambda^4}\right)\frac{|K_w|^2}{\rho^2}D^6 \quad ;D=\text{Drop diameter} \qquad (11)$$

$$;K_w = (m^2-1)/(m^2+2)$$

where m is the complex refractive index of water, and $|Kw|$ is about 0.96 for water, 0.42 for ice spheres. The total scatter from rain and water droplets will then simply depend on the reflectivity factor:

$$\int N_D D^6 dD \qquad (12)$$

where N is the number of drops in a unit volume. This will be modified later by other considerations. Now an important difference in the scattering cross Sections of clear air turbulence and rain scatter becomes evident; while turbulence has a very strong dependence on the scattering angle, rain scatter is independent of the angle for linear polarization perpendicular to the plane of scattering, or proportional to $\cos^2(\theta)$ for linear polarization in the plane of scattering.

The troposcatter system is clearly more sensitive to rain scatter. The greater attenuation experienced in precipitation, however, causes the received power in rain, relative to that in clear-air conditions, to depend on the intensity of the rain. This trade-off is very important. It was expected that rain on the path would

simply attenuate the signal so much that it would decrease the reliability of the link. It has been shown, however, that the trade-off is sufficient, so that statistically the link is no less reliable during precipitation.

A comparison of the scatter cross Sections of rain and turbulent clear air conditions shows (Figure 2.3) that extremely clear air conditions are required for turbulence to provide a significant portion of the scattering cross Section and thereby dominate the mode of scattering. Because this plot is for RADAR at a scattering angle of 180°, compensation should be made for troposcatter for small angles due to the effectively enlarged scattering cross Section of turbulence. Therefore, the proper placement of the lines is about 20 dB higher than in the Figure shown.

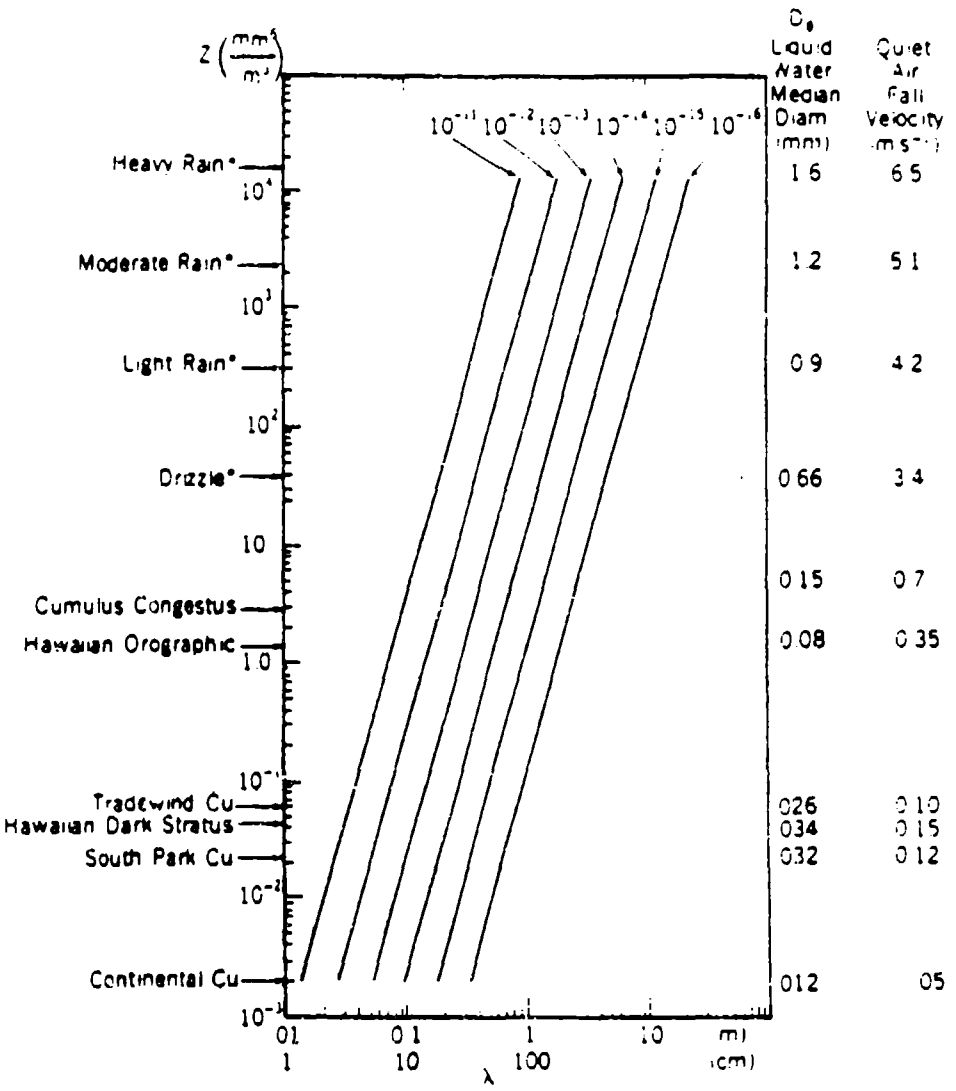

Figure 2.3: Plot of the structure constant under conditions for which scatter contributions from CAT and rain are expected to be equal [Gossard 1991]. Note that there is a required upward shift of 20 dB of the lines for the Prospect Hill-Mt Tug path.

2.6 Terrain Diffraction

Terrain diffraction plays an important role in transhorizon communication; it can even dominate the propagation process. Diffraction is most important when there is a common edge (such as a mountain peak) at the horizon, located at a very small angle to both the transmitter and receiver. Under the right conditions, it is possible that diffraction from several consecutive edges can dominate. Further, during times with unusually high refractive index variation, the radio horizon can be altered to a high degree so as to lower the angles with any distant edges. The Prospect Hill - Mt.Tug path is not expected to be significantly affected by this phenomena. The angles with the horizon are large (see footnote 5 for a listing of some important parameters), and even during 'super-refractivity' conditions, the waves must diffract around several edges. If diffraction occurs, there would be an increase of the power at the lowest height viewed by the system (corresponding to the shortest path). The Doppler shift associated with that power would also be very small. Neither of these characteristics are observed for any extended period of time on the path.

2.7 Aircraft Scatter

The most important anomalous form of scatter is from aircraft. Aircraft in the common volume on the Logan-Lebanon route are detected clearly by rapidly vanishing high-level fields along with a strong Doppler signature. By analyzing the data in terms of median, rather than mean, quantities, such 'shot noise' is expected to have minimal effect.

Chapter 3

The System and its Channel Characteristics

3.1 General

Troposcatter systems consist of a transmitter, the tropospheric scatter channel, and a receiver located beyond the radio horizon. A high-gain receiver antenna picks up the minute amount of transmitted energy scattered towards it from the atmosphere. The directions in which the antennas point most often define a great circle path (the shortest distance path). Both dish antennas are highly directive, such that a small 'common volume' is defined within their circular 3-dB beamwidths. Because of the low pointing of the antennas this common volume is roughly cylindrical along the great circle path. In actuality, although the beam leaving the transmitting antenna is of an in-phase cylindrical shape mimicking the antenna face, the beam spreads to a slightly conical shape as it is diffracted in the atmosphere. For our particular path the Ku-frequency (12.4-18 GHz, though nowadays said to lie in the J frequency range) volume ranged from 1.1 km in height above sea level, or 400 m above the mountain range below, to 2.3 km above sea level, and horizontally covered roughly 60 km, over a 161 km long path between Mt.Tug in Lebanon, NH, and Prospect Hill, Waltham, MA[4]. Since the common volume is closer to the Mt.Tug side and the antenna is for the Ku-band of the same size, this antenna defines the limits of the common volume. Simultaneous measurements were made at a lower, more commonly used frequency in the C-band (4-8 GHz, nowadays in the G-band), with larger antennas resulting in a smaller common volume ranging from 1.1 to 1.7 km in height and 40 km horizontally. (The beamwidth is given by $\theta = \alpha\lambda/D$, where α is a constant determined from considerations of antenna shape and pattern.) The axes of the antennas were pointed in the same directions so that the experiment is a multi-frequency measurement of roughly the same volume. Not only the scatterers within the volumes defined by the half-power points are important; energy retransmitted from the entire volume encapsulating these two transmit-receive points and beyond also reaches the receiver, albeit weighted by the antenna pattern. Of course, it is also affected by the aforementioned relations of the different scattering modes.

---

[4] Prospect Hill - Mt.Tug Bistatic Scatter System

Frequency	15.731 GHz	4.95 GHz
Distance	160.9 km	
Trans. Height	159.4 m	
Rec. Height	493.8 m	
Trans. Aperture	3 ft	29 ft
Trans. BW	26.49 mrad	8.36 mrad
Rec. Aperture	3 ft	10 ft
Rec. BW	26.49 mrad	25.25 mrad
Scattering Angle	35.23 mrad	34.61 mrad
Modulation	400 MBit/Sec	None
Carrier Power	225 W	30 W
Rec. Noise Level	-144 dBm	-147 dBm

Several factors other than the types of scattering described earlier affect the magnitude of the received power. These include the effects of the antenna pattern and the so-called 'aperture-to-medium' coupling as well as the path geometries.

The far-field antenna power density patterns are derived from the two-dimensional Fourier transforms of the field in the antenna aperture, for the case of the paraboloid reflectors resulting in (normalized, Gt will denote the magnitude along the axis):

$$f^2(\theta) = \left\{ \frac{8J_2[(\pi D\sin\theta)/\lambda]}{[(\pi D\sin\theta)/\lambda]^2} \right\}^2 \quad \begin{array}{l} ;\ \theta\text{=angular distance from beam axis} \\ ;\ D\text{=antenna diameter} \end{array} \tag{13}$$

The antenna pattern then consists of a main beam and a number of sidelobes well outside of the common volume. As a result, there is severe suppression of the power received from scatterers outside the common volume, though this suppression is not uniform. Nevertheless, it is conceivable that strong enough scatterers outside the common volume relative to scatterers within the common volume could significantly add to or even drown the effect of lesser scatterers inside the common volume.

Not only the strength of the scatterers but also the extent to which the scatterers fill the volume plays an important role. A large volume of scatterers will retransmit more energy toward the receiver than a lesser volume of otherwise equal scatterers.The far-field antenna gain function is given by:

$$G(\theta,\phi) = \frac{4\pi A_e(\theta,\phi)}{\lambda^2} \quad ;A_e = kAf^2(\theta) \cong .65Af^2(\theta) \quad ;A = \frac{\pi D^2}{4} \tag{14}$$

$$G(\theta,\phi) \cong \frac{6D^2 f^2(\theta)}{\lambda^2}$$

As antennas increase in size and thus decrease in beamwidth to achieve higher gains, there is therefore an accompanying reduction of the volume of scatterers. This so-called 'aperture to medium coupling loss' is accounted for by the standard references used for design [CCIR,1990, Rice et.al, Tech.Note101] by a simple formula relating the loss to the sum of the two antenna gains. This method lacks, however, in that it fails to address the question of beamfilling or geometric structure of turbulence or other scatterers. For instance, if it is found that, for a significant portion of the time, thin turbulent layers contained within a small portion of the common volume contribute to the received power, then it is reasonable to assume that use of an antenna with higher gain would not entail a coupling loss, since any reduction in the size of the common volume would still contain the scatterers. A correction factor taking into account layer thickness

is introduced in the models [Ottersten 1969, Crane 1980, p185], but encounters difficulties if the structure is more complex.

The coupling effect also plays an important role as to the relative importance of the scatterers inside and outside of the common volume. It might appear that for precipitation the antenna function and for turbulence the added angle dependence given in equation 9 might eliminate all impact of scatterers in a region outside the common volume. By virtue of its large volume, though, the summed effects from such a region may in fact be greater than from the common volume for the precipitation case. For instance, if there is rainfall directly above the transmitter, such as would enhance forward scatter at these frequencies, a very large angular region of the transmitting antenna beam would then be filled by scatterers, corresponding to a large volume covered by the receiver. The effect from the rain, even when absent from the common volume could thereby produce a signal even stronger than the norm.

3.2 Channel Characteristics

Along with the attenuation caused by absorption and scattering, the channel causes additional, time-variant, fading of the signal level. The fading is categorized into short-term and long-term fades. The rapid fading (on the order of seconds) is the result of random phase additions of the scatterers causing constructive and destructive interference. In accordance with theory, the power level is Rayleigh distributed with respect to the fast fade; since the large number of scatterers with uniformly distributed phases result in a gaussian process, the in-phase and quadrature components are normally distributed. The slow fade (on the order of tens of minutes), which is the result of changes in the weather, has been empirically determined to be log-normally distributed. In terms of the diurnal and seasonal changes there is, generally, an increase in the signal level during the warmer hours of the day, and during the warmer and more humid seasons. The design of troposcatter communications systems is based on estimates for channel conditions of the 'worst month' of the year; new statistical methods for doing so have recently been developed [Crane 1990].

Complete characterization of the channel requires not only knowledge of the signal level variation; the Doppler signature and the delay structure also provide crucial design parameters. Only when this characterization of the channel has been made complete can determination of the bandwidth, proper coding, and diversity schemes be made.

3.2.1 Delay Spread

The pathlength associated with each scatterer results in a particular time delay between the time of transmission and reception. The sum of the power received from all equidelay paths constitutes the total

power received at any one delay. Equidelay paths, usually expressed in nanoseconds, form near ellipsoids around the sites. Due to the angular dependence - from the antenna gain function and scattering cross Section definitions - and a greater amount of absorption, the contribution from scatterers at greater delays is sharply diminished. The exact shape of the power-vs-delay signature - the multi-path intensity profile - depends on the spatial distribution and nature of the scatterers. Figure 3.1 a-b shows two typical clear air profiles.

A quantitative measure of the delay signature, the delay spread of the signal, is defined as the distance (in nanoseconds) between the half-power points of the multipath intensity profile. This is a very important quantity since its reciprocal is a measure of the coherence bandwidth of the channel; the time dispersion of the signal indicates the potential intersymbol interference (ISI) on very rapid data streams.

For turbulent scatter, the main source of reradiated energy will derive from the common volume. It is possible, therefore, to consider the delays to represent different heights in that region. This is the direct result of the angular dependence of the scattered power given in equation 9. Turbulence-scattered power received at any one delay is the sum of powers reradiated from all points on a corresponding spheroidal shell; the planes are defined by the interSection of ellipsoids (associated with particular delays) and the common volume. Within the common volume, horizontal deviation from the center along the ellipsoid causes little weighting by the relation given in eqn. 9. Vertical deviation, however, leads to significant change in the scattering angle, even within the common volume . For a uniformly turbulent-scatterer filled volume, computer models show, the received power theoretically yields a vertical profile roughly like that of a rapidly rising exponential, followed by a slower exponential decay, see Figures 3.2a) and b). Because of this general shape, the delay spread is expected to be small during clear air conditions. During ducting, or conditions where thin, high-intensity, layers dominate the scattering process, the spread will be minimal.

The multi-path intensity profile aids also in discerning the mode of operation of the channel. Clearly, if there is only one layer causing specular reflection, the delay profile would show a narrow spike, characterized by very slow motion, randomly positioned in the common volume. No such spikes exist. If, however, the volume consists of many, thinly layered, reflecting surfaces, it could be very difficult to distinguish them from a scattering process caused by turbulent motion by simply looking at the multi-path intensity profile.

It is not possible with certainty to make any height-to-delay association in the case of rain, since the angular dependence of Equation 9 is lacking in the cross Section equation for rain (Equation 11). It is at times possible, of course, that this association is in fact accurate. It is evident from Figure 2.3 that very clear conditions are necessary for a completely accurate vertical positioning of the scatterers by inference

from the delay profile. The delay spread, therefore, is very large during precipitation. In fact, under the right conditions, the delay signature can be virtually flat, even when the received power is very high. Computer modelling shows that a locally limited volume of rain, positioned at different Sections across the region, results in a variation of received power of less than 10 dB. There are some indications by which it could still be possible to estimate where the rain is located, if it is locally limited at all. For instance, rain directly above the transmitter would be accompanied by substantial increase in the variance.

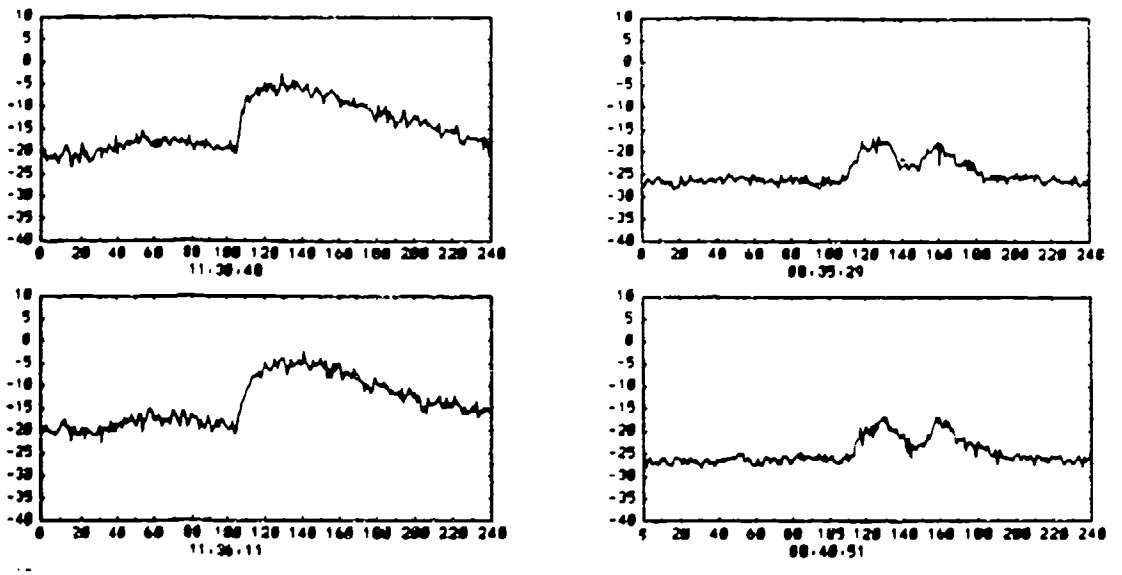

a) b)

Figure 3.1: Power vs. delay signatures during a) clear air, uniformly filled common volume, b) clear air, layering structure.

In order to find the power associated with each delay it is necessary to first establish a relative time reference. To aid in this, a 1023 bit long phase-modulated pseudo-random noise code generator was applied to the Ku band transmission. An identical device , switching the phase of a correlating signal at the same rate, was applied at the receiver end. The power received, when the transmitted signal is at a delay such that the incoming and correlating signals are in phase, is 1023 times the power at an out-of-phase delay. The correlating device is then clocked to skip one bit to form the next 1023 bit long position, and the power at another delay can be recorded. The device is called a RAKE correlator. The envelope of the power as a function of delay yields the multipath intensity profile. Since the rate of the PRN code is 400 MBit/sec, the time-resolution of the device is 2.5 ns, yielding in the clear-air case a spatial resolution of roughly 30 m. This is a much greater resolution of low tropospheric RADAR data than has been achieved before.

Resolution volumes of similar size have been achieved using RADAR [e.g. Woodman 1980] but not at such low altitudes.

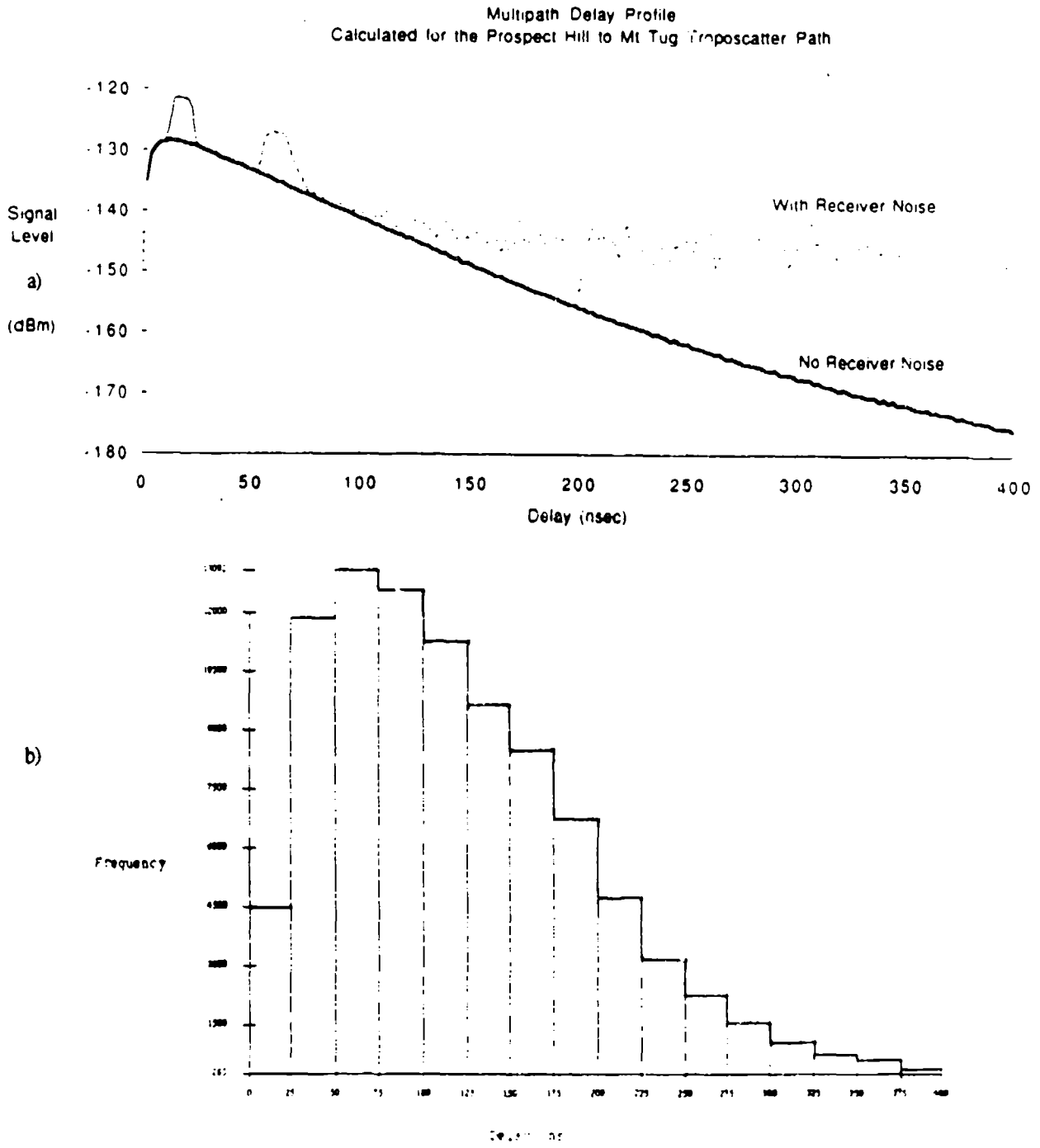

Figure 3.2: a) Theoretical plot of delay signature of the signal level, showing also the effect of two strongly turbulent, 100m thick, layers. b) Histogram of the delay signature summed over a week's observations, in terms of number of measurements above the 3-dB points, implying a uniform distribution of the thin layers with height.

While the delay spread limits the uncoded bandwidth of the channel as 1/(delay spread), coding and various demodulation schemes can improve this ratio, subject to the limits of the signal-to-noise ratio. The RAKE correlator is in fact the optimum receiver for processing the wide-band signal (i.e. where bandwidth >> information rate). Without coding a typical delay spread of 150 ns would allow for a bandwidth of about 7 MHz; with the RAKE receiver the theoretically achievable bandwidth equals the bit resolution, i.e. the code rate or 400 MBit/sec.

3.2.2 The RADAR Equation

Power reception is straight-forward for the volume forward scatter model, once the scattering cross Section has been determined. The power density incident on the scatterer is:

$$S_i = \frac{P_t G_t(\theta,\phi)}{4\pi r_x^2} \quad ;x = \text{position of scatterer relative to transmitter}$$

The power radiated by the scatterer toward the receiver is:

$$S_r = \frac{S_i \eta(\theta,\phi)}{4\pi r_\rho^2} \quad ;\rho = \text{position of receiver relative to scatterer}$$

The total power at the receiver is therefore:

$$P_r = S_r A_e = \frac{\lambda^2}{4\pi} G_r(\theta,\phi)$$

Taking into account line losses and the specific attenuation losses from the atmosphere the final equation then becomes:

$$\frac{P_r}{P_t} = \frac{\lambda^2}{(4\pi)^3} g_t g_r l_t l_r \int_{Vol} f_t^2(\theta) f_r^2(\theta) \eta(x) \frac{dx}{r_t^2 r_\rho^2} 10^{-(1/10)\left\{\int_0^x \alpha ds + \int_x^d \alpha ds\right\}} \qquad (15)$$

where d is the location of the receiver relative to the transmitter [Crane 1981]. The scattering cross Sections are as given in chapter 2. This equation can be fitted to yield the power received at any delay, the total power etc, by simply changing the values (i.e. Cn for clear air) in the scattering cross Section. Such

changes effectively simulate different atmospheric conditions. By doing so, layered turbulence structures on top of weak background turbulence have been modeled, as have different rain configurations.

3.2.3 Mean Doppler Frequency of the Doppler Spread

The Doppler frequency shift in the received signal was measured at each delay as well as the power. It is estimated from the in-phase and quadrature components of the received signal by knowing the frequency which caused the shift. The in-phase and quadrature components of the signal are created for this express purpose. The Doppler roughly measures the component of motion of the scatterers along the vertical axis; it is estimated by the pulse-pair algorithm. The mean Doppler is simply the power-weighted average of the Doppler shift of the entire volume of scatterers. Any motion of a scatterer - other than along the line of the great circle path (or, rather, other than along the equidelay planes) - will in effect either lengthen or shorten the path of the scattererd energy. The motion will cause a negative or a positive Doppler shift, respectively, of the wave. For a symmetric path, the horizontal components of the scatterers will cancel each other out; the motion away from and toward the center carry equal weighting from the antenna functions and the scattering cross Sections, and in equal amounts lengthen and shorten the path of the wave. (This assumes that the horizontal wind is uniform over the common volume, a reasonable assumption.) Vertical motion, on the other hand, does not cancel out. Downward motion, for instance, always has a component that shortens the path, none that lengthen it. A clearly positive Doppler is therefore detected during precipitation.

Small amounts of rain may not have sufficient downward motion over the entire volume to cause a large Doppler shift. Therefore it is theoretically possible to have rain on the path, but for the data to be considered clear air data. During clear air, and possibly during some cases of precipitation, the Doppler at different delays represents the motion of the scatterers at different heights. It is possible to observe the process of various meteorological phenomena using these signatures, such as slowly falling snow melting to form rapidly falling rain.

The Doppler spread is a measure of the rapidity of fading on the path. It is defined as the distance between the half-power points on the power spectrum. Like the delay spread, this is an important measure. It is crucial in determining the keying distances for frequency and phase modulation schemes. Since the delay spread is much smaller than the coherence time (1/(Doppler spread)), the fading is always slow compared to the signal rate. The signal transmission will therefore be frequency-nonselective. It is important to understand that the Doppler spread is the frequency-spread at any one delay (usually the one associated with the greatest power), and that the Doppler shift is the shift in the spectrum at any one delay. This is in

contrast to the mean Doppler, which is an average measure over the entire volume. Figure 3.3 shows a typical spectrum.

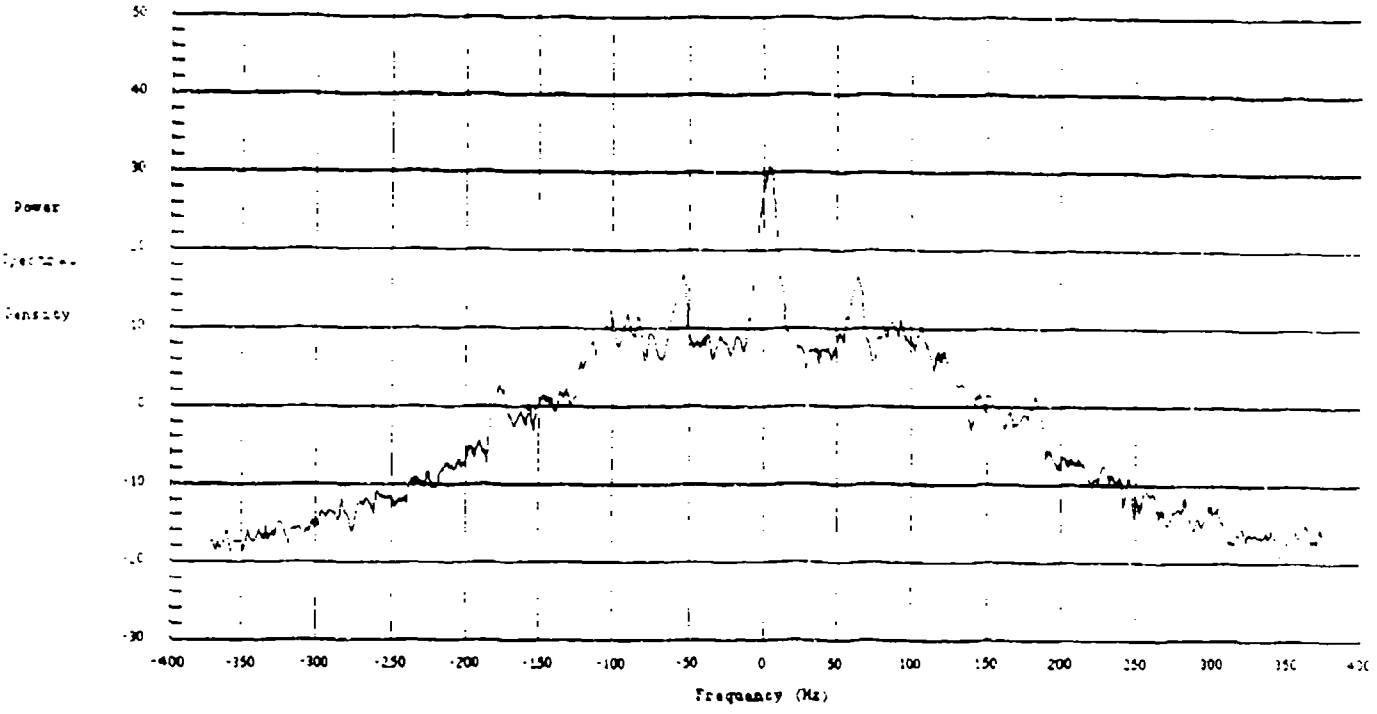

Figure 3.3: a) frequency spectra at the maximum power delay tap, showing Doppler shift and spread.

There are several factors that together cause the Doppler spread. There is a component from equation 3, since the total velocity variance is an integral of the spectrum E(k). The Doppler spread would be directly proportional to the turbulent dissipation rate, if this was the only component. Unfortunately, however, there is additional broadening of the spectrum: by the volume averaging of the scatterer contributions within any one delay shell, by the time averaging of several measurements, and by the wind shear. While it may be possible to separate out the variance due to turbulent activity in some RADAR measurements, this is not possible on our path since the wind shear component is by far the dominating mode. Even in uniform wind with no shear, there would be a range of wind components in the direction toward and away from the center of the path.

3.3 Particulars of the Prospect Hill - Mt.Tug Path

There are practical problems associated with installing a troposcatter system. These have resulted in alterations of the channel characteristics described above, unique to the Mt.Tug - Prospect Hill path. Most significant among these is the offset, or misalignment, of the antennas. It is the result of the practical 'definition' of the great circle path when using less sophisticated equipment.

In practice, aligning the antennas is done by scanning the horizon with the receiver antenna until the position corresponding to the highest power is found. This is a time-average operation, and is subject to change with different weather conditions. Furthermore, in the mountainous terrain between Boston and Lebanon, irregularities in the local horizons of the antennas will offset even the 'true' maximum power position. The lower picture in Figure 3.4 shows how the antennas could most closely 'match' if the receiver was pointed at a valley, instead of along the great circle path - where it would point at an intervening mountain.

This misalignment or irregularity in the local horizon plays an important role in the interpretation of the data. As shown in the Figure, even if there is only a uniform horizontal wind, the components of the wind will no longer cancel out. As shown, westerly and easterly winds yield negative and positive Doppler signatures, respectively. The upper picture in Figure 3.4 shows that, even if the antennas are aligned, intervening mountains can cause such Doppler shifts.

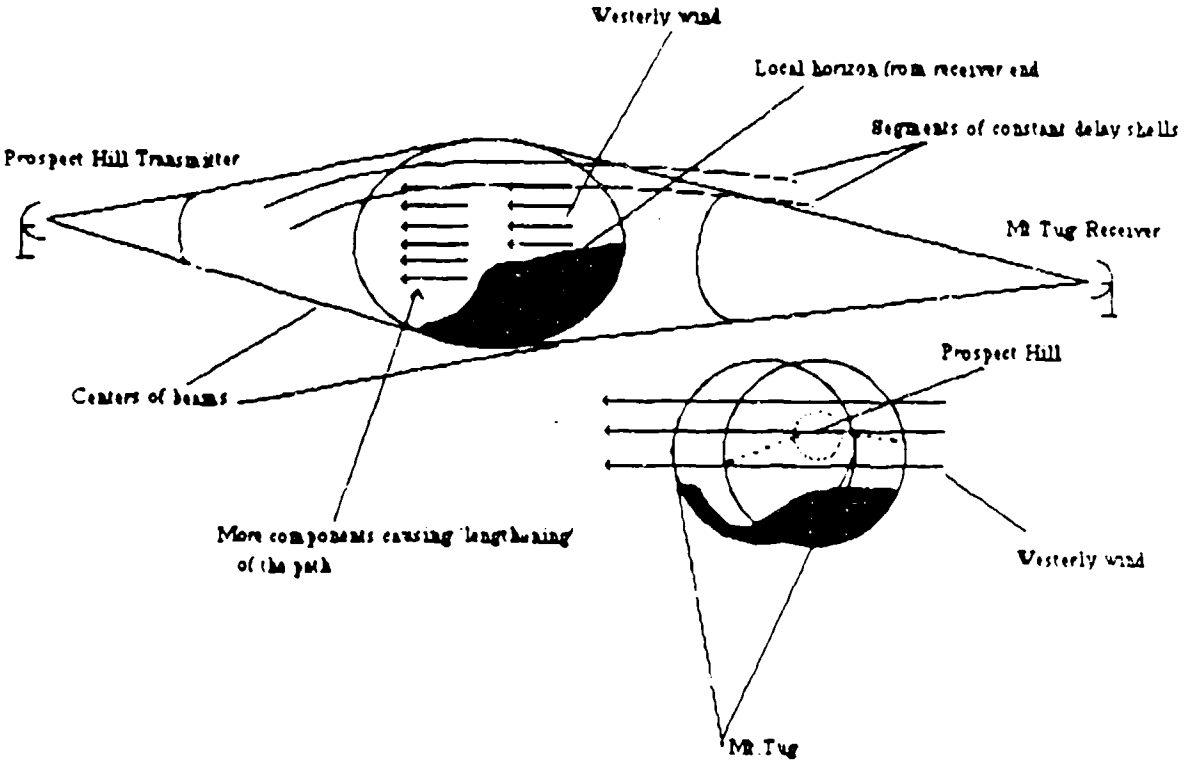

Figure 3.4: The local horizon and/or alignment offset of the antennae, causing a negative Doppler signature during westerly winds.

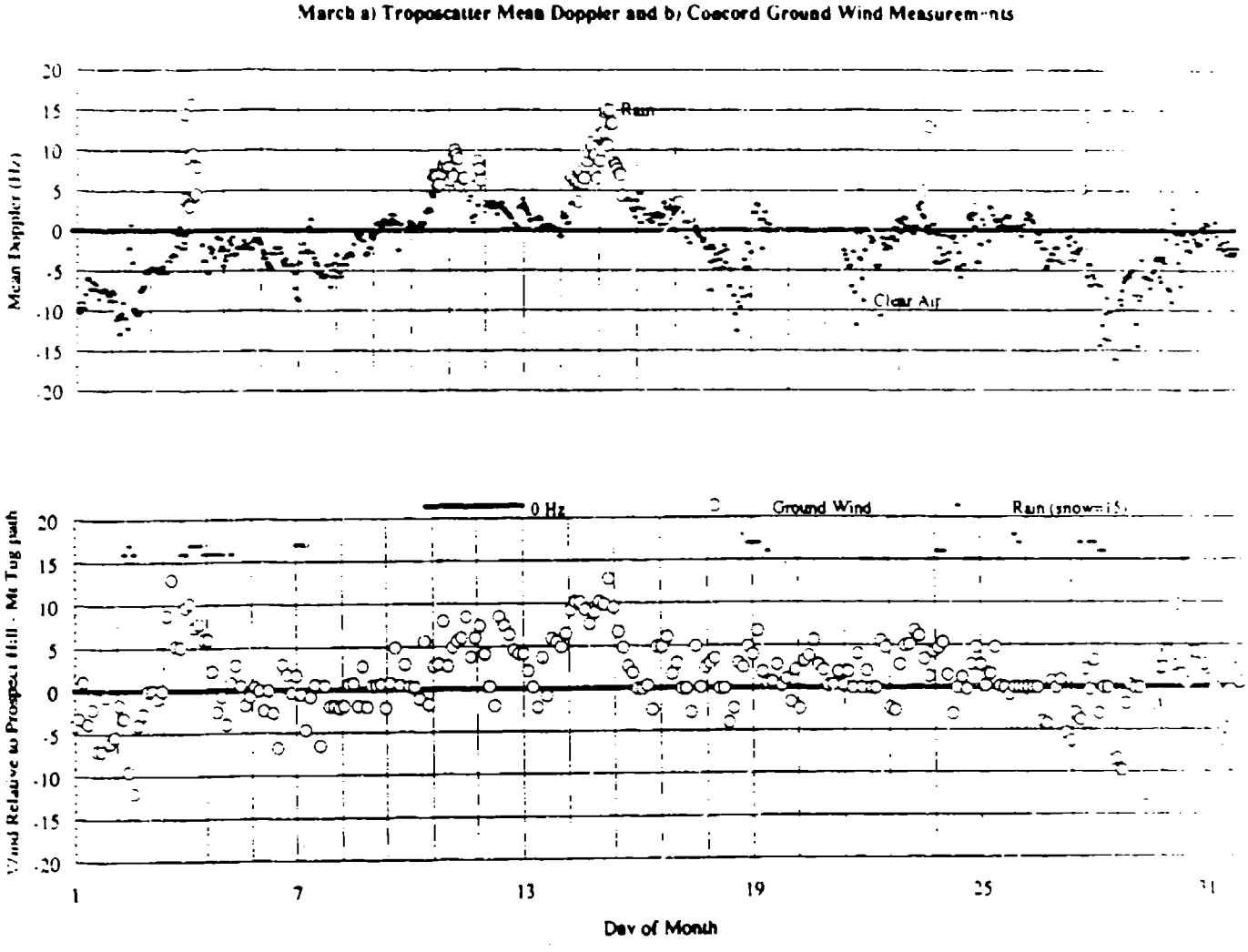

Figure 3.5: March troposcatter mean Doppler shift measurements of lower troposphere and Concord ground wind measurements

The fact that the component in the vertical direction due to the horizontal wind is small, is counteracted by its greater absolute value; vertical movement is usually on the order of cm/sec, but horizontal winds measured several m/s. It is quite conceivable that a westerly wind under just the right circumstances could completely cancel out the effects of rain on the Doppler signature, and eliminate any detection of rain on the path. Figure 3.5 shows the Doppler (hourly median values) signature for the month of March. A second plot shows an estimate of the impact wind might have, from ground measurements of the wind at Concord, NH [NOAA Mar. 1991]. The slow, more or less continuous, changes of the Doppler due to changes in the regional wind, are interspersed with positive rain signatures showing sudden increase in the Doppler. Correlation between the graphs is expected to be very rough since the Concord reading is a point measurement at a different altitude. Nevertheless, the impact of the wind is clearly important, especially during strong winds.

More precise interpretation of the data may be achieved by comparison of the data with MIT RADAR measurements made along part of the Prospect Hill - Mt.Tug path. These are only made during conditions of rain, however. It may be necessary to adjust all the data, once a determination of the impact of the misalignment has been made - including the data from previous years - if the impact is considered significant.

Another minor detail that should be clarified is that the PRN code generator operated at less than an optimum level. Rather than a 30 dB difference (=1023) between signal and noise, it has in reality been approximately 18 dB. (This is the case because of hardware inaccuracies in the state-of-the-art PRN code generators operating at extremely high rates.) This reduces the sensitivity of the system, and more of the delay spread measurements during low signal reception were discarded. (When the signal is very low, the noise floor of the PRN generator would be of the same level as the signal, yielding a flat response - indicating an infinite delay spread.)

Chapter 4
Data Collection and Processing Procedure

4.1 General

After the initial hardware processing, the data were collected on a personal computer system on Mt.Tug. It was then transferred to the Thayer "T1" VAX where it was permanently stored on magnetic tapes. Most of the subsequent processing was done on that machine; some of the final arrangement and plotting of the data was then done on the Northstar system.

As is common practice for troposcatter systems, the data were analysed in terms of median values. It is expected that this will remove statistical anomalities similar to shot noise, such as occasional scatter from aircraft - see Figure 4.1 for a timeseries of the mean Doppler shift, showing both aircraft scatter and a more extended period of rain. Averaging processes are also expected to efficiently remove the Rayleigh fast fading process effects. With large amounts of data, the statistics of the median value should approach that of the mean of the process.

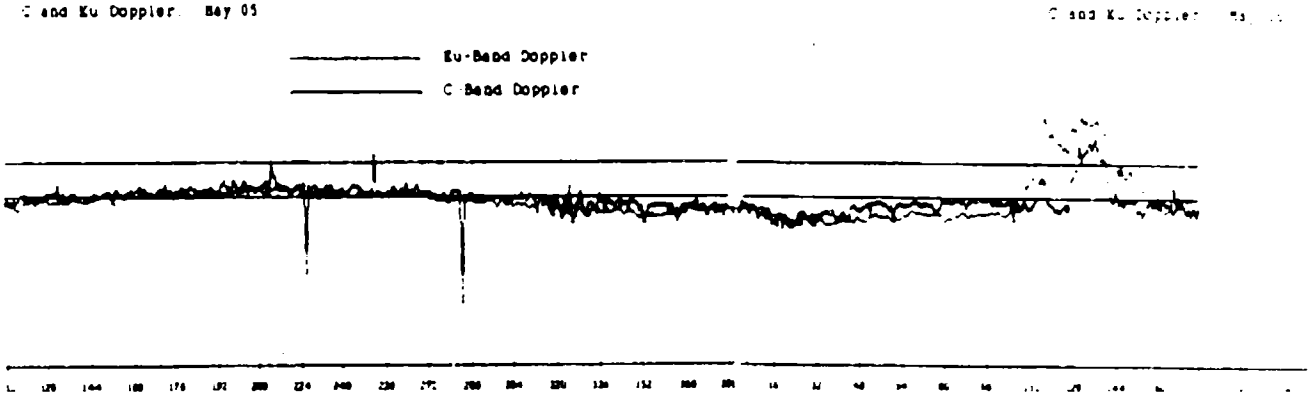

Figure 4.1: Timeseries of C and Ku band mean Doppler shifts. Note the close agreement at the two frequencies, except during rain, where the Ku band Doppler is higher. Each mark numbers the 16 measurements made during an hour.

4.2 Data Collection

The data collection consisted, mainly, of recording the in-phase (i) and quadrature (q) components of the power output of a 120 Hz low pass filter, and from them calculating the total power and Doppler frequency shift. This was first done at every 'tap' of the 1023 long PRN code. Once this had been accomplished, a

'window' of 241 taps length was centered around the tap with the maximum power received. To quicken the process, subsequent recording of the data were only made on the window. This length was considered sufficient to aquire an accurate estimate of the delay profile. Due to the relative, unpredictable, drift of the codes (caused by relative drift of the 5 MHz Cesium beam frequency standards), the window was re-centered once every hour. Thus the power for the entire 1023 taps code was recorded at the beginning of the hour, followed by sixteen 241 tap windows of recorded power and Doppler. Averaging of the 'i' and 'q' components was also done; 60 measurements of each were averaged, sampled at a rate of 250 Hz. At the end of the hour data were recorded and processed for a spectrum; the processing was done on site to reduce data. The Doppler and power measurements were calculated on site from the raw data for the same reason. The data for the spectra were collected at the 'maximum power' tap. The data from the spectra yield independent estimates of the Doppler spread and the Doppler offset. Note, however, that these spectral estimates are relevant to one tap only, not to the entire volume.

There were few serious problems with the data collection other than what was caused by the relative frequency drift. A few, easily recognized, isolated incidents did occur when faults in the code clocking at the receiver end, caused the PRN generator to skip a random number of taps. This had been a considerable problem during the fall, but was fixed while the transmitter was down during that time.

4.3 Data Processing

The hourly sixteen 241 taps long windows formed the basis for the statistical estimates of power, Doppler and delay spread. The total power is the result of summing the power (subtracting the noise power) in the window. The mean Doppler is the power-weighted average of the Doppler at each tap. An estimate for the '2σ' delay spread was initially based on the variance of the power with regard to the taps. This was soon found to be insuffiently accurate (because of the large size of the window) and the distance between the half-power points were found exactly. Finding the peak power (which was then halved before finding the 'crossing points') involved some averaging. The estimate for the delay spread is therefore a slightly conservative one. No estimate for the delay spread was made when the power was too low relative to the noise power.

The noise power was initially estimated at the beginning of every hour; it is the lowest short (5 taps) segment of powers found when scanning all the taps. This lowest power is, generally, located far away from the region containing the signal. This same criterion was used subsequently for the smaller windows. For a delay profile with a large spread, however, no distancing from the region containing the signal is possible. For that reason, if the noise power found in the 1023 long code sequence was lower than that found in any tap in the window, then the noise power from the long sequence was substituted for the one

found in the window. This reveals an inherent weakness in the results, albeit small, since channel characteristics can change considerably over the span of tens of minutes.

Finding the total power and mean Doppler required finding the 'onset' tap, that is, the tap which corresponds to the shortest path possible across the mountains. Furthermore, no meteorological processes can be studied without an exact knowledge of the location of the onset tap. Finding the onset is difficult only because of the unpredictable nature of the relative frequency drift. After trying various algorithms for finding the onset, a method whereby the user inputs the hourly onset peaks was determined to be the only practical solution. The method consists of the following. The first delay profile 'window' of every hour in any given day is plotted, as in Figure 3.1. The onset tap is guessed at and entered into the computer. The processing program interpolates between the points to find the onset taps for the remaining 15 windows for that hour. It does so by using the relevant maximum power taps and the user-provided onset taps.

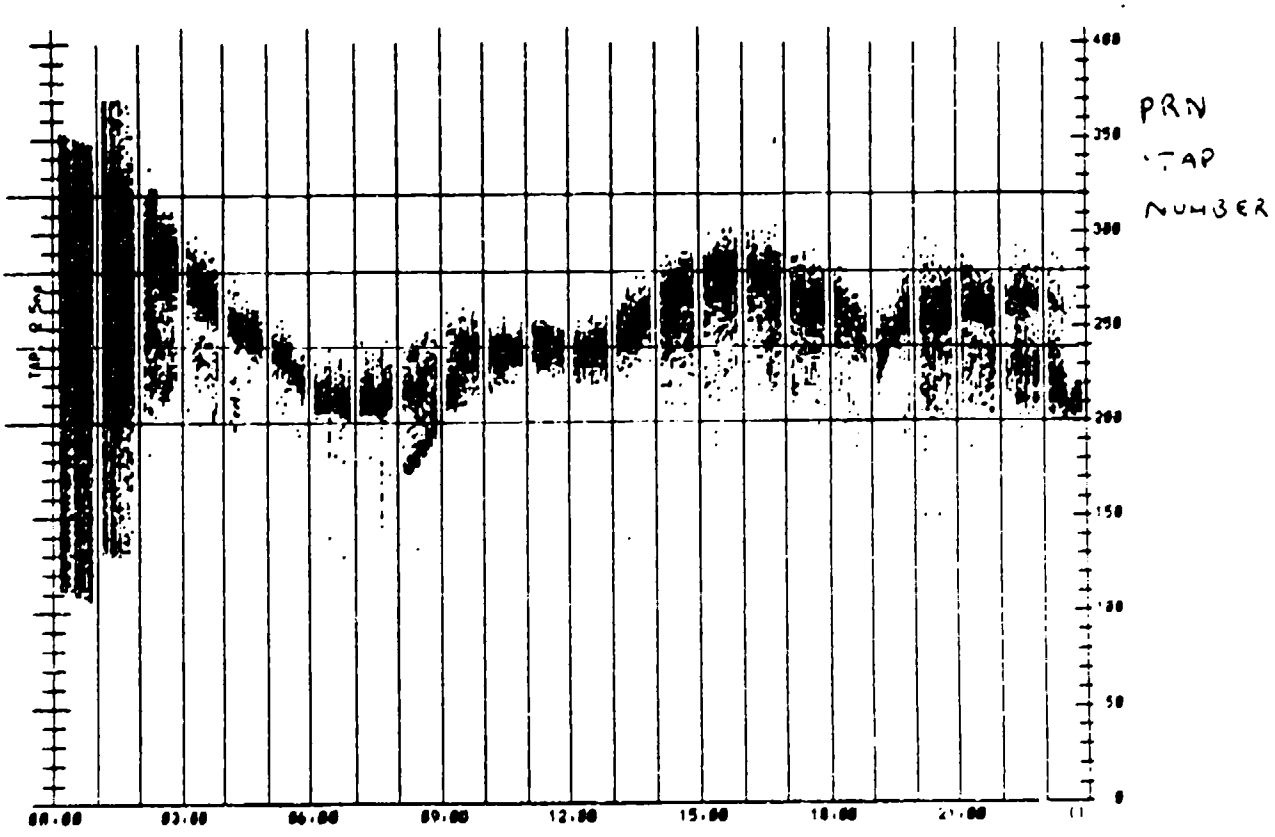

Figure 4.2: Delay profile generated by plotting the points above the 3-dB power levels.

For as short a time-span as an hour, the relative drift was assumed, for simplicity, to be linear. The computer then plots a picture for the whole day, showing all the points of the delay profile above the 3-dB

points, as shown in Figure 4.2. In other words, 24 (hours) times 16 delay profiles are plotted, effectively showing motion and thickness of significant events. Note that there is no absolute power reference in this plot; at any one time, points above the 3-dB point refer to the maximum found in that particular delay profile. If the transitions on this graph are not smooth, new possible onset taps are guessed at, and a new graph generated. This process is iterated until a smooth plot has been generated. It is this process, then, that evaluates the validity of the guesses of the onset. Once this stage has been accomplished can the onset taps be used in the other algorithms. Exact knowledge of the onset is especially important for the delay spread estimate, which otherwise would be tainted by side-band and code repetition "noise".

4.4 Data Classification

For ease in comparing the data with previous measurements, the same classifications and criteria were used for the wide band system; any further correction of the data other than what is presented here, if deemed necessary, will be made in conjunction with corrections of all previous data.

Once the median values for each hour had been found, the data were classified into three categories according to the mode of propagation:

1) Turbulent volume scatter. This was the default mode, considered clear air.
2) Rain scatter. Since the Ku band is more sensitive to rain, it was used to detect it. If the median level was above +2.5 Hz, and the maximum above +6 Hz, that hour was designated a rain period.
3) Ducting. This was only detected when the C band was in use, because of its higher sensitivity to this phenomena. It was identified by the presence of very strong signals, and near-zero Doppler shifts.

The data were then Sectioned according to hour of the day, the quarter day interval (morning: 04:00-10:00, afternoon: 10:00-16:00, evening: 16:00-22:00, night: 22:00-04:00), and according to season (Winter: January-February, Spring: March-May, Summer: June). Note that EST was used throughout the experiment. Further, variations in the data about their median values were recorded as the number of hours in strong attenuation (>10 dB less than the median signal level), attenuation (5-10 dB less than the median), normal, amplification (5-10 dB stronger signal than the median), and strong amplification (>10 dB above the median level) conditions. During times when both the C and Ku band data were available, a 5x5 matrix for these categories were created for comparison of the two bands during different propagation modes. Cumulative distributions were created from the data, for investigation of their statistical behaviour. The next chapter details these results and plots comparisons of the different quantities when appropriate, along with a discussion and conclusion of the same.

Chapter 5
Results and Analysis

5.1 Introduction

Figures 5.1 through 5.6 show an example of the 'raw' median value time series, for the month of June. The distributions of the measurements shown is typical for all the months observed. Atypical, however, is the extended period of low signal received during the 15th to 17th of June - most clearly seen in the Ku band data, Figure 5.1 - and in the extended period of ducting during the 19th to 20th of June. Since this may be atypical behaviour for the channel, and because of the limited amount of data (this month constitutes the entire summer data set), the variation of the signal behaviour for this month is expected to be higher than normal.

Rain is identified on the path by its high Doppler shift in the Ku band, Figure 5.3. Occasionally, it can also be discerned by high Doppler shift in the C band. This may occur, as it did during the 15th of June, when the Ku band records such a low signal that it loses the signal on the 1023 PRN code. This occurs when the signal is not detectable, by a simple search, above the self-noise of the PRN generator. When it happens - unusual for extended time periods - no accurate Doppler estimate in the Ku band can be made. (In fact, the pulse-pair algorithm provides such a sensitive measure of the Doppler shift that, if the appropriate region of the PRN code could be identified, a good estimate could often be achieved even with the signal hidden in the noise.) This represents a slight change in the detection scheme from previous years, necessary because of different noise levels of the different systems.

Figure 5.3 also reveals a flaw in the algorithms that determine whether or not rain occurs on the path. The flaw originates in the antenna alignment offset described in Section 3.3, during easterly winds. Isolated, large, positive Doppler shifts are indicative of periods of rain, as during the 12th of June. There are, unfortunately, times with slow, smooth, changes in the Doppler shifts - corresponding to the slow changes in wind direction and speed (see Section 3.3) - causing Doppler shifts above the 'rain detection' threshold. An example can be seen during the 18th of June. Even with the adjustments of the algorithms that have been used (involving the maximum Doppler shifts for the hour - a median of the 16 measurements must be above 2.5 Hz and the maximum for that hour above 6 Hz for the hour to be considered a rain period), these periods, falsely identified as rain periods, could in the worst case constitute as much as 10-20% of the entire rain data base. Conversely, a strong westerly wind can counteract and overcome positive rain Doppler. During such times, rainy conditions would be considered clear air conditions. This probably occurs less often, but an accurate measure is difficult to obtain. The detection schemes in this thesis are, nonetheless, exactly as during previous years, except for the slight alteration described above. This provides continuity, and hence a basis for comparison.

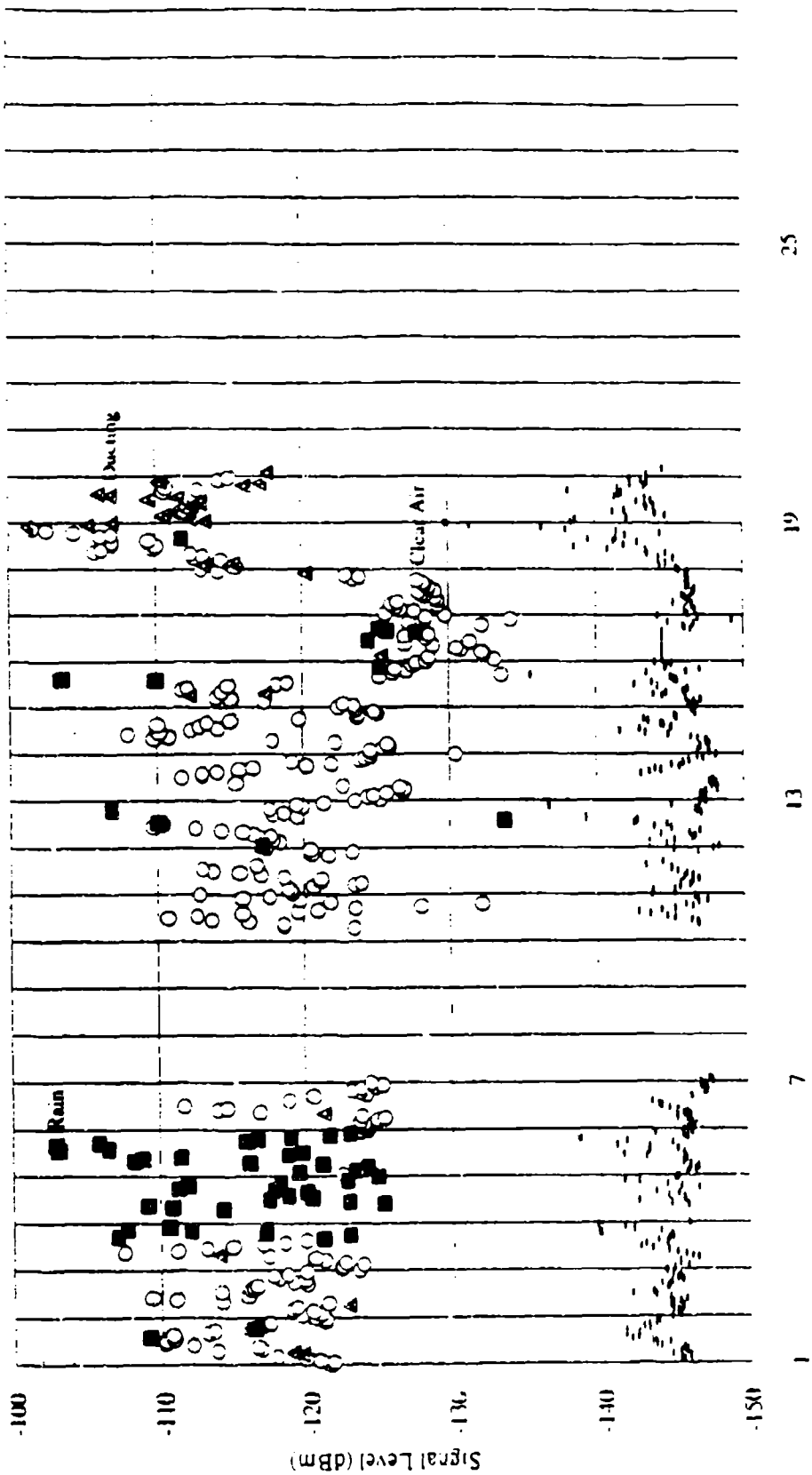

Figure 5.1 Ku band received power levels for the month of June, 1991.

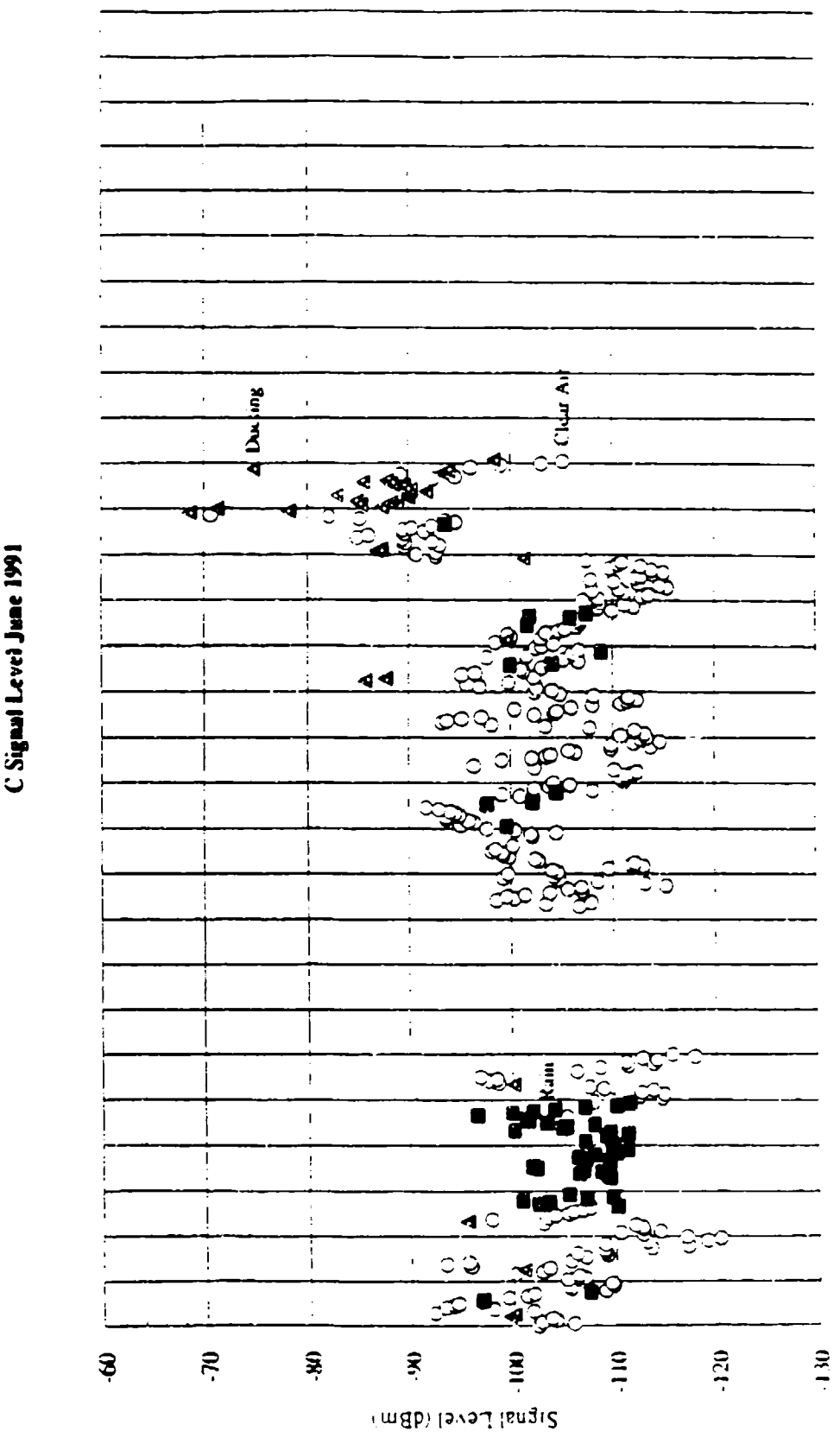

Figure 5.2: C band received power levels for the month of June, 1991.

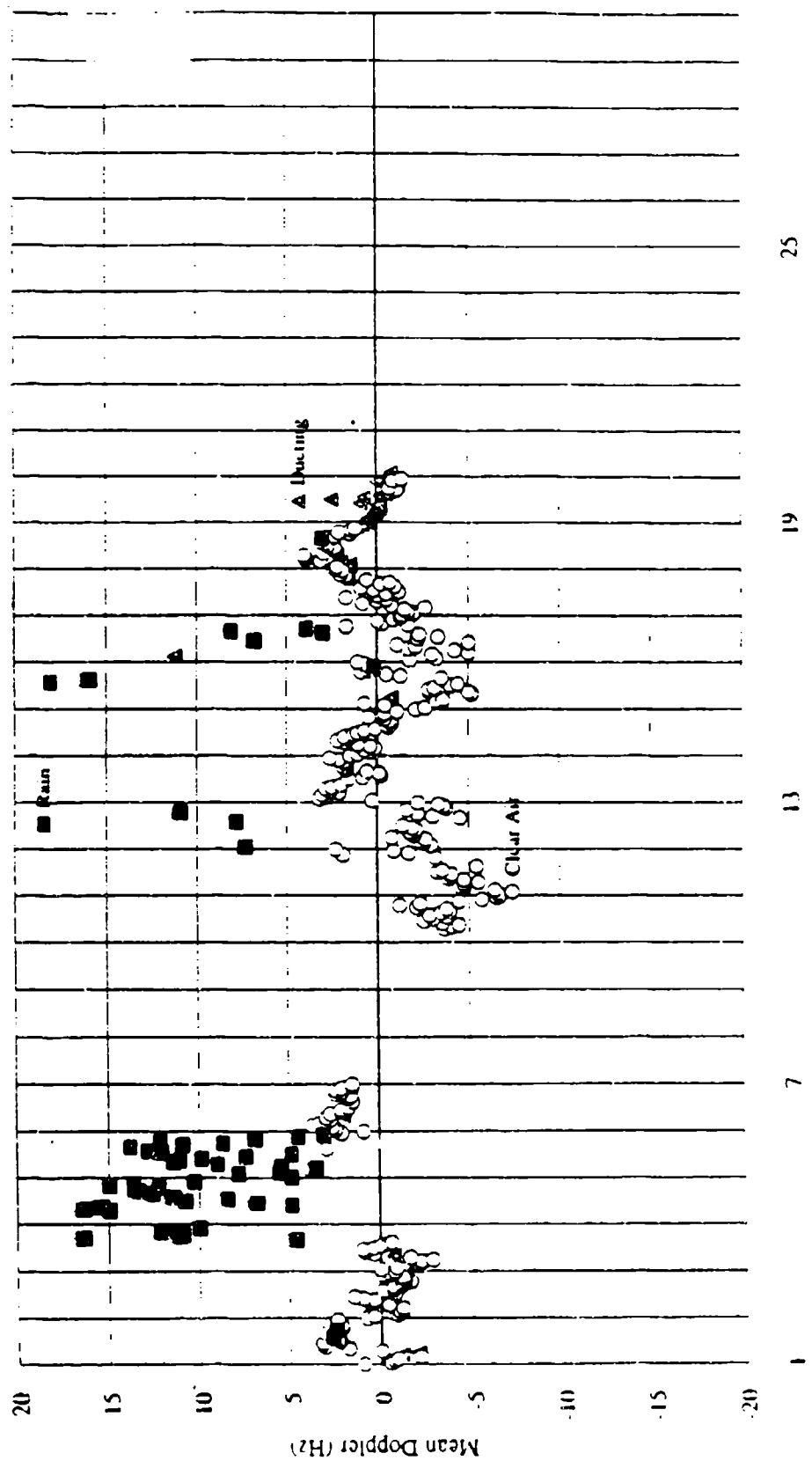

Figure 3.3 Ku band mean Doppler frequency shift for the month of June, 1991

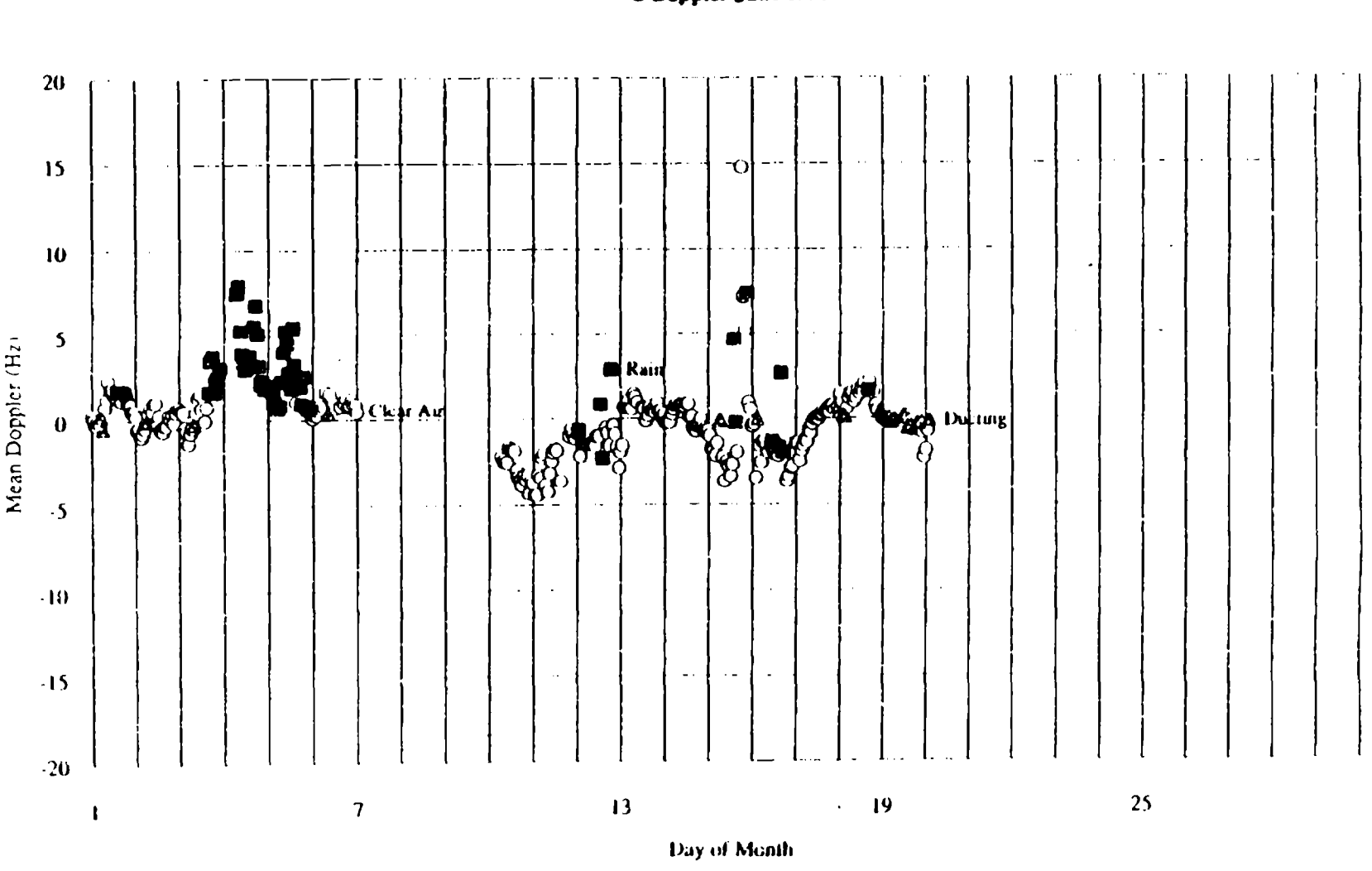

Figure 5.4. C band mean Doppler frequency shift for the month of June, 1991.

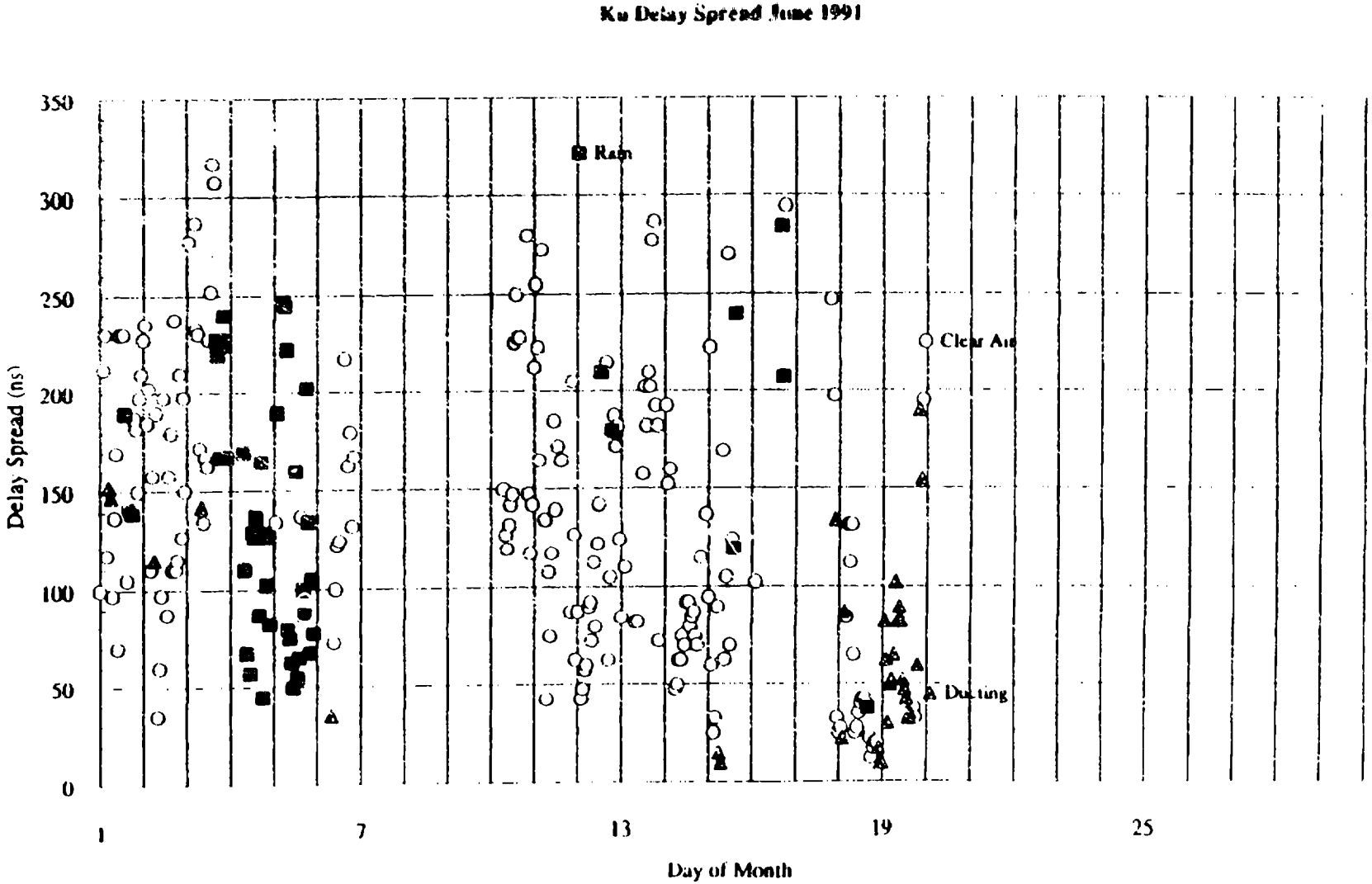

Figure 5.5: Ku band delay spread for the month of June, 1991.

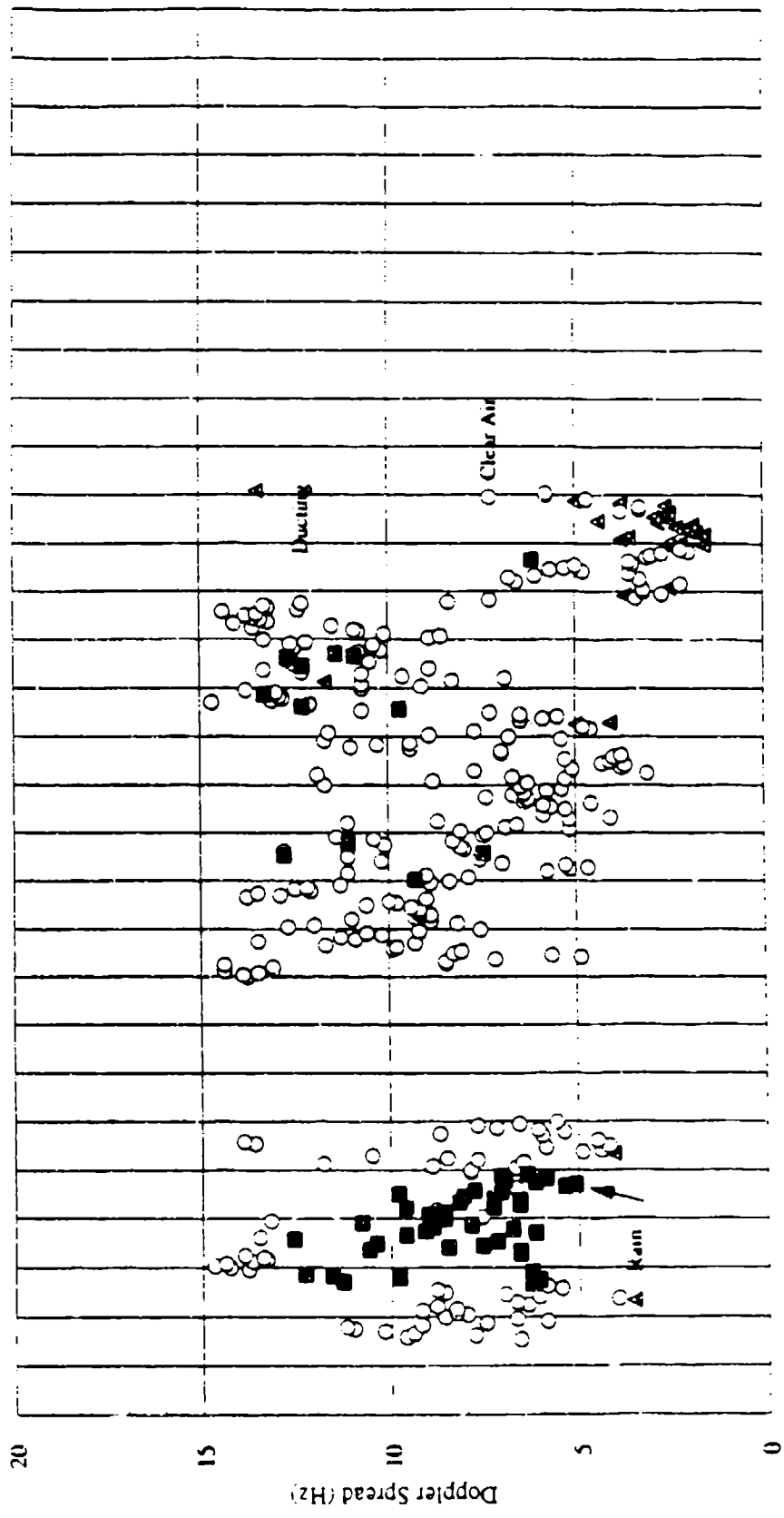

Figure 5.6 Ku band Doppler spread for the month of June, 1991.

Previous estimates of the multipath delay spread showed much less sensitivity than the present estimate. The range of the previous estimate had been contained within the 100 to 200 nanosecond lines for almost all the measurements. Figure 5.5 shows how drastically the estimate has improved, although there is little change in the median of median values. The estimate of the variance about that median will improve, indicated by its increase from previous years. This will represent a significant increase in the percentage of time that the available bandwidth is expected to be lowered (and raised, although that is of less concern), as compared to previous estimates. This is because there are phenomena (ducting, thin layer scattering dominance) during which the real multipath delay spread is small. However, the less sensitive 'two-sigma' delay spread estimate used previously would not reveal such sharply contoured signatures. Note that several hours have been deleted from the multipath plot. This is done when the received signal levels are too low for an accurate measure of the spread to be obtained. This occured, for instance, during the 15th to the 17th of June.

Ducting on the path is discerned best by the C band measurements. A low C band Doppler median measurement and an unusually high signal level median (also as compared with the Ku band signal level) qualifies the hour considered for the ducting category.

5.2 Period of Study

Table 5.1 details the number of hours of data that were used in the statistical summaries of this chapter. Due to a break down of the transmitter in the fall of '90, no data were recorded until the beginning of January '91. During the first few days of transmission, a permanent collection scheme was developed. Data from those days will not be included in the statistical study since inconsistencies would result. Subsequent collection was virtually uninterrupted through the middle of April. At this time the local cable TV company - whose antennas are located at the receiver site - claimed that the project caused interference with several TV channels, wherefore its operation was temporarily shut down. The complaint had followed soon after the installation of an additional amplifying stage in the Ku band front end. (This had been done in preparation for the multi-frequency experiment.) The interference seemed intermittent, probably dependent on the transmission conditions of the TV channel. Various attempts to reduce the interference were made, until the addition of a narrowband filter finally cleared any noticeable effects on the TV stations. For this reason, data collection was intermittent in late April and during May. During June, more hardware problems with the transmitter caused loss of data during a few days. A final transmitter break down on June 21st marks the end of the data collection campaign.

Ku band:	Winter 91	Spring 91	Summer 91	Total number of hours
Clear Air	796	1164	270	2230
Rain	4	134	56	194
Ducting		10	33	43
Total	800	1308	359	2467

C band:	Winter 91	Spring 91	Summer 91	Total number of hours
Clear Air		244	270	514
Rain		29	56	85
Ducting		10	33	43
Total		283	359	642

Table 5.1: Summary of Observation Period (Hours)

5.3 Comparison of C-band and Ku-band Signal Levels

Since the C band was used as a reference standard for the Ku band, it is important to distinguish dissimilar behaviour of the signals. To this end, the 5x5 signal level matrices in table 5.2 are listed, for the three modes of propagation. In this case, it was convenient to combine the data from May and June - the only months when both bands were in operation - rather than separate the data into the seasons. This is also an appropriate step in order to increase the data base for the comparison, especially so since the June data shows unusually high meteorological activity (see Section 5.1). The categories of the attenuated and amplified states are determined by comparison of the data with the median levels. For Table 5.2, the medians used are those of the corresponding modes of propagation. In the Figure 5.7 - 5.9 plots, the median level shown is that of the clear air observations.

Table 5.2: Relative Behaviour of Ku and C band Signals

C band:	S. Atten.	Atten.	Normal	Ampl.	S. Ampl.
Ku band					
[5]S. Atten.	0	5	11	7	0
Atten.	2	30	46	2	0
Norm.	17	54	199	51	14
Ampl.	0	1	19	17	24
S. Amp.	0	0	5	5	10

Total number of hours: 514

Ku band median value: -118.7 dBm; C band median value: -106.3 dBm

a) Clear Air

5 S. Atten: Strongly attenuated relative to the normal medial signal level (more than by 10 dB), atten: attenuated (5 to 10 dB), Amp: amplified (5 to 10 dB), and S.Amp: strongly amplified (more than 10 dB).

C band:	S. Atten.	Atten.	Normal	Ampl.	S. Ampl.
Ku band					
S. Atten.	0	0	2	2	0
Atten.	0	8	9	1	0
Norm.	0	7	26	2	2
Ampl.	0	2	11	5	0
S. Amp.	0	0	7	1	0

Total number of hours: 85

Ku band median value: -116.2 dBm; C band median value: -104.0 dBm

b) Rain

C band:	S. Atten.	Atten.	Normal	Ampl.	S. Ampl.
Ku band					
S. Atten.	0	1	0	0	0
Atten.	2	4	0	0	0
Norm.	2	5	21	2	1
Ampl.	0	0	2	0	2
S. Amp.	0	0	0	0	1

Total number of hours: 43

Ku band median value: -113.2 dBm; C band median value: -90.2 dBm

c) Ducting

From Table 5.2 a) and Figure 5.7 it is evident that the behaviour of the two signals is similar; by far the greatest portion of the signal levels is in adjacent categories - the deviations about the respective median levels differ by less than 10 dB. The majority of the measurements, 55%, however, are in different categories, and 22% of those are in non-adjacent categories. It is in place, therefore, to question both the appropriateness of the propagation mode categories considered, and the methods of determining the mode of propagation for any given hour. Some divergent areas, such as the region with attenuated Ku band signal and amplified C band signal, may be statistical artifacts. They could also be an indication that refinement of the theory - by considering more categories - is necessary. It is clear, however, that the regions with the greatest digressions from the median levels in Figure 5.7 - with amplified Ku band signals accompanied by normal C band signal levels, and with strongly amplified Ku band signals accompanied by strongly amplified C band signals - in fact correspond to the identified rain and ducting groups, as evidenced by Figures 5.8 and 5.9. No mechanism, however, explains the very small group of data where the Ku band, unlike the C band, is attenuated. It seems, therefore, that any difficulties encountered are primarily the result of inexact categorization methods, rather than the result of use of faulty categories. If this is the case, the Figures indicate that it affects only a small portion of the data. With this in mind, a conclusion drawn from these tables is that turbulent volume scatter is the main mode of propagation at both Ku and C bands, and that the categories as well as categorization methods are appropriate.

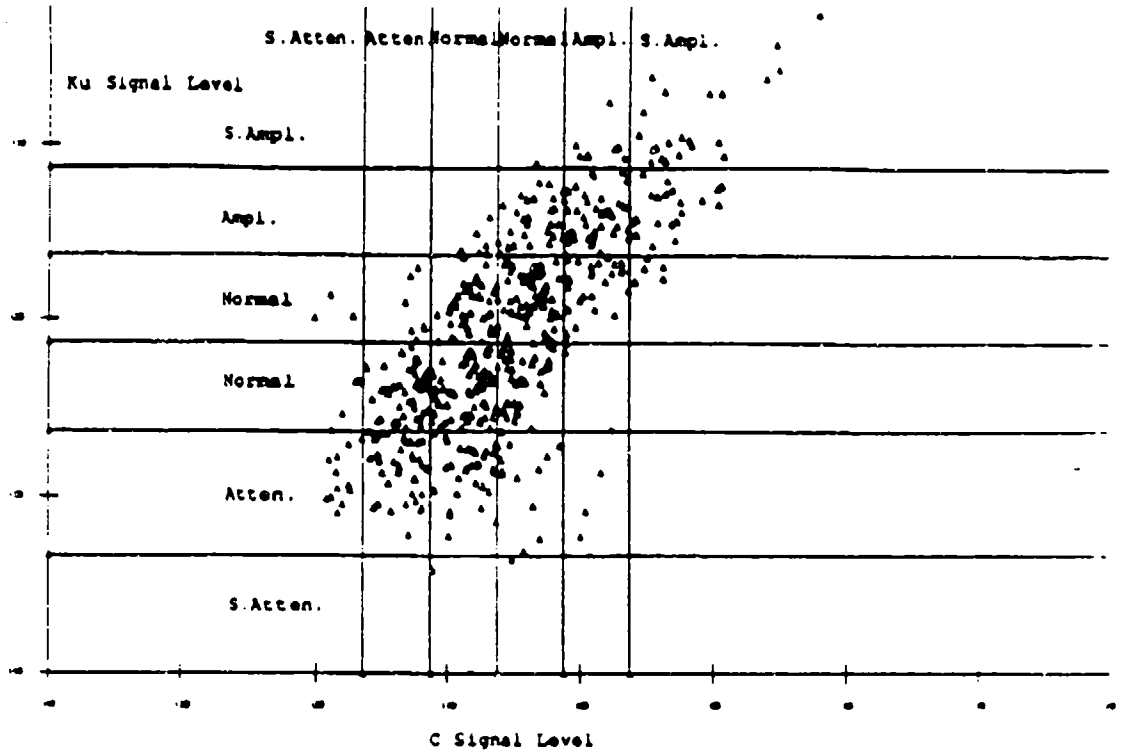

Figure 5.7: Ku vs C signal levels, Clear Air, May/June 1991.

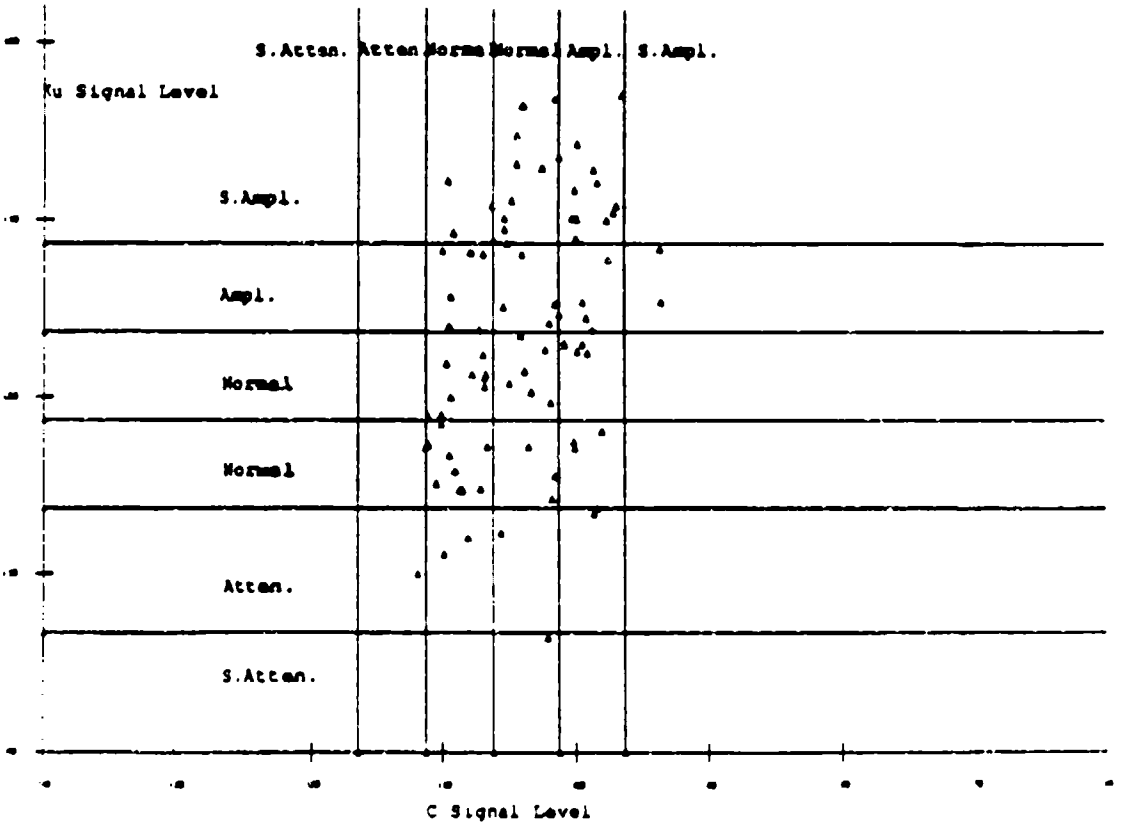

Figure 5.8: Ku vs C signal levels, Rain, May/June 1991.

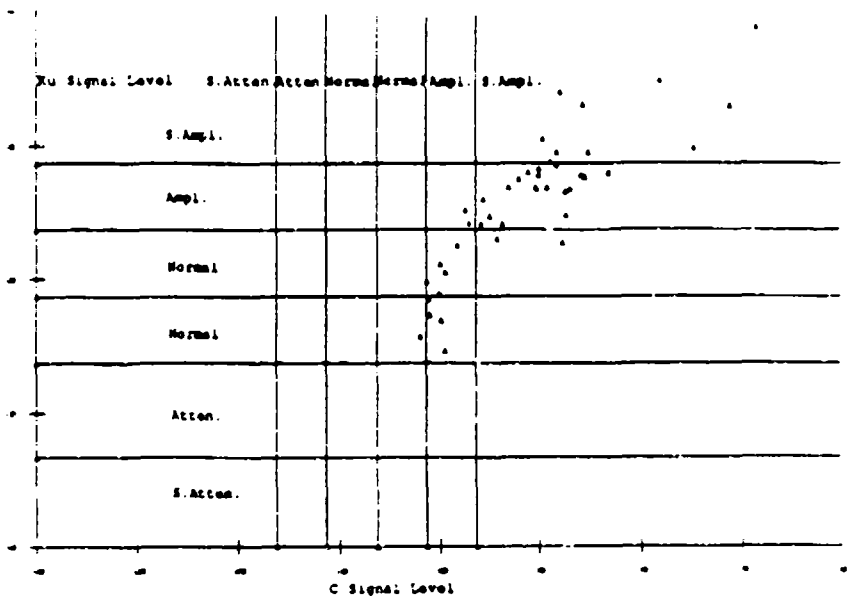

Figure 5.9: Ku vs C band signal levels, Ducting, May/June 1991.

5.4 The effect of Rain on Ku band Transmission

Figure 5.8 also shows the effect of precipitation on the received signal levels; for a larger portion of the time than during clear air conditions, the Ku band signal level is amplified (the C band shows less change). As expected, the Ku band signal, with a wavelength smaller than that of the C band signal, is much more sensitive to the rain effects (see Eqn.11). Table 5.3 clarifies the relationship between the distribution of turbulent volume scatter signal levels to the distribution of rain scatter signal levels.

	Clear Air hours / %	Rain hours / %	Rain w/ respect to Clear Air Median
Median of all hours	-121.6 dBm	-113.5 dBm	
Strong Attenuation (no. hours)	27 / 3.4%	0 / 0%	0 / 0%
Attenuation	152 / 19.1%	0 / 0.0%	0 / 0.0%
Normal	416 / 52.3%	3 / 75%	0 / 0.0%
Amplification	139 / 17.5%	1 / 25%	2 / 50.0%
Strong Amplification	62 / 7.8%	0 / 0%	2 / 50.0%
Total number of hours	796 / 100%	4 / 100%	4 / 100%

a) Winter

	Clear Air hours / %	Rain hours / %	Rain w/ respect to Clear Air Median
Median of all hours	-120.8 dBm	-119.5 dBm	
Strong Attenuation (no. hours)	82 / 7.0%	6 / 4.5%	3 / 2.2%
Attenuation	199 / 17.1%	25 / 18.7%	21 / 15.7%
Normal	642 / 55.2%	62 / 46.3%	59 / 44.0%
Amplification	177 / 15.2%	16 / 11.9%	21 / 15.7%
Strong Amplification	64 / 5.5%	25 / 18.7%	30 / 22.4%
Total number of hours	1164 / 100%	134 / 100%	134 / 100%

b) Spring

	Clear Air hours / %	Rain hours / %	Rain w/ respect to Clear Air Median
Median of all hours	-119.7 dBm	-117.0 dBm	
Strong Attenuation (no. hours)	11 / 4.1%	2 / 3.6%	1 / 1.7%
Attenuation	52 / 19.3%	12 / 21.4%	6 / 10.7%
Normal	139 / 51.5%	20 / 35.7%	26 / 50.%
Amplification	55 / 20.4%	16 / 28.6%	11 / 19.6%
Strong Amplification	13 / 4.8%	6 / 10.7%	12 / 21.4%
Total number of hours	270 / 100%	56 / 100%	56 / 100%

c) Summer

Table 5.3: Distributions about median levels, Ku band, clear air and rainy conditions.

The first column of rain data lists the number of rain hours with the various reception levels (as described in Section 4.4) with respect to the median value of the rain hours. The last column shows the same hours with respect to the median of the clear air hours. As is seen in these three tables, rain has the effect of increasing the median signal levels, and reduces the amount of low-level fields, skewing the distributions upward. The rain data from the winter months are scarce, but the other seasons contain sufficient data for statistical reliability. In all, only 4 of the 2467 hours, or 0.16%, were dominated by strong attenuation caused by rain, relative to the clear air median signal level. Concern for the effect rain has on the path is more appropriate with regard to high-level interference fields. In fact, plot A17 in Annex A, shows that, for the Ku band, high-level fields are as common during rain as during ducting conditions. It should be noted, however, that the high-level fields correspond to light rainfall, and that the low-level fields are caused, in general, by stronger rainfall on the path. For design purposes, therefore, it is insufficient to consider all rain as a single mode of propagation. A study must be made of the expected distributions of rainfall on any particular path, prior to system design.

5.5 Diurnal Variations

Figures 5.10 through 5.14 show the diurnal variations of the quantities in question for the spring. A complete set for the other seasons are listed in Annex A, Figures 1 through 8. Figure 5.10 shows little variation in the Ku band clear air signal level. During the mid-day hours there is amplification of the signal by only 2 dB. An increase during this time is expected in clear air because of the increased turbulent activity when the sun warms the earth's surface. The hot, more turbulent, air rises, reaching the lower edge of the common volume by about 10 am. There is a progression of the diurnal variation that has been obscured by the averaging of the data (from March through May) in Figure 5.10. Each month shows an increasing difference between the mid-day hours and the rest of the day. During the summer this difference becomes quite large, and is non-existent during the winter hours observed. The diurnal variation of signal levels during rain is greater, but also the result of fewer hours of data. It is the result of a more variable meteorological process, and the received signal level is more dependent on the location and horizontal extent

of the rain, than is the clear air signal level. This variation during rain is, therefore, considered statistically indeterminate. The plot shows yet another view of the superior transmission conditions provided by the rain. Ducting occured only during a few hours for the time period that the C band was operational during the spring (May). The signal levels are clearly higher even in the Ku band, not only in the C band (Figure 5.11) where its effect is the greatest. As can be seen from Figure 6 in Annex A (June has a greater amount of C band data, and more measurements during ducting), the greatest coupling into the ducts occurs during the night and early morning hours. The effect on the Ku band signal levels (Figure 5, Annex A) is as high as a 15 dB increase above the clear air levels. For the C band the increase is up to twice that Figure.

Figure 5.12 and 13 show the Doppler shifts on the path. The prevailing westerly winds result in a clear air negative Doppler shift signature of about 3 Hz. This is the result of path asymmetry, as described in Section 3.3. Had the antennas been aligned over a path with a uniform horizon profile, the Doppler shift would have been well within 1Hz. There is a decrease of the average offset throughout the three seasons, caused by less strong and persistent westerly winds. The Ku band shows more sensitivity to motion of the scatterers; the Doppler shift is roughly proportional to the signal frequency.

The delay spread increases during rain, and is very much smaller during ducting. During the winter (Figure 3, Annex A) this difference is the greatest, and during the summer the difference is the smallest. From experience with the hourly delay plots it is expected that, if more precise methods of discerning rain on the path are used, this difference will be augmented. The estimates for the median delay spreads during rain in this report are, therefore, expected to be somewhat low.

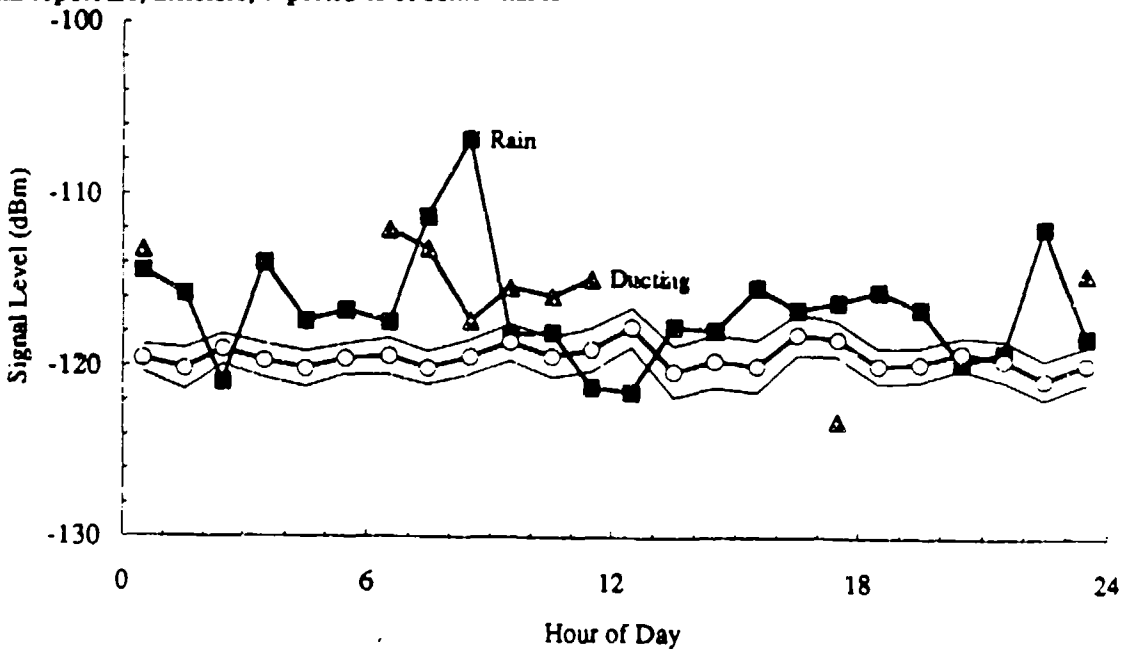

Figure 5.10: Average diurnal variation in Ku band signal level, spring, 1991.

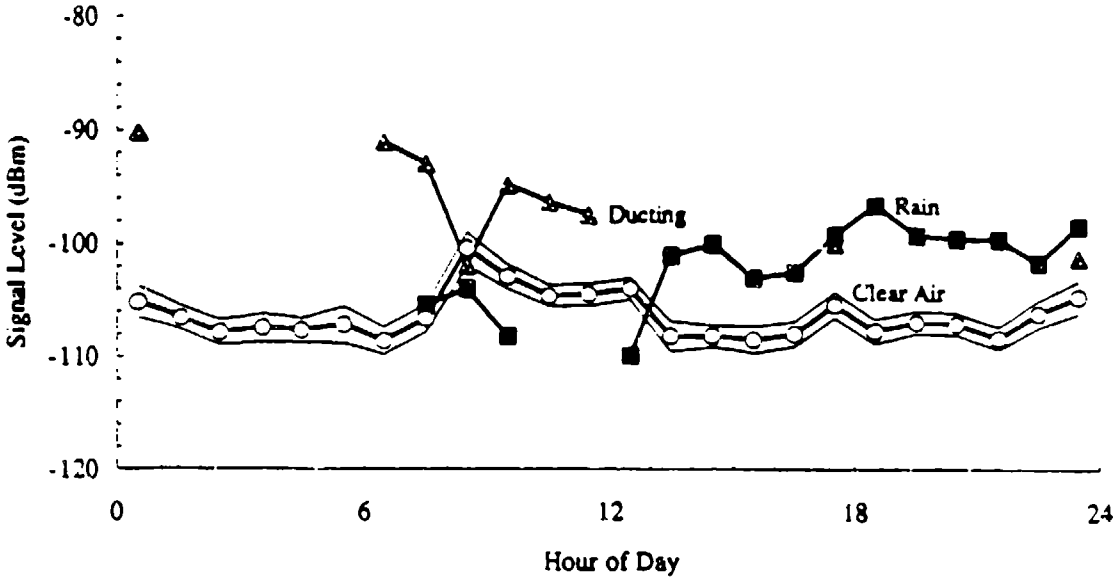

Figure 5.11: Average diurnal variation in C band signal level, spring, 1991.

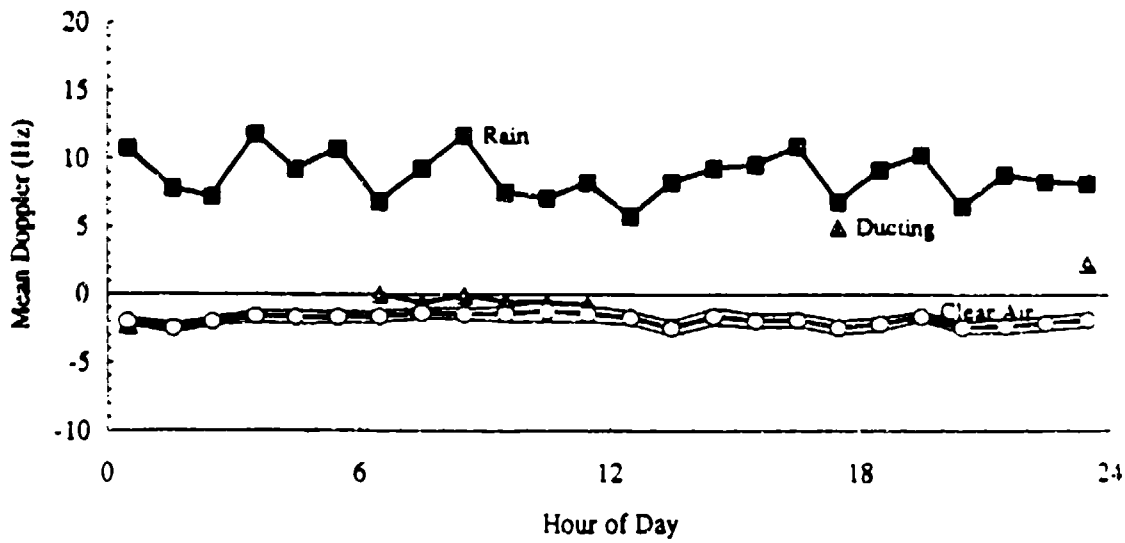

Figure 5.12: Average diurnal variation in Ku band Doppler frequency shift, spring, 1991.

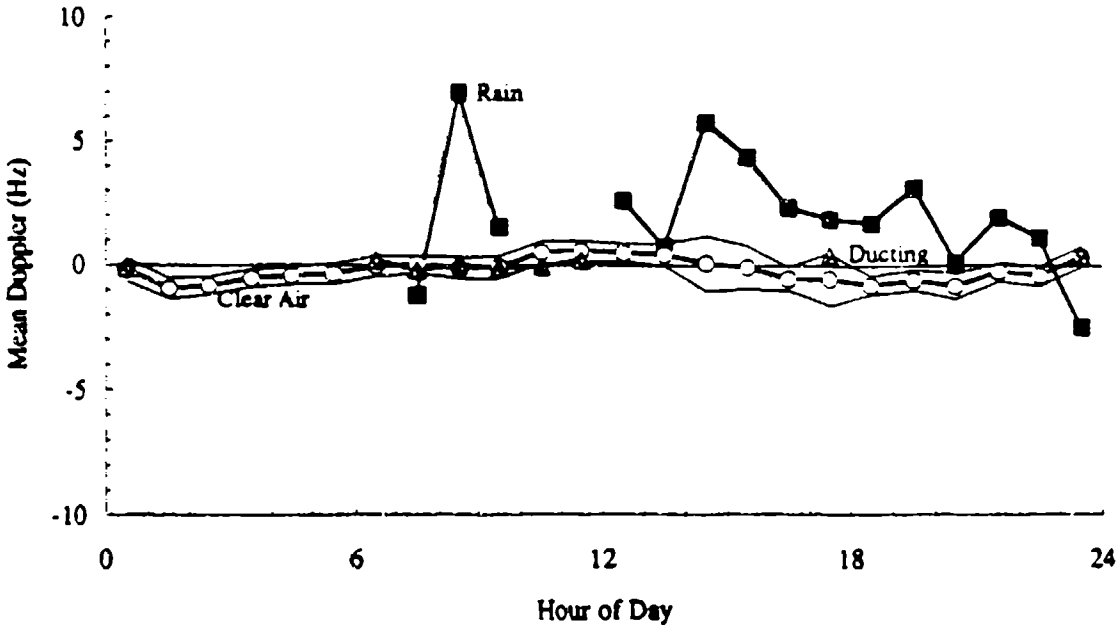

Figure 5.13: Average diurnal variation in C band Doppler frequency shift, spring, 1991.

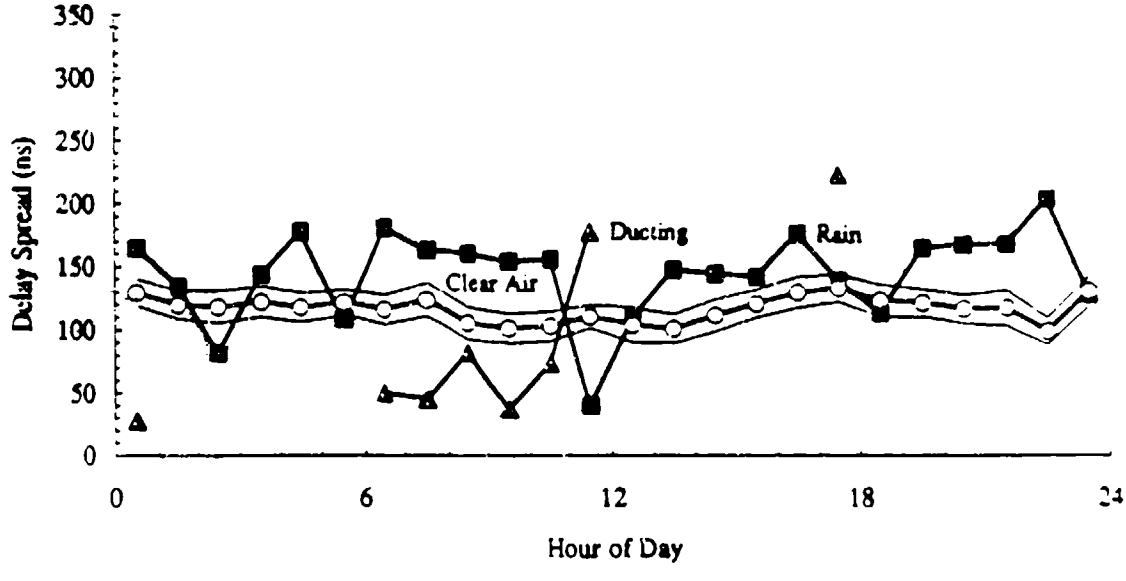

Figure 5.12: Average diurnal variation in Ku band delay spread, spring, 1991.

Table 5.4 summarizes the behaviour of the received signal levels, as well as the Doppler shift and delay spreads, during June, 1991. Similar summary sheets for the winter and spring measurements are listed in Annex B. The first standard deviation value is the estimator of the series of median values; the second value is the standard deviation of the median of medians given in the column above it. The signals show clear variation during the day; Ku band signals are strongest in the afternoon by 6 to 8 dB. The C band shows a variation of 5 to 6 dB. There is a weak negative Doppler shift due to the prevailing westerly winds. The delay spread shows very large standard deviation values compared to previous years; this is the result of the improvement in the algorithm estimating this quantity. The data for the Doppler spread values was not divided into these same groups, but simply recorded for each season as a whole. Previous experience has shown that this measurement is very insensitive for the lower range, probably because of external noise (60 Hz) affecting the data. These values are listed at the end of each table.

Table 5.4: Summer 1991 - Quarter Day Summaries - Clear Air

	Ku Carrier Level/ Xmission Loss (dBm)	Ku Doppler Shift (Hz)	Ku Delay Spread (ns)	C Carrier Level/ Xmission Loss (dBm)	C Doppler Shift (Hz)
Night					
Hours	72	72	44	72	72
Average	-122.7/167.5	-0.5	152.5	-106.9/151.7	-0.4
Std. Dev. (series / median)	4.4 / 0.20	2.6 / 0.21	70.2 / 6.5	6.5 / 0.33	1.5 / 0.1
Morning					
Hours	69	69	45	69	69
Average	-120.5/165.3	-0.5	97.5	-102.8/147.6	-0.4
Std. Dev.	6.2 / 0.2	2.8 / 0.13	62.5 / 6.1	7.6 / 0.3	1.5 / 0.11
Afternoon					
Hours	65	65	35	65	65
Average	-114./158.8	-0.1	140	-101.3/146.1	0.2
Std. Dev.	6.6 / 0.12	2.4 / 0.12	71.6 / 5.0	6.3 / 0.25	1.6 / 0.18
Evening					
Hours	64	64	46	64	64
Average	-120.5/165.3	-0.3	142.5	-108.0/152.8	0.3
Std. Dev.	6.8 / 0.25	2.0 / 0.28	79.0 / 5.0	8.7 / 0.34	4.0 / 0.24
Doppler Spread:	Hours: 264	Median: 8.6	StDev: 3.3		

Table 5.5 reinforces the conclusions about the effect of rain on the transmitted Ku band signal. The signal levels are higher, during almost all of the day, than the clear air measurements. There is also a slight increase in the C band signal level during summer rain. It is evident that the Doppler shift is the clearest indicator of rain on the path. The rain Doppler spread is comparable to the clear air values during this season. There is insufficient data to discern any diurnal variations from this table.

Table 5.5: Summer 1991 - Quarter Day Summaries - Rain

Night					
Hours	7	7	5	7	7
Average	-122.7/167.5	7.3	167.5	-109.6/154.4	1.9
Std. Dev.	5.3 / 1.0	2.5 / 1.0	89.3 / 30.2	4.3 / 0.70	1.2 / 0.28
Morning					
Hours	8	8	8	8	8
Average	-114.3/159.1	11.1	110.0	-109.2/154	4.0
Std. Dev.	5.6 / 1.3	4.4 / 0.98	84.6 / 17.7	3.8 / 0.69	2.6 / 0.84
Afternoon					
Hours	17	17	13	17	17
Average	-118.7/163.5	8.4	127.5	-102.3/147.1	3.0
Std. Dev.	8.8 / 1.2	4.8 / 1.1	61.3 / 10.3	3.4 / 0.45	2.4 / 0.49
Evening					
Hours	24	24	23	24	24
Average	-116.5/161.3	10.9	140.0	-107.1/151.9	2.3
Std. Dev.	6.5 / 0.81	4.5 / 0.54	68.0 / 9.7	4.7 / 0.44	2.0 / 0.46
Doppler Spread:	Hours: 54	Median: 8.7	St.Dev: 2.2		

Table 5.6 shows the same quantities during ducting conditions. As expected, the signal levels are considerably higher, peaking during night hours in the C band, where ducting is of greater impact. The delay spreads are extremely small compared to that of either rain or turbulent scatter. This is expected, since the power scattered toward the receiver will come from the vertically limited duct. Note that this result also applies to the Doppler spread measurement. It is much smaller during ducting, as one would expect, because of the stability of the ducting region.

Table 5.6: Summer 1991 - Quarter Day Summaries - Ducting

Night					
Hours	11	11	10	11	11
Average	-113.2/158	0.8	30.0	-87.3/132.1	0.1
Std. Dev.	6.5 / 0.77	3.2 / 0.11	44.0 / 22.4	10.3 / 1.6	0.20 / 0.1
Morning					
Hours	13	13	13	13	13
Average	-112.5/157.3	-0.2	82.5	-90.0/134.8	-0.1
Std. Dev.	4.8 / 0.58	1.1 / 0.2	46.9 / 11.6	6.5 / 1.2	0.21 / 0.45
Afternoon					
Hours	6	6	6	6	6
Average	-111.4/156.2	0.7	42.5	-89.2/134	-0.2
Std. Dev.	3.1 / 0.63	1.8 / 0.31	17.7 / 11.7	1.7 / 1.2	0.31 / 0.17
Evening					
Hours	3	3	3	3	3
Average	-115.9/160.7	-1.1	155.0	-93.5/138.3	-0.3
Std. Dev.	3.4 / 1.7	0.64 / 0.22	58.5 / 51.0	10.9 / 2.5	0.12 / 0.22
Doppler Spread:	Hours: 264	Median: 3.6	St.Dev: 2.6		

95% bounds. Since the major portions of the curves lie within these bounds (90% are expected to), it is evident that the lognormal model provides an excellent appproximation to the signal level distributions. Annex A lists a more complete set of these distribution curves for different conditions.

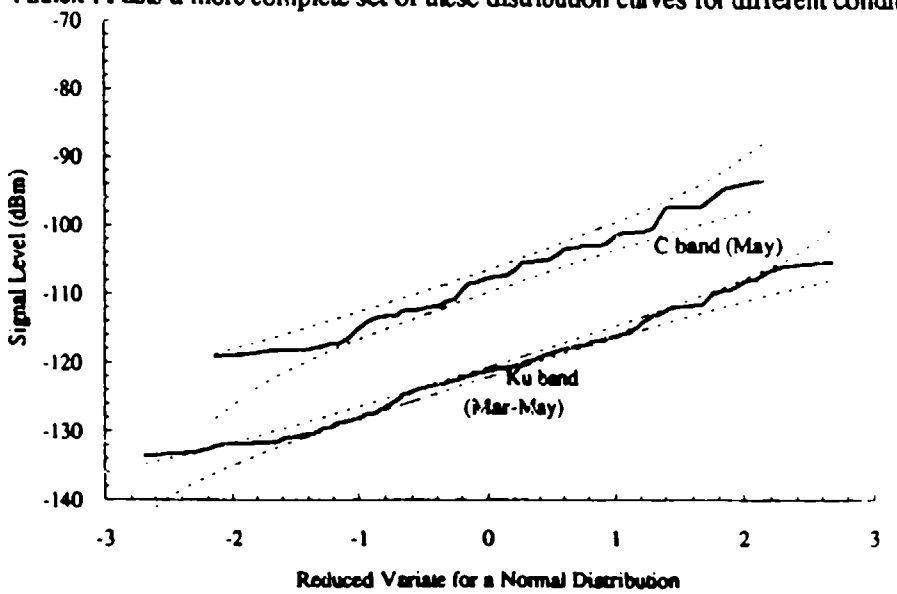

Figure 5.15: Sample cdf for Ku and C signal levels, night, spring, 1991, clear air.

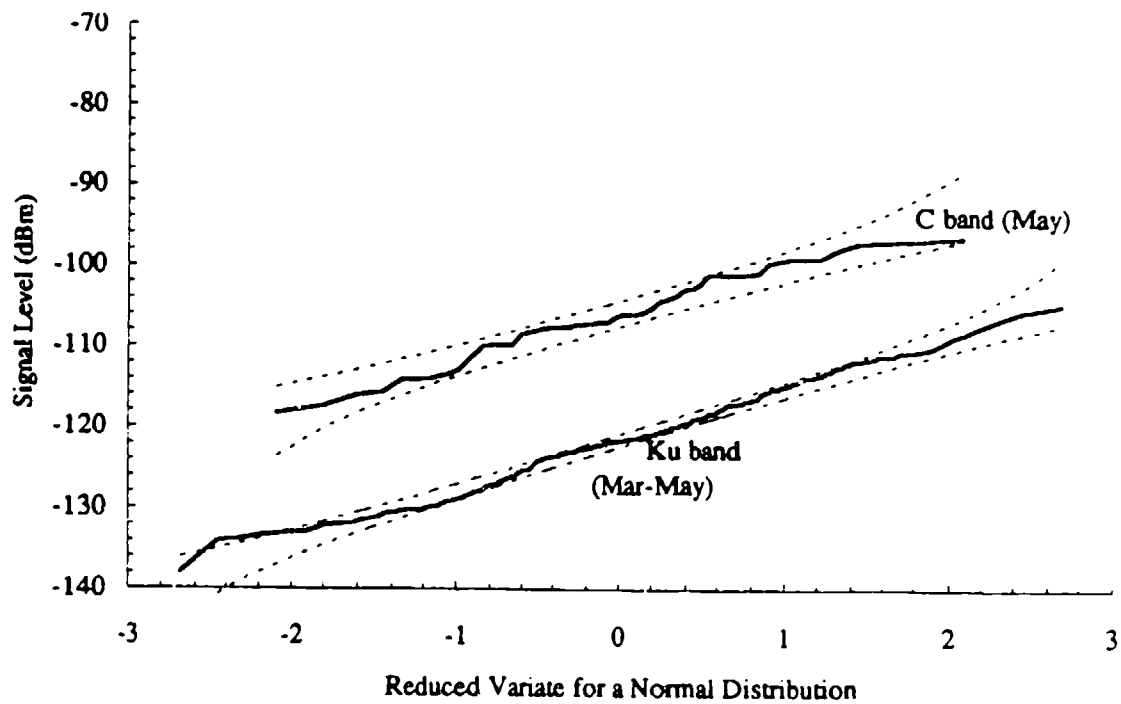

Figure 5.16: Sample cdf for Ku and C signal levels, morning, spring, 1991, clear air.

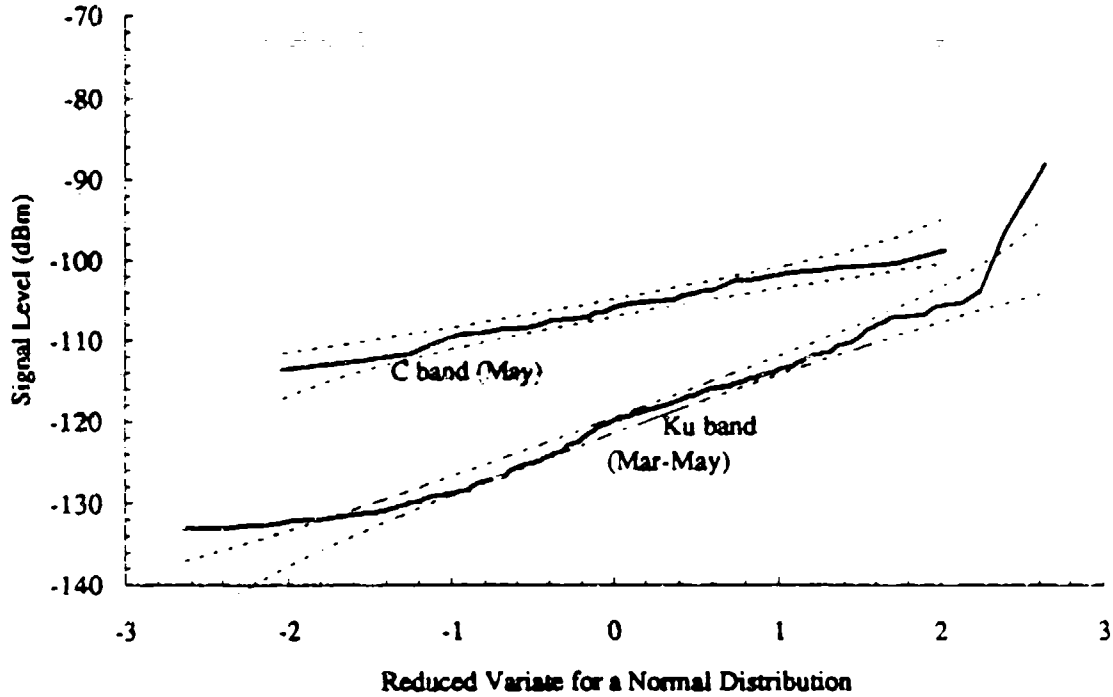

Figure 5.15: Sample cdf for Ku and C signal levels, afternoon, summer, 1991, clear air.

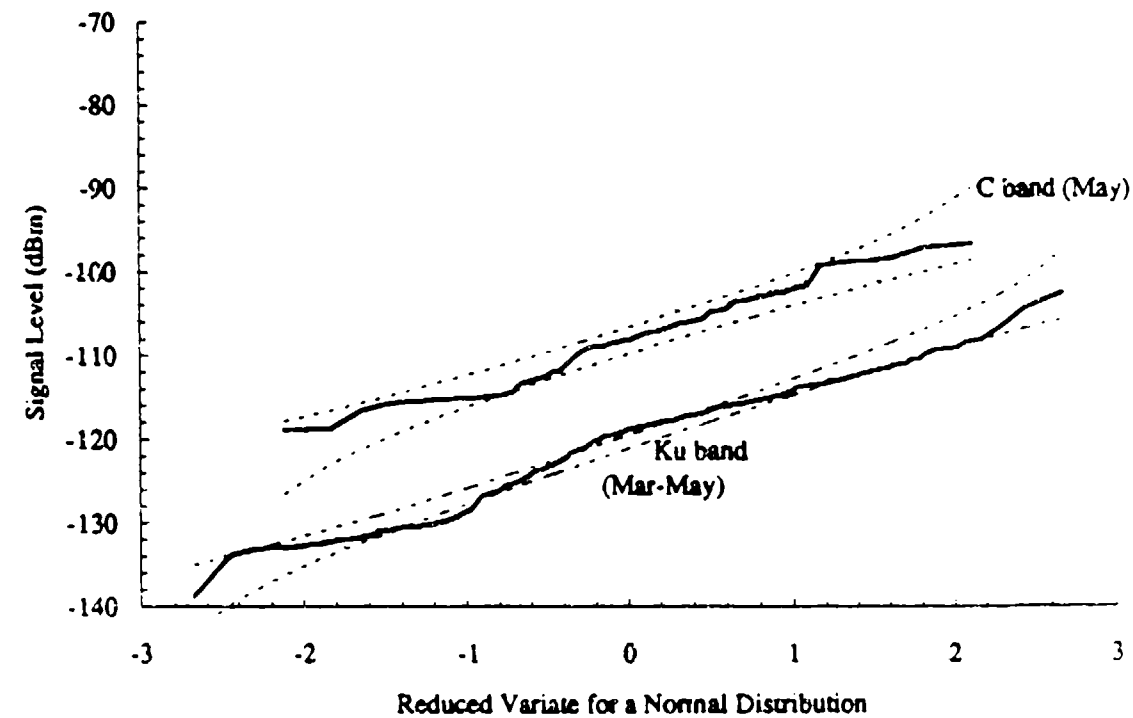

Figure 5.16: Sample cdf for Ku and C signal levels, evening, summer, 1991, clear air.

The CDFs are also applied to the other quantities; the Doppler spread and delay spread cdf's are given in Figures 5.19 and 5.20. The Doppler spread distributions show little difference between rain and clear air, in the estimate of their median values, but is substantially lower during ducting. The range of the Doppler spread during rain, however, is considerably smaller than the range during clear air. Note the full range of the delay spread estimates in Figure 5.18, and the excellent fit within the normanl distribution 5% and 95% bounds.

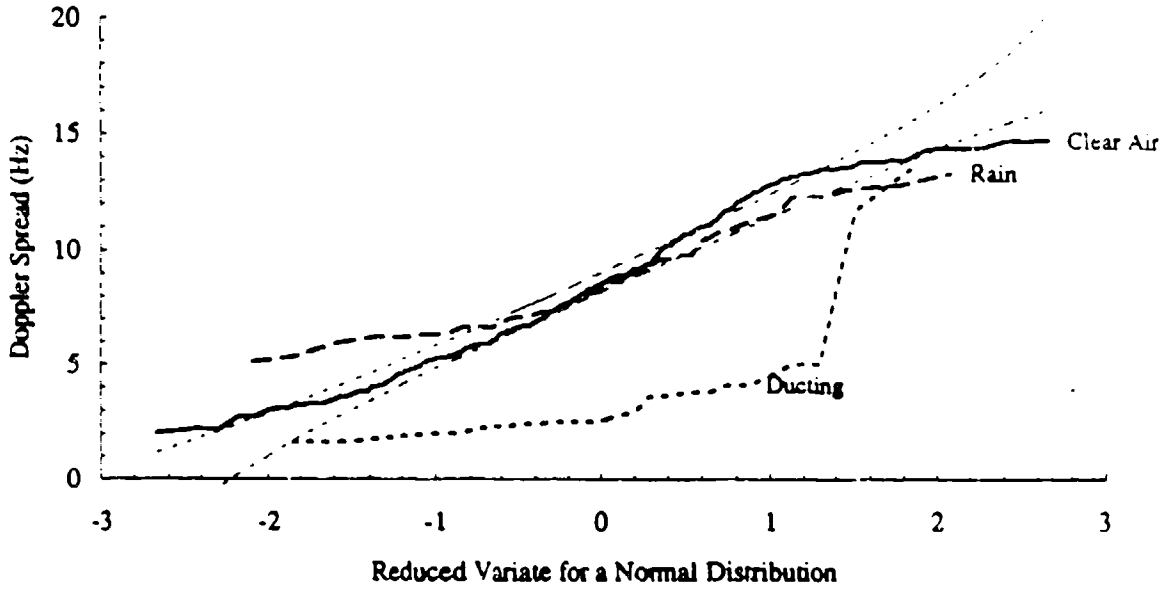

Figure 5.19: Sample cdf for Ku Doppler Spread, all conditions and hours, summer, 1991.

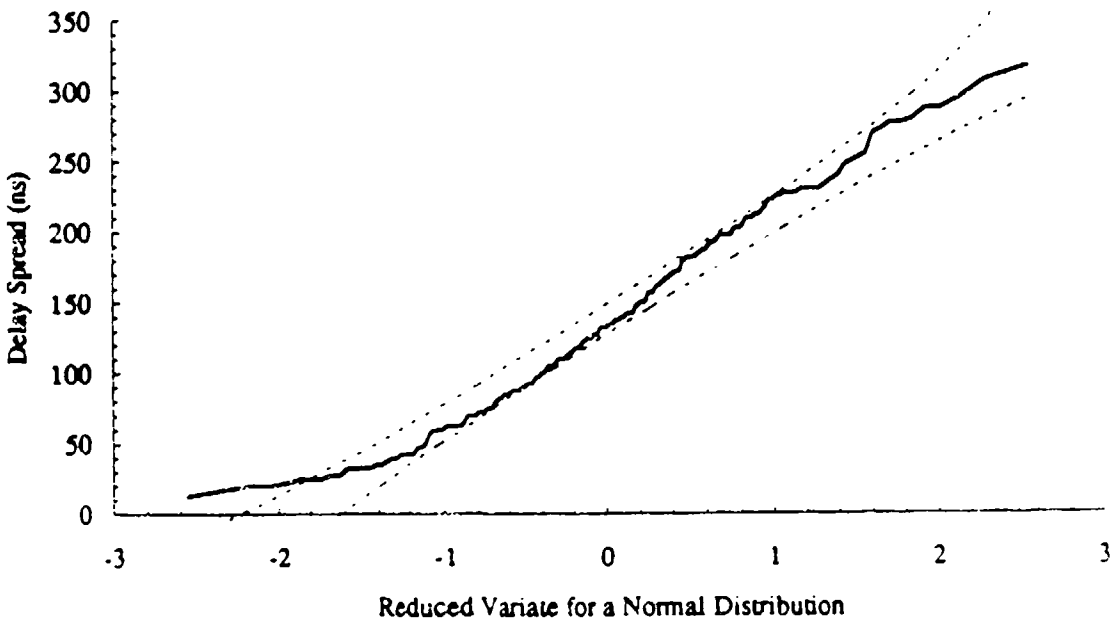

Figure 5.20: Sample cdf for Ku delay spread, clear air, all hours, summer, 1991.

5.6 Seasonal Variation

The seasonal variation of three quantities are of primary interest with regard to seasonal change. Again, a more complete set of CDFs, showing seasonal variation, is provided in Appendix A. The first plot, Figure 5.21, shows the diurnal variation of the Ku signal levels for all three seasons. The summer shows a great 'hump' during the warmer hours of the day, but its night-time level is barely higher than the level during the other seasons. The second plot, Figure 5.22, shows the greater dominance of westerly winds during the colder seasons. With this in mind, if the data is to be revised at a later stage, these months should be investigated first for accurate categorization of rain data. (Since the amount of offset is a mild indicator of the amount of rain data that could, potentially, have been defined, erroneously, as clear air data.) The third plot depicts the seasonal change of the delay spread. As mentioned earlier, the spread is as much as 50% higher during the summer than winter hours. This result is in spite of the fact that the lowest average signals were observed during the winter months. (If the signal is too low, there is a risk that the delay spread measured will be unduly large; it is clear that this risk has been minimized sufficiently, by the thresholds set in order for the recorded data to be used in the statistical presentation.) Another view of the seasonal changes is presented in Appendix A, plots A14-16. For all three cases of power, Doppler spread, and delay spread, higher values were observed during the summer season.

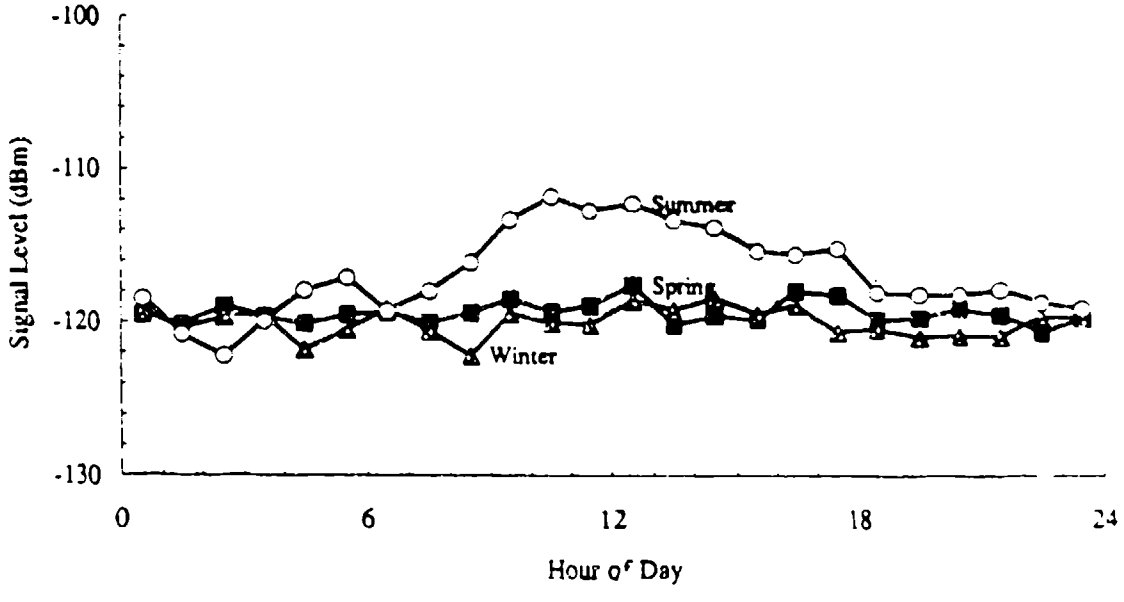

Figure 5.21: Diurnal variation of Ku signal levels for three seasons, clear air.

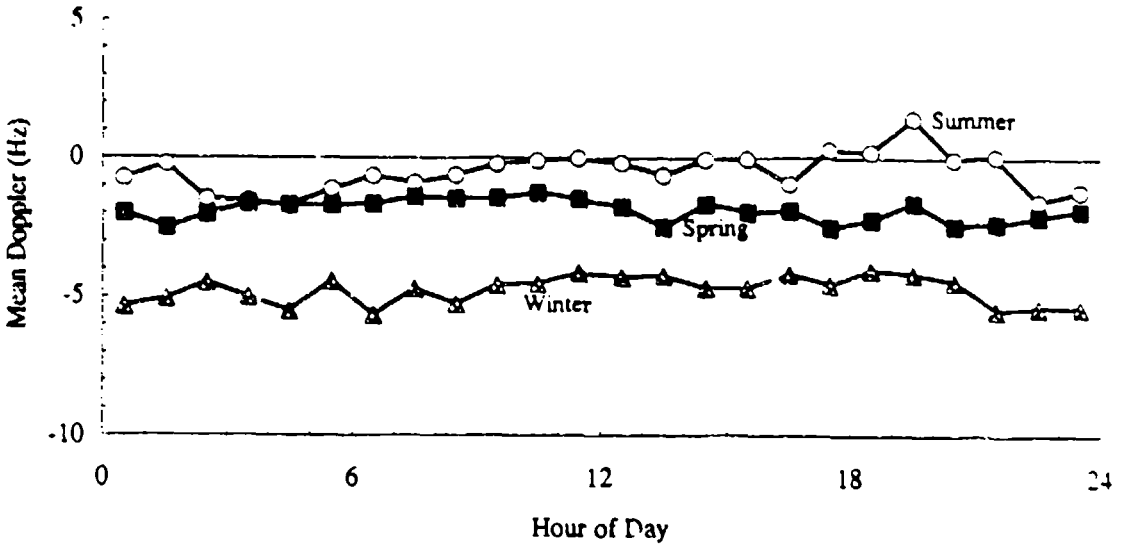

Figure 5.22: Diurnal variation of Ku Doppler shifts for three seasons, clear air.

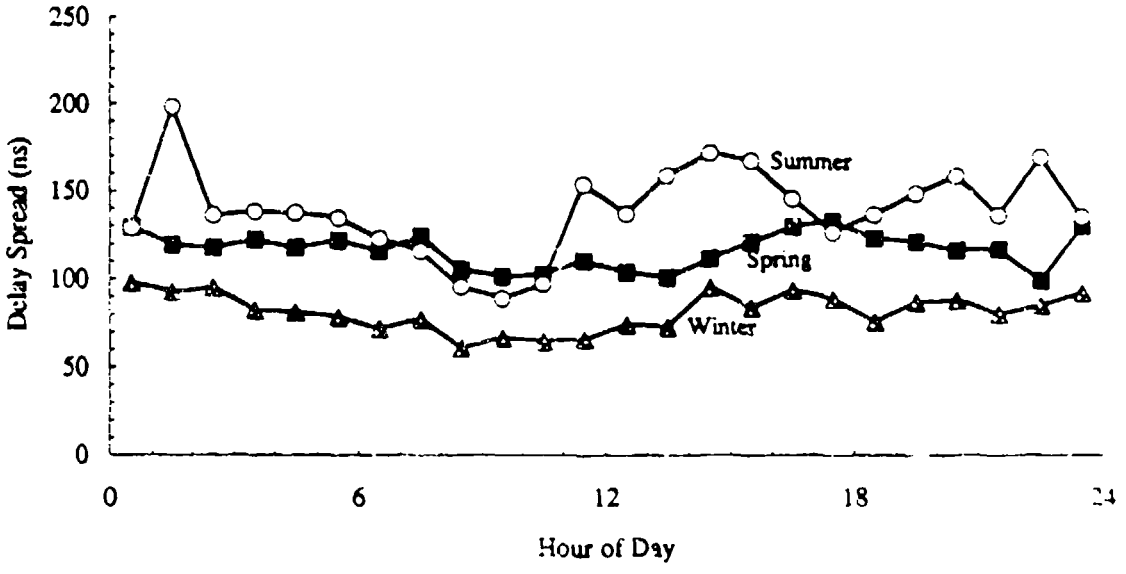

Figure 5.23: Diurnal variation of Ku delay spread for three seasons, clear air.

5.7 Conclusion

The measurements taken during 1991 show, in agreement with results from the initial stages of the data collection campaign, that the signal levels can be modeled by the lognormal probability distributions, and that the delay and Doppler spreads can be modeled by normal probability distributions. The median values have been shown to be consistent with the thin layer, turbulent volume forward scatter model [Crane 1991]. It is therefore possible to predict both the high and low-level fields expected from the path, by using the distributions and the median levels predicted by the theoretical model. Moreover, rain on the path, unless large amounts of heavy rainfall are expected, will not adversely affect the wave propagation. Care must be taken, however, to guard against the variations in the delay spread - this may in fact be of more concern than signal level deterioration, and its seasonal variations may be of more concern than the variations due to precipitation.

Future work on the project would focus on a comparison of the 1991 data set with data from the previous few years, and a study on a monthly, rather than seasonal, basis with a complete set of data; this would yield estimates for the 'worst month' characteristics. The effects of the antennae misalignment must also be dealt with, perhaps by comparing the data with independent weather RADARs. Although a fairly substantial portion of the data categorized as rain could be in error because of the misalignment, this is not expected to affect the conclusions made here.

Annex A

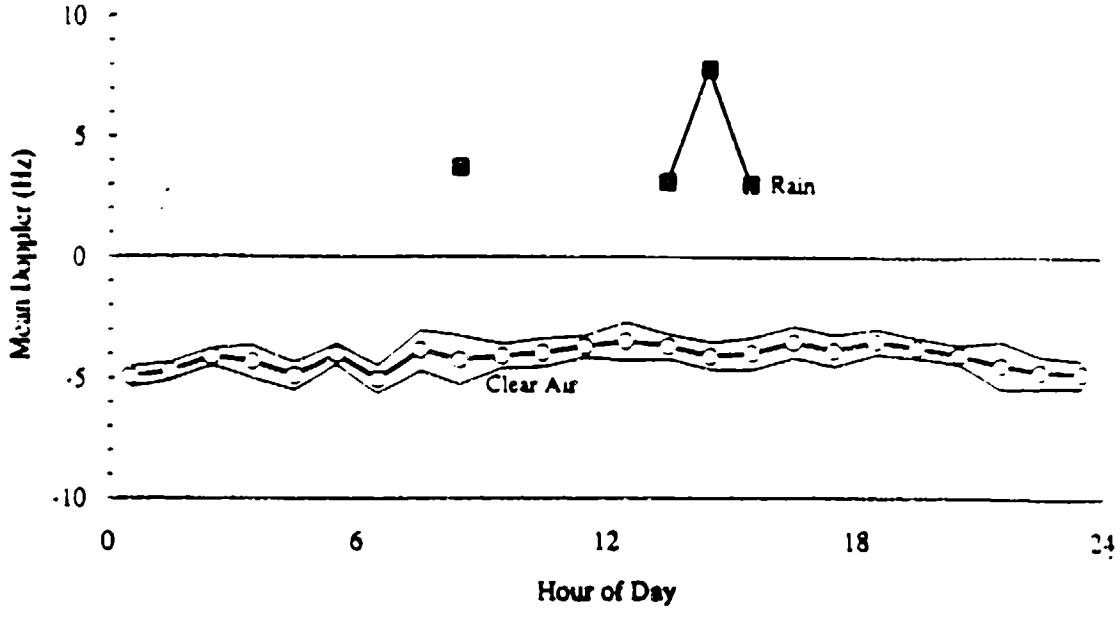

A1 Plot of Average diurnal variation in Ku band signal level, winter, 1991.

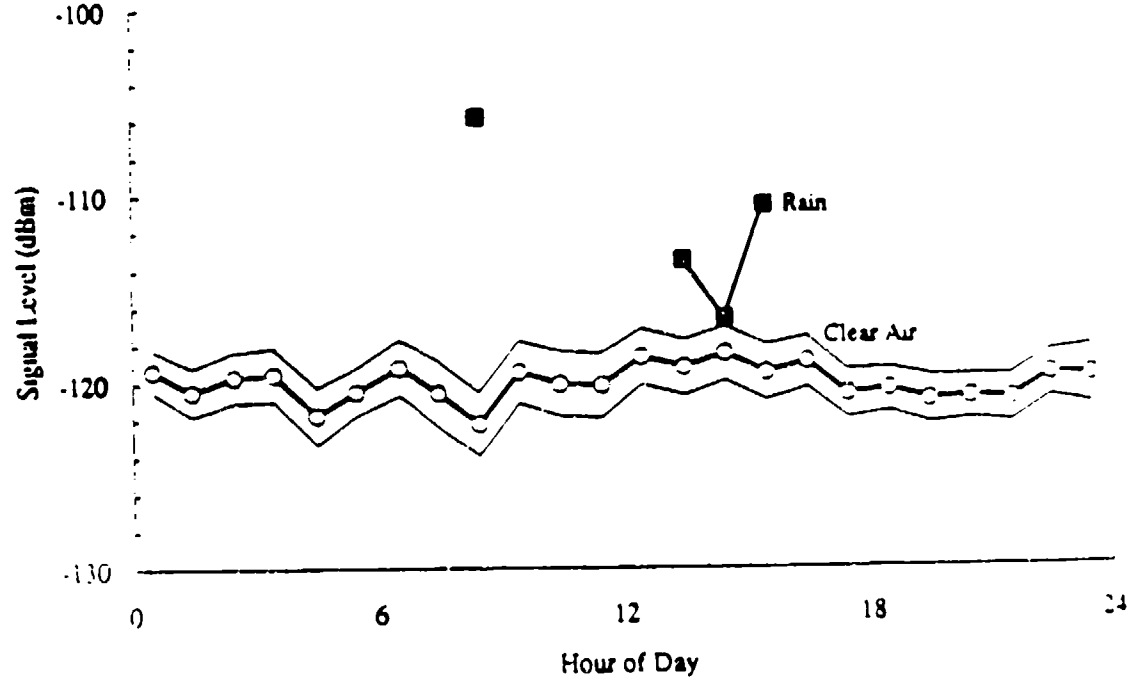

A2 Plot of Average diurnal variation in Ku band mean Doppler frequency, winter, 1991.

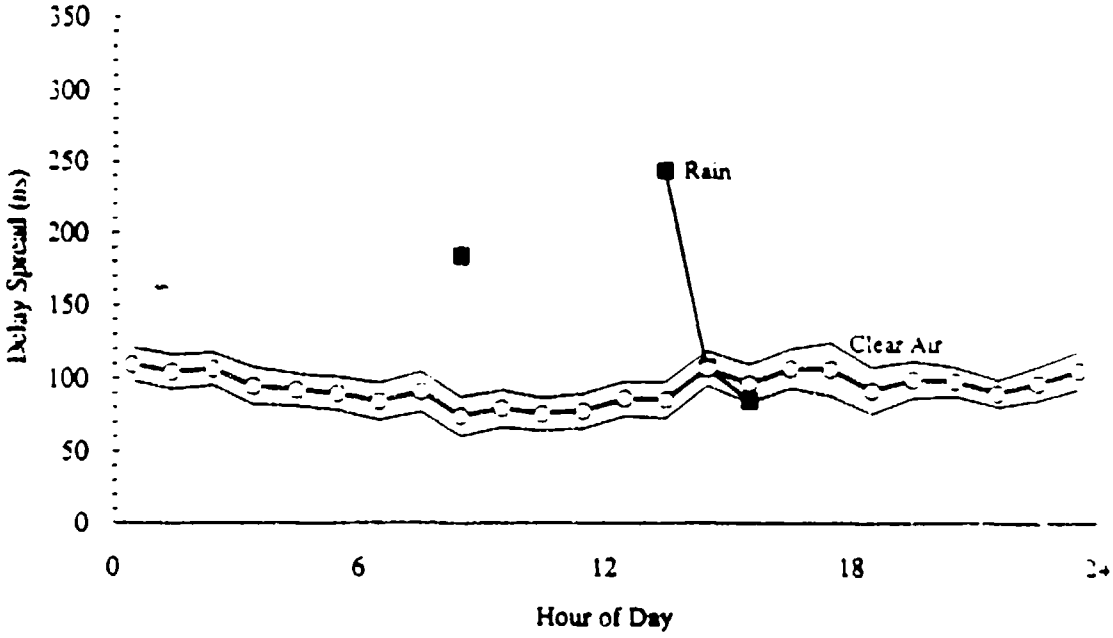

A3 Plot of Average diurnal variation in Ku band delay spread, winter, 1991.

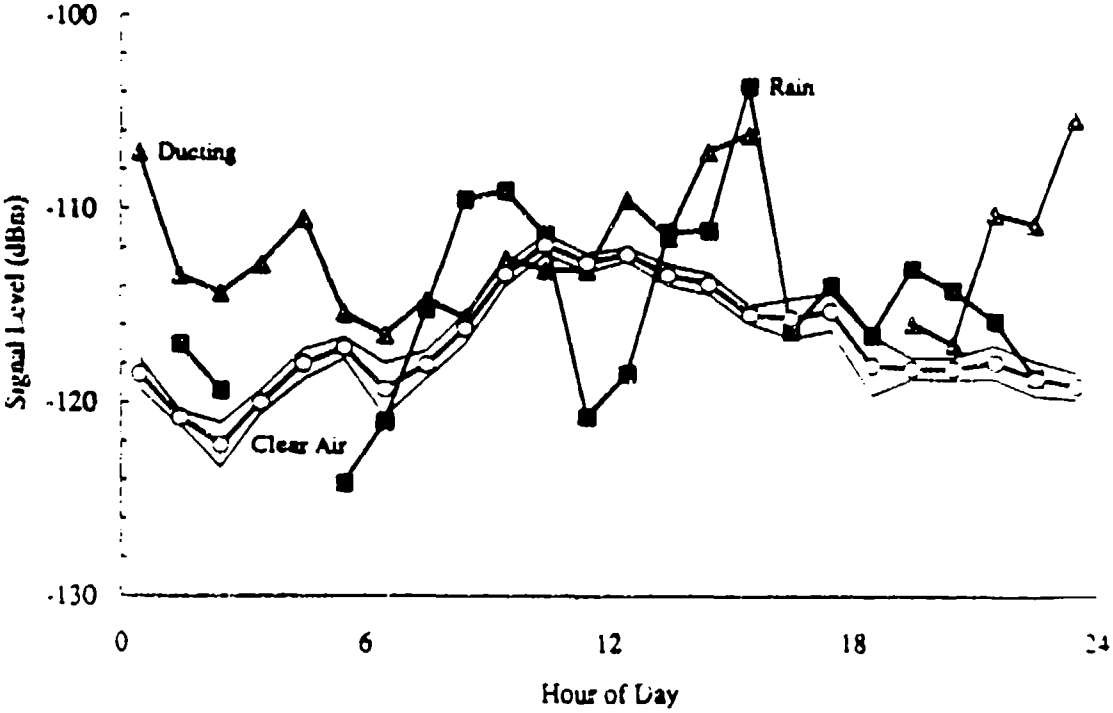

A4 Plot of Average diurnal variation in Ku band signal level, spring, 1991.

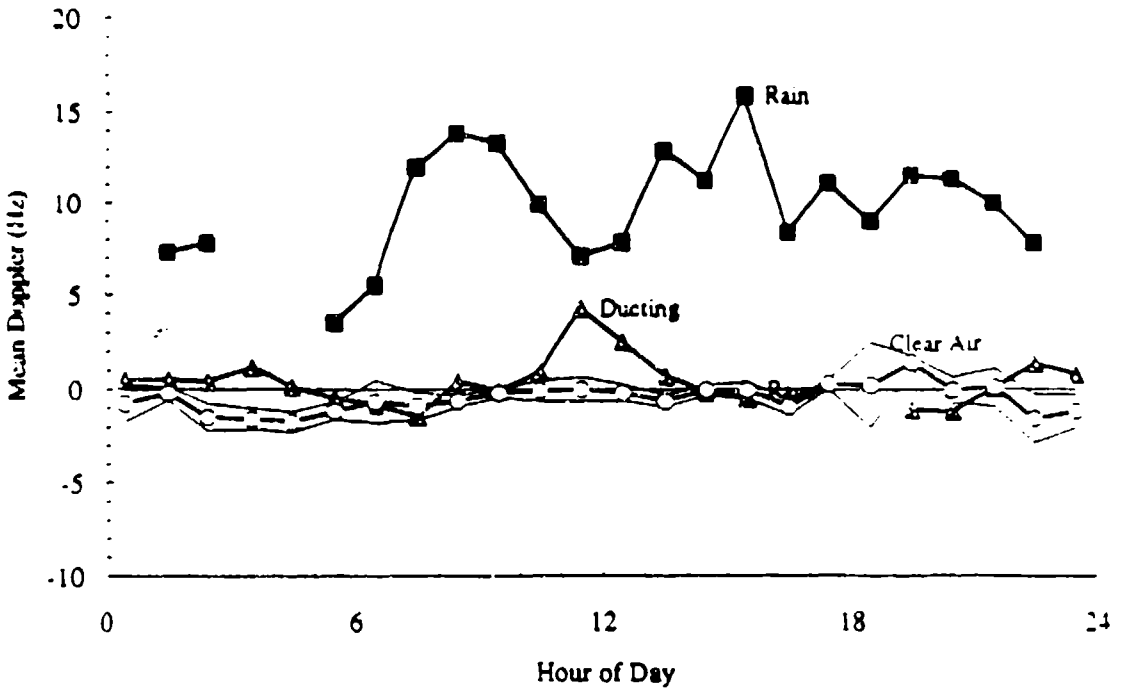

A5 Plot of Average diurnal variation in Ku band mean Doppler frequency, spring, 1991.

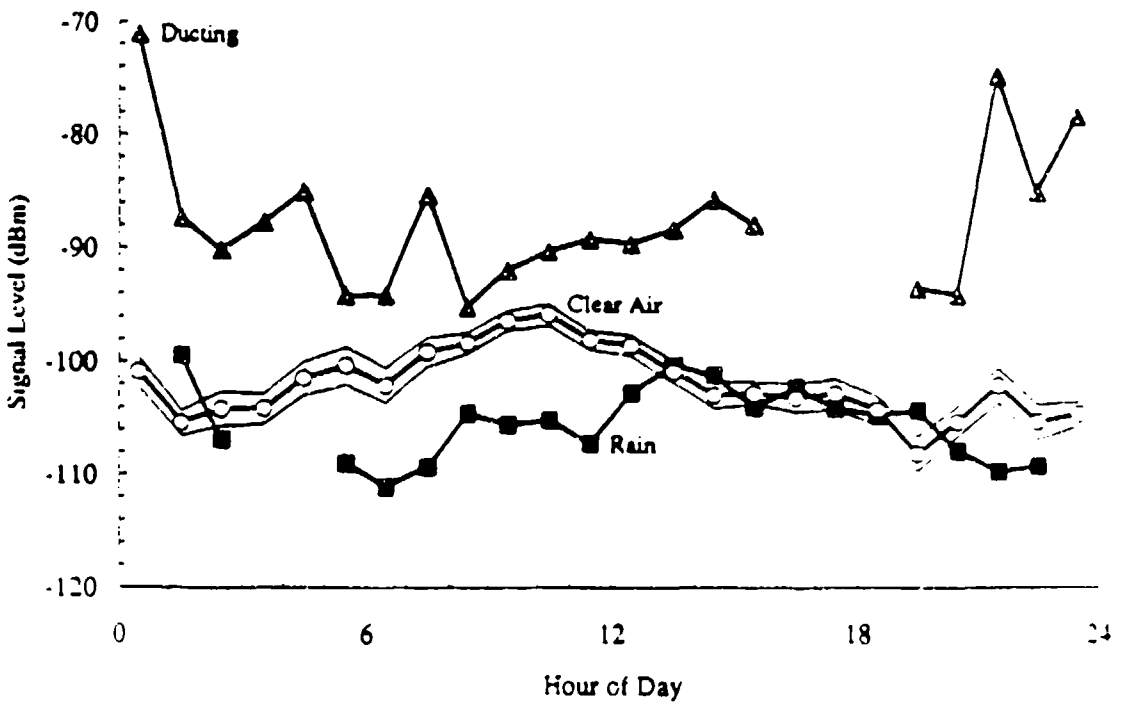

A6 Plot of Average diurnal variation in C band signal level, spring, 1991.

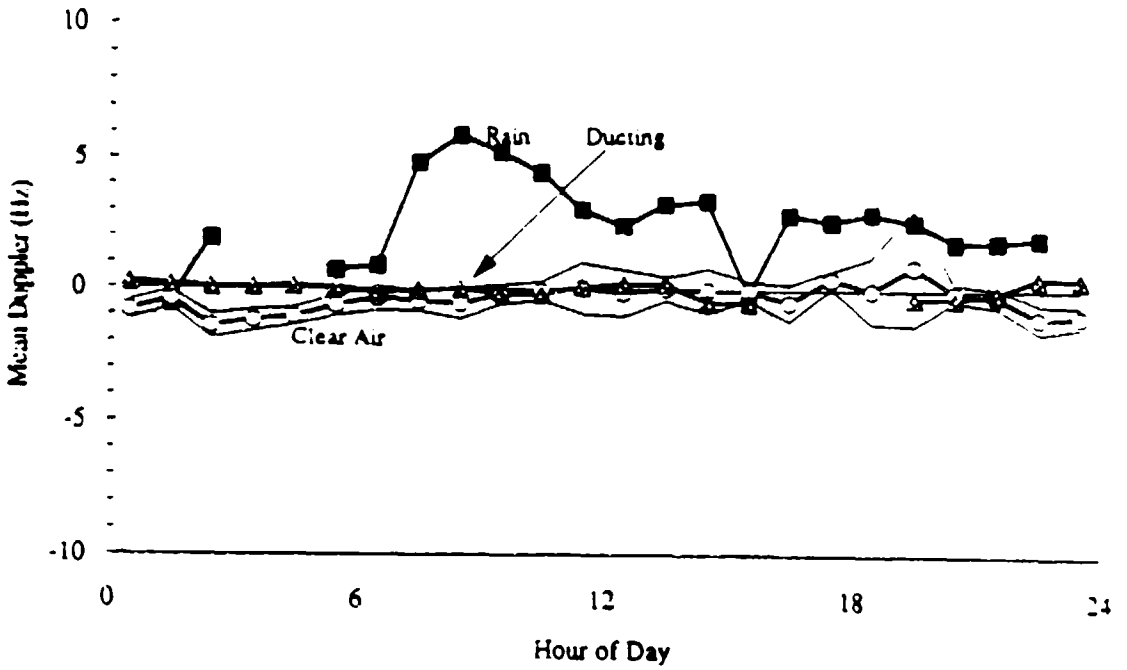

A7 Plot of Average diurnal variation in C band mean Doppler frequency, spring, 1991.

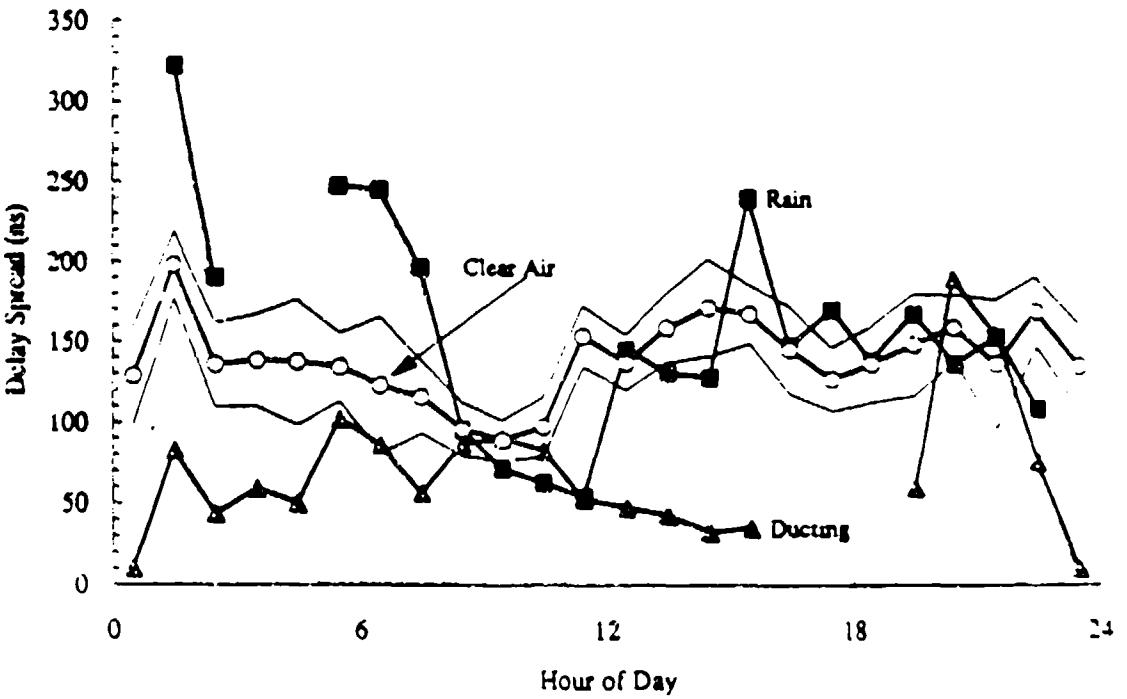

A8 Plot of Average diurnal variation in Ku band delay spread, spring, 1991.

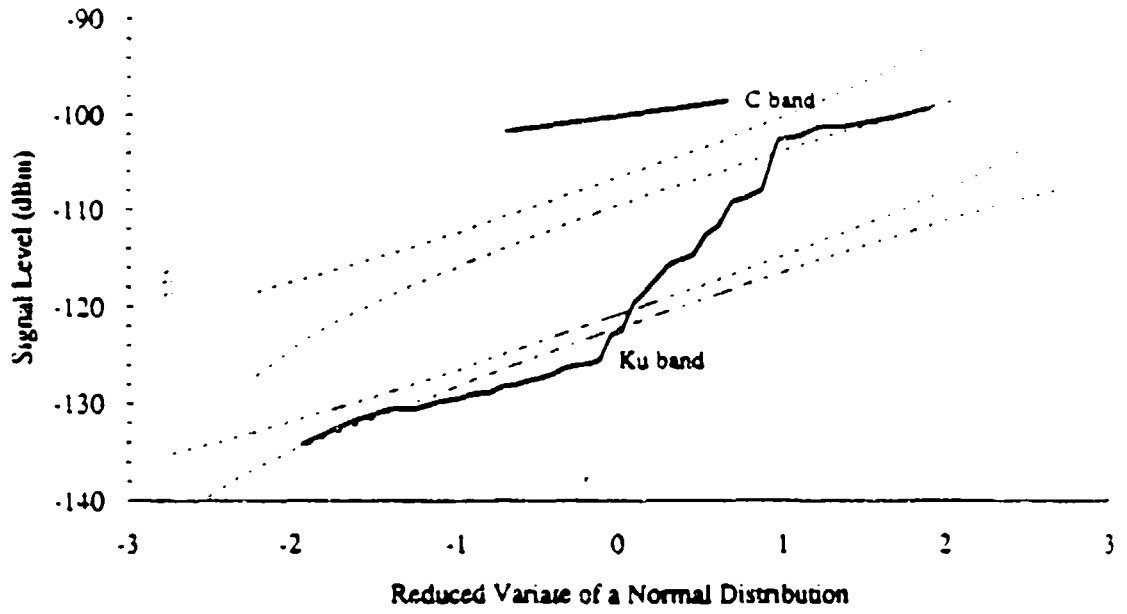

A9 Sample CDF for Ku and C signal levels, rain, night, spring, 1991 (bounds of clear air).

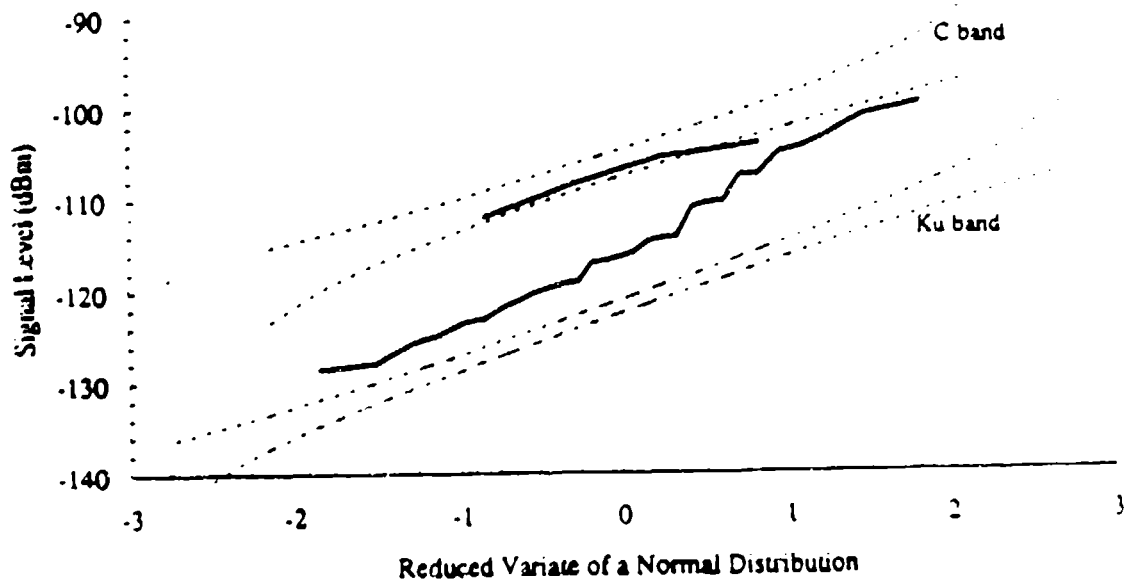

A10 Sample CDF for Ku and C signal levels, rain, morning, spring, 1991.

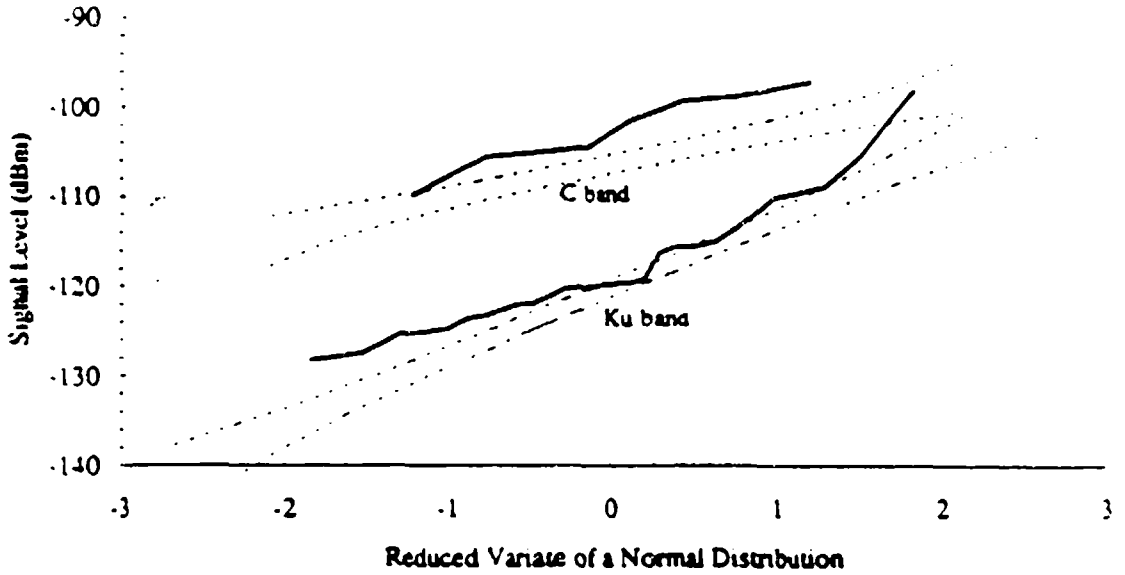

A11 Sample CDF for Ku and C signal levels, rain, afternoon, spring, 1991.

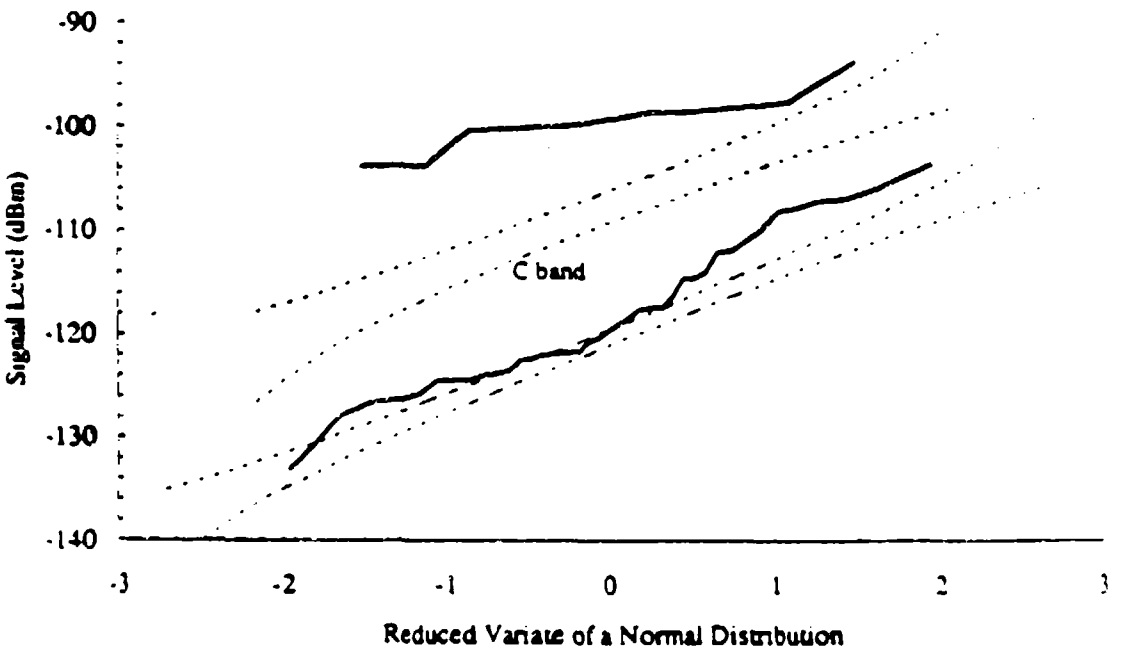

A12 Sample CDF for Ku and C signal levels, rain, evening, spring, 1991.

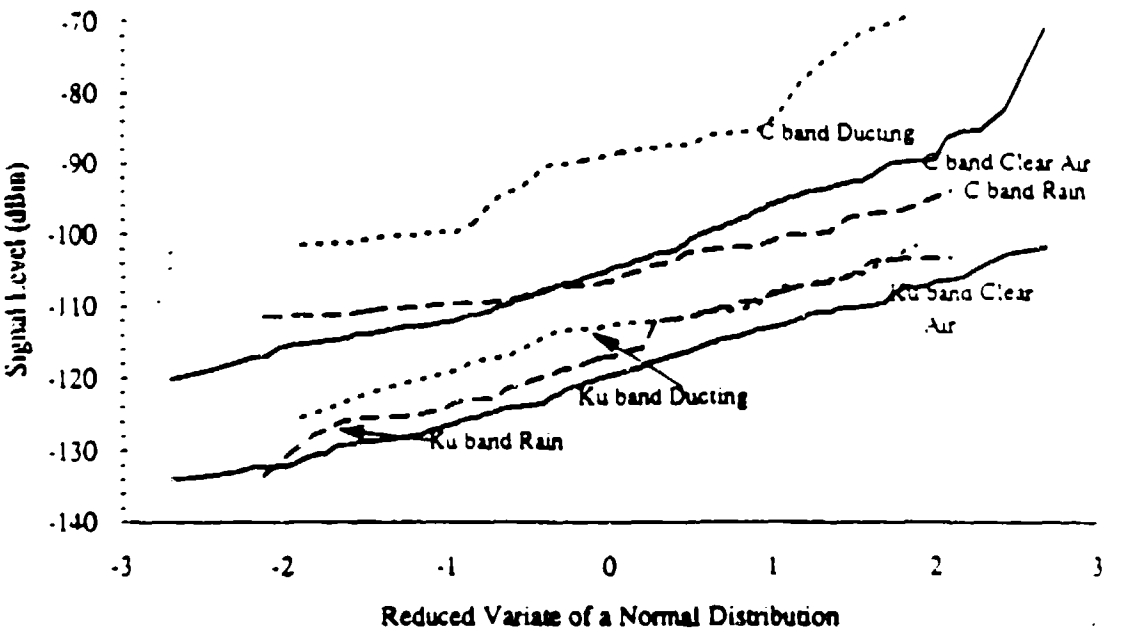

A13 Sample CDF for Ku and C signal levels, all conditions, all hours, summer, 1991.

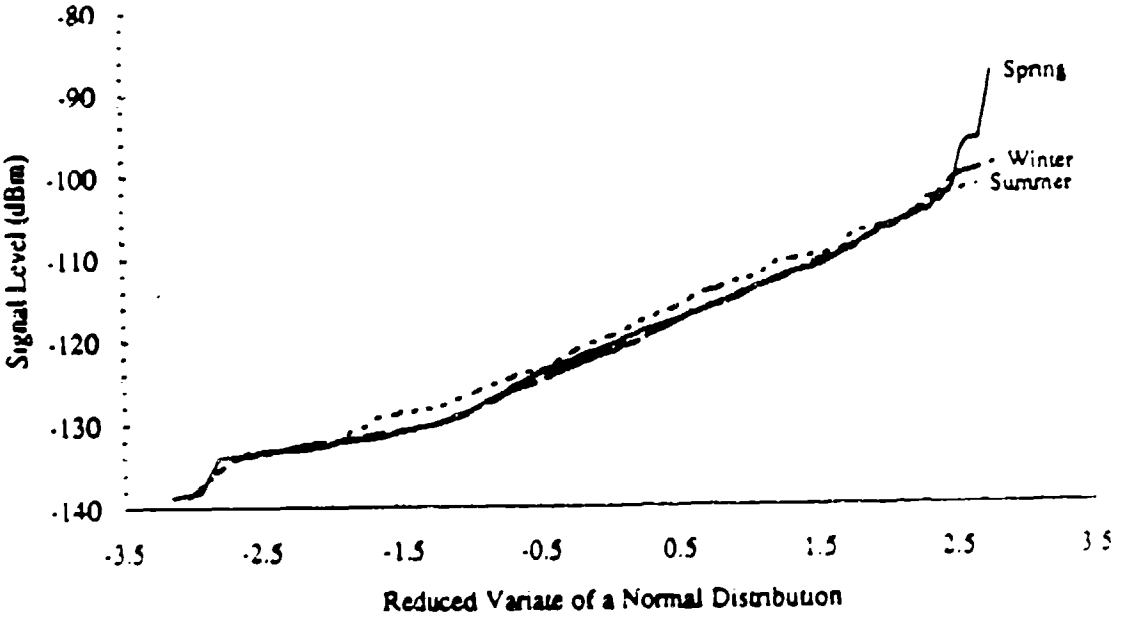

A14 Sample CDF for Ku signal levels, all three seasons, clear air, 1991.

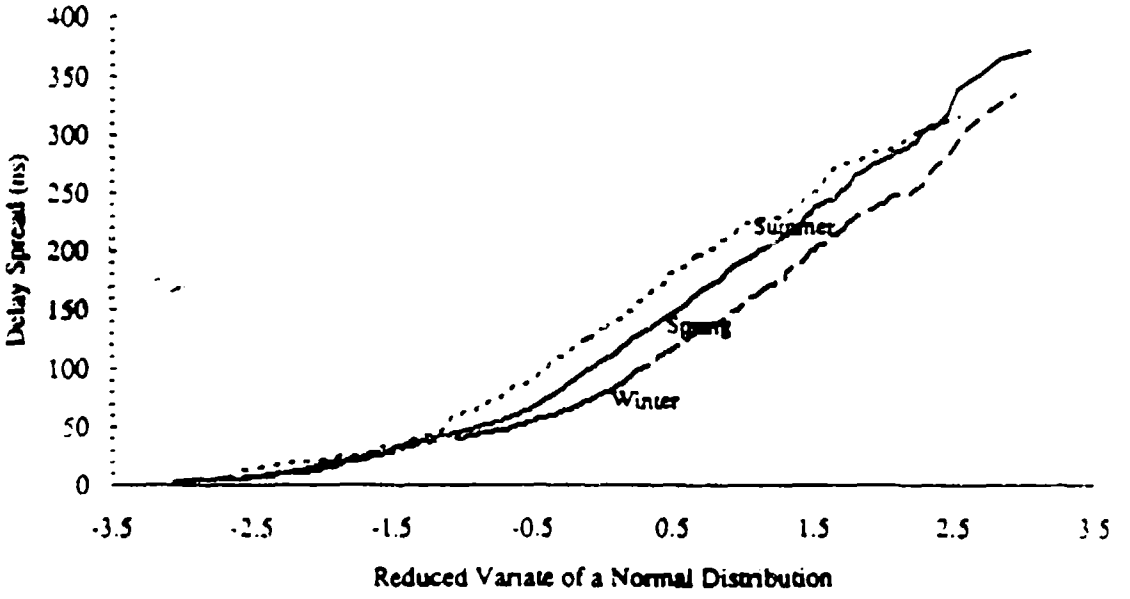

A15 Sample CDF for Ku delay spread, all three seasons, clear air, 1991.

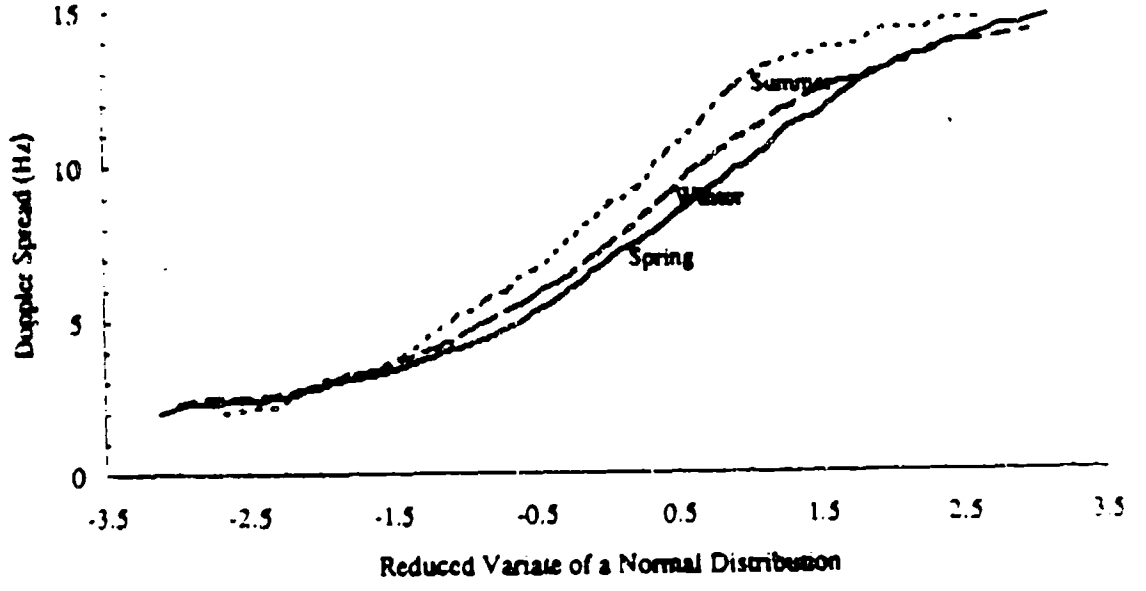

A16 Sample CDF for Ku Doppler spread, all three seasons, clear air, 1991.

Annex B

Summary tables for spring and winter 1991:

Table B1: Spring 1991 - Quarter Day Summaries - Clear Air

	Ku Carrier Level/ Xmission Loss (dBm)	Ku Doppler Shift (Hz)	Ku Delay Spread (ns)	C Carrier Level/ Xmission Loss (dBm)	C Doppler Shift (Hz)
Night					
Hours	305	305	222	70	70
Average	-121.4/166.2	-1.6	105.	-107.7/152.5	-0.9
Std. Dev. (series / median)	5.9 / .26	3.3 / .10	76.6 / 2.9	6.0 / 0.3	2.0 / 0.10
Morning					
Hours	303	303	223	59	59
Average	-121.7/166.5	-1.	105.	-106.9/151.7	-0.4
Std. Dev.	6.2 / 0.25	3.5 / 0.11	66.8 / 3.0	5.5 / 0.32	1.6 / 0.1
Afternoon					
Hours	263	263	229	52	52
Average	-119.9/164.7	-1.3	97.5	-107/151.8	0.4
Std. Dev.	7.7 / 0.34	3.3 / 0.14	67.9 / 2.9	3.7 / .26	1.1 / 0.16
Evening					
Hours	291	291	250	63	63
Average	-118.8/163.6	-1.8	110.	-107.6/152.4	-0.5
Std. Dev.	6.6 / 0.27	3.3 / 0.11	71.7 / 3.	6.0 / 0.26	1.9 / 0.14
Doppler Spread:	Hours: 1153	Median: 6.7	St.Dev: 2.8		

Table B2: Spring 1991 - Quarter Day Summaries - Rain

Night					
Hours	36	36	26	3	3
Average	-122.9/167.7	7.8	140.0	-100.1/144.9	0.8
Std. Dev.	11.3 / 1.1	3.8 / 0.38	76.3 / 12.1	1.4 / 1.4	1.9 / 0.54
Morning					
Hours	29	29	28	4	4
Average	-116.3/161.1	9.	145	-108.2/153.	1.1
Std. Dev.	8.1 / 1.0	3.6 / 0.65	79.2 / 15.14	3.2 / 0.87	3.2 / 1.4
Afternoon					
Hours	30	30	28	8	8
Average	-119.9/164.7	7.0	122.5	-104.4/159.2	2.3
Std. Dev.	7. / 0.97	4.6 / 0.63	76.2 / 11.7	4.4 / 0.69	3.3 / 0.86
Evening					
Hours	39	39	35	14	14
Average	-119.8/166.6	8.0	157.5	-99.5/144.3	1.4
Std. Dev.	7.1 / 0.89	3.9 / 0.44	69.3 / 9.9	2.4 / 0.66	3.2 / 0.68
Doppler Spread:	Hours: 124	Median: 8.1	St.Dev: 2.6		

Table B3: Spring 1991 - Quarter Day Summaries - Ducting

Night					
Hours	2	2	2	2	2
Average	-114.5/159.3	-2.3	27.5	-101.1/145.9	-0.1
Std. Dev.	0.9 / 1.5	3.3 / 3.1	72.5 / 34.9	7.7 / 1.2	0.35 / 0.6
Morning					
Hours	4	4	4	4	4
Average	-115.3/160.1	-0.6	45.0	-94.8/139.6	-0.1
Std. Dev.	2.2 / 0.37	0.39 / 0.19	19.3 / 7.2	4.1 / 1.2	0.17 / 0.28
Afternoon					
Hours	3	3	3	3	3
Average	-115.8/160.6	-0.8	90.0	-97.0/141.8	0.2
Std. Dev.	0.58 / 0.57	0.39 / 0.25	53.9 / 16.5	0.79 / 2.5	0.29 / 1.5
Evening					
Hours	1	1	1	1	1
Average	-123.1/167.9	5.0	222.5	-99.9/144.7	0.4
Std. Dev.	0.0 / 3.7	0.0 / 5.0	0.0 / 51.3	0.0 / 1.6	0.0 / 0.5
Doppler Spread:	Hours: 5	Median: 8.3	St.Dev: 4.5		

Table B4: Winter 1991 - Quarter Day Summaries - Clear Air

	Ku Carrier Level/ Xmission Loss (dBm)	Ku Doppler Shift (Hz)	Ku Delay Spread (ns)
Night			
Hours	207	207	159
Average	-121.8/166.6	-4.0	87.5
Std. Dev. (series / median)	6.9 / 0.34	3.3 / 0.13	63.9 / 3.0
Morning			
Hours	183	183	145
Average	-122.1/166.9	-3.9	70.0
Std. Dev.	6.3 / 0.4	4.2 / 0.18	57.2 / 3.1
Afternoon			
Hours	185	185	169
Average	-119.7/164.5	-3.3	72.5
Std. Dev.	7.1 / 0.39	3.5 / 0.15	60.1 / 3.1
Evening			
Hours	220	220	179
Average	-122.2/167	-3.5	80.0
Std. Dev.	6.2 / 0.31	2.5 / 0.16	62.6 / 3.4
Doppler Spread:	Hours: 752	Median: 7.3	St.Dev: 2.9

Table B5: Winter 1991 - Quarter Day Summaries - Rain

Night			
Hours	0	0	0
Morning			
Hours	1	1	1
Average	-115.8/160.6	375	185
Std. Dev.			
Afternoon			
Hours	3	3	3
Average	-113.5/158.3	3.1	107.5
Std. Dev.	2.5 / 0.	2.7 / 0.	80.4 / 0.
Evening			
Hours	0	0	0
Doppler Spread:	Hours: 4	Median: 5.8	St.Dev: 0.7

Bibliography

Anderson, B.T.,"Observations and Analysis of Tropospheric Scatter Propagation During Rain at 16 GHz and 5GHz", M.E.Thesis, Thayer School of Engineering, Dartmouth College, Hanover, NH, 1989.

Atlas, D., and K.R. Hardy, Radar analysis of the clear atmosphere: Angels, *Proc. XV Gen. Assem. URSI*, 401-469

Booker, H.G., and W.E. Gordon, A theory of radio scattering in the troposphere, *Proc. IEEE, 38*, 401-412, 1950

C.C.I.R., "Effects of the Atmosphere", Section 5C, in *Recommendations and Reports of the C.C.I.R., 1978*, volume V, Propagation in Non-Ionized Median, International Telecommunications Union, 1990.

Chandra, S.N., "Establishing a Wideband (400 MBit/sec) Receiver at the Ku band for a 161 km Troposcatter Communications Link", M.E.Thesis, Thayer School of Engineering, Dartmouth College, Hanover, NH, 1990.

Crane, R.K., A review of radar observations of turbulence in the lower stratosphere, *Radio Sci.*, 15, 177-193, 1980.

Crane, R.K., A Review of Transhorizon Propagation Phenomena, *Radio Science*, 16(5), 649-669, 1981.

Crane, R.K., "Tropospheric Scatter Propagation at 5 and 15 GHz: Preliminary Results fo a 161 km Path", Interim Report on Research Conducted Under Post-Doctoral Program, Rome Air Development Ctr., 1988

Crane, R.K., Worst-month rain attenuation statistics: a new approach, Thayer School of Engineering, Dartmouth College, Hanover, NH, 1990.

Crane, R.K., "5/15 Scattering Study", Rome Laboratory, Rept RL-TR-91-45, Hanscom AFB, MA 1991.

Crane, R.K., and R. Prabhu, "Wideband Troposcatter", Final Report on research Conducted under Contract to Georgia Inst. of Tech. on Subcontract E-21-T29-S1 to their Prime Contract No. F30602-88-D-0025 with Rome Laboratory, Hanscom AFB, Ma., Thayer School of Engineering, Dartmouth College, Hanover, NH, 1991.

Dewan, E.M., Optical Turbulence Forecasting: A Tutorial, Report to the Hauscom AFB, Ma., 1980.

Eklund, F., and S. Wickerts, "wavelength Dependence of Microwave Propagation Far Beyond the Radio Horizon," *Radio Science*, 3, 1066-1074, 1968.

Doviak, R.J., and D. Zrnic, *Doppler Radar and Weather Observations*, Academic Press, Orlando, FL, 1984.

Gossard, E.E., W.D. Neff, R.J. Zamora, and J.E. Gaynor: The fine structure of elevated refractive layers: Implications for over-the-horizon propagation and radar sounding systems, *Radio Science*, 19, 1523-1533, 1984.

Gossard, E.E., D.C. Welsh, and R.G. Strauch, Radar-measured height profiles of Cn and turbulence dissipation during October 1989 at Denver, 1991

Hall, M.P.M., *Effects of the Troposphere on Radio Communications*, Peter Peregrins Ltd. for the Institution of Electrical Engineers, New York, NY, 1979.

Hoppe, M.H., "The study of Ku-band Tropospheric Scatter Channel During Clear Air Conditions via Data Collected on the Link Between Prospect Hill in Waltham, MA, and Mt.Tug in Enfield, NH," M.E. Thesis, Thayer School of Engineering, Dartmouth College, Hanover, NH, 1989.

Levins, C.L., "Establishing a Receiver Station for the Study of a Ku-band Troposcatter Channel", M.S.Thesis, Thayer School of Engineering, Dartmouth College, Hanover, NH, 1986.

Ottersten, H., Atmospheric structure and radar backscattering in clear air, *Radio Science.*, 4, 1179-1193, 1969.

Prabhu, R., "Observations and Analysis of a Troposcatter Propagation Channel at the Ku band", M.S. Thesis, Thayer School of Engineering, Dartmouth College, Hanover, NH, 1991.

Proakis, J.G., *Digital Communications*, 2nd ed., McGraw-Hill Book Company, New York, NY, 1989.

Rice, P.L., A.G. Longley, K.A. Norton and A.P. Barsis, "Transmission Loss Predictions for Tropospheric Communications Circuits", Tech Note 101, Vols 1 and 2, National Bureau of Standards, Washington DC, 1965.

Richter, J.H., High-resolution tropospheric radar sounding, *Radio Science*, 4, 1260-1268, 1969

Skolnik, M.I., The frequency dependence of tropospheric scatter propagation and its relation to stratified turbulence, Naval Research Lab., Washington DC, 1974

Stamboulis, P.A., "The Study of a tropospheric Scatter Channel via System Modeling and Analysis of Data Collected from Ku and C-band Links," M.S. Thesis, Thayer School of Engineering, Dartmouth College, Hanover, NH, 1987.

Sullivan, M.J., "The Establishment of a Dual Frequency troposcatter Receiver Station for the Use in a Statistical Study of the Feasibility of Troposcatter Communications in the Ku band," M.E. Thesis, Thayer School of Engineering, Dartmouth College, Hanover, NH, 1987.

Tatarskii, V.I., *The effects of the turbulent atmosphere on wave propagation*, Natl. Tech. Inf. Serv., Springfield, Va., 1971.

Woodman, R.F., "High-altitude resolution stratospheric measurements with the Aricebo 430-MHz radar", *Radio Science*, 15, 417-422, 1980.

MISSION

OF

ROME LABORATORY

Mission. The mission of Rome Laboratory is to advance the science and technologies of command, control, communications and intelligence and to transition them into systems to meet customer needs. To achieve this, Rome Lab:

a. Conducts vigorous research, development and test programs in all applicable technologies;

b. Transitions technology to current and future systems to improve operational capability, readiness, and supportability;

c. Provides a full range of technical support to Air Force Materiel Command product centers and other Air Force organizations;

d. Promotes transfer of technology to the private sector;

e. Maintains leading edge technological expertise in the areas of surveillance, communications, command and control, intelligence, reliability science. electro-magnetic technology, photonics, signal processing, and computational science.

The thrust areas of technical competence include: Surveillance, Communications, Command and Control, Intelligence, Signal Processing, Computer Science and Technology, Electromagnetic Technology, Photonics and Reliability Sciences.